

SCALE-UP OF MECHANICALLY AGITATED
FLOTATION PROCESSES
BASED ON
THE PRINCIPLES OF DIMENSIONAL
SIMILITUDE

By

Marius Truter

Thesis submitted in partial fulfilment of the requirements for the Degree

of

MASTER OF SCIENCE IN ENGINEERING
(MINERAL PROCESSING)

in the Department of Process Engineering

at the University of Stellenbosch

Supervised by

Prof C Aldrich

Stellenbosch

December 2010

Declaration

I, the undersigned, hereby declare that the work contained in this thesis is my own original work and that I have not previously in its entirety or in part submitted it at any university for a degree.

A handwritten signature in black ink, appearing to read 'A. H. van der Merwe', written above a horizontal line.

Signature

10 September 2010

Date

Copyright © 2010 Stellenbosch University

All rights reserved

Abstract

The use of dimensional analysis to scale-up mechanically agitated flotation processes and to identify deficiencies in froth flotation plants was explored. The full range of operating variables was considered, such as particle size distribution, reagent suite, conditioning time, retention time, machine geometry, aeration, solids suspension, power requirements and turbulence. Dimensional analysis offers a methodology to combine variables into dimensionless groups to guide the scale-up process based on the notion of similarity. Ten dimensionless groups were developed and combined with metallurgical variables, such as liberation, reagents dosage and flow diagrams to produce a scale-up and evaluation tool, applicable to any mechanically agitated flotation process. In many hydrodynamic studies, the researchers considered hydrodynamic variables based on rotor diameter. In this case the hydrodynamic variables based on rotor diameter represent mechanism "ability", while parameters based on cell diameter are considered "requirement".

Dimensionless groups have also been applied to the definition of basic parameters of the kinetic constant, such as floatability, bubble surface area flux and froth recovery factor. It also showed that the bubble surface area flux has a maximum with increased aeration, where similar models do not show this dependence.

Analysis by computational fluid dynamics and Perspex modelling revealed valuable insight into the inner working of the Wemco flotation machine, such as air dispersion, turbulence levels, separation zones and solids concentration. Design changes to the rotor, disperser, hood and geometrical lay-out produced a marked improvement in flotation conditions. It also supported certain dimensionless numbers measured in full scale plants.

Case studies confirmed that almost all flotation plants, irrespective of the minerals floated, suffer from the same deficiencies. Dimensional similitude offers a unique tool to identify these deficiencies and to predict the effect of recommended improvements. In almost every case where the fundamental requirement of similarity was applied, an improvement in performance was observed. Finally a new algorithm is proposed for the scale-up of flotation plants and the application is demonstrated in the design and testing of a pilot plant.

Opsomming

Die gebruik van dimensionele analise in die opskaal van flottasieprosesse en die identifisering van flottasieaanlegprobleme is ondersoek. Die volle bereik van bedryfsveranderlikes is ondersoek, soos partikelgrootte, kondisioneringstyd, retensietyd, geometrie, lugvloei, suspensie van vastestowe, turbulensie en drywingsvereistes. Dimensielose analise is die proses waardeur veranderlikes deur wiskundige manipulasie gekombineer word in dimensielose groepe. Tien dimensielose groepe is ontwikkel en is tesame met metallurgiese veranderlikes soos vrystelling, reagensdosering en vloei-diagramme gekombineer om gebruik te word om gelykvormigheid te bewerkstellig. Hierdie proses is van toepassing op enige flottasieproses gebaseer op meganiese geagiteerde toerusting.

Dimensielose groepe is ook gebruik in die definisie en kwantifisering van turbulensie, agitatie, geometrie, suspensie van vastestowe, verspreiding van lug en drywingsvereistes. Daarbenewens is die groepe gebruik in die definisie van die basiese veranderlikes van die kinetiese konstante soos lugborreloppervlakvloei, suspensie, en herwinning in die skuimfase. Die groepe is ook gebruik in die bewys dat die lugborreloppervlakvloei 'n maksimum het met toename in lugvloei. In baie gevalle word hidrodinamiese veranderlikes uitgedruk in terme van die rotordiameter en in hierdie studie word dit beskou as meganisme "vermoë". Die hidrodinamiese veranderlikes gebaseer op sel-diameter word beskou as "behoefte".

Berekeningsvloeidinamika en Perspex modellering het waardevolle insig verskaf in die binne-werking van die Wemco flottasiemasjien soos lugverspreiding, turbulensie en partikelkonsentrasie en is ook gebruik om sekere dimensielose getalle wat in volskaalse aanlegte gemeet is, te verifieer. Gevallestudies het bevestig dat feitlik alle flottasieaanlegte, ongeag die soort mineraal, gebuk gaan onder dieselfde afwykings. Dimensionele analise bied 'n eenvoudige benadering om hierdie afwykings te identifiseer en om die effek van veranderings te voorspel. In alle gevalle waar die beginsels van gelykvormigheid slaafs gevolg is, het 'n merkbare verbetering in prestasie voorgekom.

Ten slotte is 'n nuwe opskaleringsalgoritme ontwikkel en is die toepassing daarvan gedemonstreer deur die ontwerp en toets van 'n loodsaanleg, gebaseer op die Wemco geometrie.

TABLE OF CONTENTS.

CHAPTER 1: INTRODUCTION.....	1
CHAPTER 2: A LITERATURE REVIEW ON DIMENSIONAL ANALYSIS AND SCALE-UP OF FLOTATION.....	7
2.1. Dimensional analysis and dimensionless numbers.....	7
2.2. Dimensions and units.....	8
2.3. Dimensional homogeneity.....	8
2.4. Typical results from a dimensional analysis... ..	8
2.5. Methods of performing dimensional analysis.....	9
2.6. Choice of variables.....	13
2.7. Wrong choice of physical properties.....	14
2.8. Similitude.....	14
2.9. Dimensional analysis and flotation.....	14
2.10. Flotation performance and dimensionless numbers.....	18
2.11. Summary.....	19
CHAPTER 3: DIMENSIONAL ANALYSIS OF A FLOTATION PROCESS.....	21
3.1. Dimensional analysis.....	21
3.2. Relevance list and linear independence.....	22
3.3. Buckingham π-Theorem based on repeating variables.....	22
3.4. Combination of some groups.....	25
3.5. Dimensionless numbers and transformation equations.....	25
3.6. Dimensionless kinetic constant.....	27
3.7. Characterization of plant deficiencies based on a schedule of dimensionless numbers.....	39
3.8. Partial similarity.....	46
3.9. Practical plant measurements.....	47

3.10. Deficiencies in industrial plants based on the schedule of dimensionless parameters.....	59
3.11. Dimensionless comparison of industrial designs.	61
3.12. Summary for the application of the schedule of dimensionless numbers. 61	
CHAPTER 4: INTERPRATIVE RESULTS OF A CFD ANALYSIS OF FLOTATION CELL HYDRODYNAMICS.	64
4.1. Design data.	64
4.2. CFD model.	67
4.3. CFD RESULTS.....	68
4.4. Mathematical procedure to calculate the mineral recovery rate potential. 75	
4.5. Interpolation of Recovery rate potential data supplied by client.	77
4.6. Bubble particle collision frequency.....	81
4.7. Streamline plots.	82
4.8. Volume fraction distribution.....	82
4.9. Pulp Reynolds number.	82
4.10. Pulp density distribution.	82
4.11. Bubble particle collision frequency and probability for successful recovery.....	83
4.12. Interpolated mineral recovery rate potential.	87
4.13. Summary of CFD results.....	89
CHAPTER5: APPLICATION OF SCHEDULE OF DIMENSIONLESS NUMBERS TO A PHOSPHATE PLANT.	90
5.1. Background.	90
5.2. Geology.	91
5.3. Pilot plant conditions.	91
5.4. Full scale plant.	99
5.5. Schedule of dimensionless numbers.....	104

5.6. Modified E-Bank.	104
CHAPTER 6: APPLICATION OF THE SCHEDULE OF DIMENSIONLESS NUMBERS TO A PLATINUM PLANT.....	109
6.1. The Platinum Industry.....	109
6.2. Geology.	109
6.3. Mineralogy.	109
6.4. Flotation chemistry.	110
6.5. Operational Considerations.	111
6.6. Schedule of dimensionless numbers.....	113
CHAPTER 7: CALE-UP METHODOLOGY.	116
7.1. New scale-up algorithm.	116
7.2. Discussion of new algorithm.	116
7.3. Application of the new algorithm to a standard industrial design.....	117
7.4. Design of Tornado pilot plant.	119
7.5. Compliance to specification.....	122
7.6. Contribution of thesis to the subject.	122
CHAPTER 8: CONCLUSIONS AND RECOMMENDATION.....	126
8.1. Dimensionless analysis.	126
8.2. Schedule of Dimensionless numbers.	126
8.3. Main plant performance.	127
8.4. Process Characterization.....	127
8.5. Process specification.....	127
8.6. Scale-up Techniques.	128
8.7. CFD results of Wemco machine.	128
ABBREVIATIONS	130
NOMENCLATURE.....	133

REFERENCES	141
APPENDIX 1: I-BANK PILOT PLANT	144
I-Bank operational conditions.....	144
1.2. Geometrical similarity.....	145
1.3. Metallurgical similarity.....	145
1.4. Hydrodynamic similarity.....	146
1.5. Remarks.....	147
APPENDIX 2: H-BANK RECONFIGURED.....	148
2.1. Operating Conditions.....	148
2.2. New design.....	148
2.3. Remarks.....	151
2.4. Result.....	152
APPENDIX 3: 42 m³ SMART CELL.....	153
3.1. Background.....	153
Experimental set-up and hydrodynamic performance.....	153
3.3. Results and conclusions.....	153
APPENDIX 4: BANK 15.....	154
4.1. Background.....	154
4.2. Machine Changes.....	154
4.3. Conclusions.....	155
APPENDIX 5: MINERAL SPECIFICATION.....	157
APPENDIX 6: VISCOSITY IN PULP.....	168
6.1. Method by Roscoe (1952).....	168
6.2. Helephi's model (1997).....	168
6.3. Germans' Method.....	170

APPENDIX 7: DETAIL DIMENSIONLESS ANALYSIS.	171
7.1. Variables.	171
7.2. Developing of n-groups.	171
APPENDIX 8: NEW SCALE -UP ALGORITHM	178

CHAPTER 1: INTRODUCTION.

Flotation is the most important technique used in mineral separation (Wills and Napier-Munn, 2006) and is widely used not only in the mineral process industries, but also in the treatment of wastewater, de-inking, etc. (Dobias et al., 1992). Despite its widespread use, the physical and chemical phenomena constituting flotation is complex and not yet fully understood. For example, froth flotation exploits the differences in the physiochemical surface properties of mineral particles to enable selective attachment of particles to air bubbles in the flotation pulp (Dai et al., 1998; 1999; 2000). Air bubbles can adhere to particles only if they can displace the water film from the mineral surface, i.e. if the mineral exhibits some degree of hydrophobicity. Moreover, once loaded bubbles reach the surface of the froth, they can only continue to support the floated particles if the froth is stable. Collectively, all these phenomena are difficult to model, so that the design and optimisation of flotation equipment tend to be a heuristic procedure, or art rather than science. Typically design would be based on laboratory and pilot plant data that are then used to scale-up to industrial systems.

Only recently did researchers manage to identify the basic microscopic processes in flotation and started to develop the scale-up techniques to support full-scale design (Schubert and Bischofberger, 1998). As a result many flotation plants in the world today perform below expectation or design. For example,

Figure 1 shows grade-recovery data for a pilot plant (black bar) and corresponding industrial scale (empty bar) phosphate plant in South Africa (Van der Linde, 1980), where recovery on the full-scale plant is significantly lower than that on the pilot plant. Although this data might be 25 years old, the conditions and performance are still the same and the main reason for this seems to be a lack of understanding of the macro-processes. In some cases only the metallurgical scale-up was performed, because of a lack of understanding of the hydrodynamics and in other cases the hydrodynamics were adjusted without understanding the effects on the metallurgy. When referring to the principles of flotation, metallurgists and engineers often refer to "suppressed turbulence" and "high agitation" without having an idea how to quantify these requirements. Even in the basic design, manufacturers seem to contradict the fundamental principles to meet the requirements of aeration and suspension, e.g. to ensure proper aeration and solid suspension, manufacturers would design a machine with a low aspect ratio and with increase rotational speed, thereby threatening froth stability.

In the AMIRA - P9L project (Optimisation of Minerals Processes by Modelling and Simulation 1996-1999, JKMRRC) scale-up and simulation codes were developed based on first order kinetic models expressing recovery (R) as a function of time (τ) such that:

$$R = R_m \cdot (1 - e^{-k\tau}) \quad (1)$$

Very elegant techniques were developed to predict and determine the kinetic constant k as a function of F_p , S_b , and R_f . Of the three variables, S_b is the most significant and also a very useful variable to predict the improvement in k.

The other two variables are more difficult to determine and one always ends up with some constant that is unknown (AMIRA, P9L Final Report, vol. 2, pp. 158). To date, the author is unaware of any successful application of the AMIRA models in scaling up or analysing, identifying and "improving" industrial plant deficiencies.

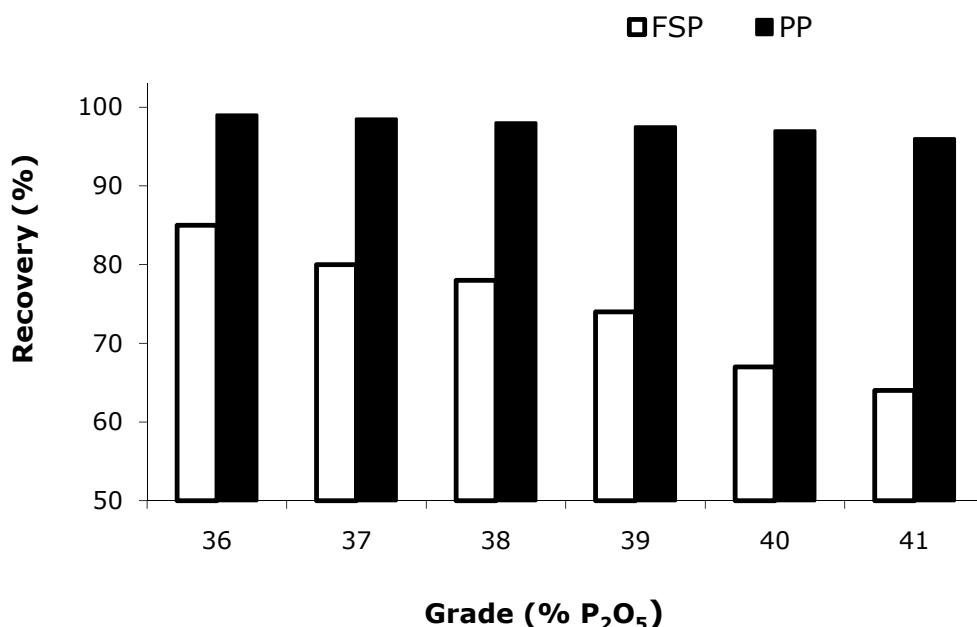


Figure 1: A typical relationship between recovery and grade, for a pilot plant (PP) and full-scale plant (FSP). The mineral is a phosphate (Van der Linde, 1980).

Another model used extensively is the Klimpel model (Klimpel, 1980).

$$R = R_m \cdot (1 - \{1 - e^{-k\tau}\} / k\tau) \quad (2)$$

Based on kinetic constants determined from laboratory scale retention time experiments, mass balance models and given flow diagrams, these models are very useful. The

difficulty is to predict the effect of hydrodynamic changes, conditioning, froth depth and liberation on k. Tables 1 & 2 show typical results of some non-metal and metal plants respectively from statistics gathered by the author at different South African plants.

In these tables, the plants are not identified for confidentiality reasons, but simply indicated as phosphate, carbonate or fluoride in the non-metal plants and Cu-1, Cu-2 (copper), Zn (zinc), and GM-1, -2, -3 (PGM) in the metal plants.

Table 1: Recovery of valuable products at non-metals plants.

Mineral (Mine)	Phosphate	Carbonate	Fluoride
Pilot Plant Recovery (%)	90	95	90
Main Plant recovery (%)	65	90	73
Revenue loss (MR/y)	100	30	30

Table 2: Recovery of valuable products at metals plants.

Mineral (Mine)	Cu-1	Cu-2	Zn	GM-1	GM-2	PGM-3
PP performance	87	93	95	92	92	72
FSP performance (%)	76	85	87	80	77	35
Revenue loss (MR/y)	100	30	20	300	100	300

No significant change of mineralogy occurred which might have had a negative impact on recovery. In some cases the reagent suites have been changed to compensate for the deficiencies in hydrodynamics. Tables 1 & 2 were compiled over six month data at the same concentrate grade. The author's estimates of lost revenue are based on the difference between the pilot plant (PP) performance and the full-scale plant (FSP) performance. To investigate these costly deficiencies, a technique based on dimensional similitude was developed. This approach will be discussed in more detail in the next Chapters. Table 3 shows that the application of dimensional similitude is appropriate in the analysis of flotation problems based on Criteria 3 and 4 in the first column of the table. Zlokarnik (1991) also claims that the timely application of dimensional similitude often leads to the discovery of forgotten variables or the exclusion of some.

Table 3: Test of appropriateness for dimensionless analysis of flotation.

1. Are the physics of the basic phenomenon unknown?	Dimensionless analysis cannot be applied.	
2. Enough is known about the physics of the basic phenomenon to compile a first, tentative relevance list.	The resultant dimensionless groups are unreliable.	
3. All the relevant physical variables describing the problem are known.	The application of dimensionless analysis is unproblematic.	#
4. The problem can be expressed in terms of a mathematical equation.	A closer insight into the dimensionless groups is feasible and may facilitate in reducing the set of dimensionless groups.	#
5. A mathematical solution of the problem exists.	The application of dimensionless analysis is superfluous.	

In the author's view, another important miss-understanding of the mechanism of mechanically agitated flotation amongst plant metallurgists and suppliers, which has fixed the approach to machine and process design over the past years, is that flotation is the random collision of sinking solid particles and rising bubbles as they move through the bulk of the machine. In fact flotation is a deliberate attempt to penetrate the velocity, pressure and tension barriers between particle and bubble.

For this reason, in mechanically agitated machines, the primary impact-collision takes place in the highly turbulent region at the tip of the rotor and behind the rotor and between the tip of the rotor and the stator where air changes into small bubbles and the particles are subjected to large centrifugal forces. Bubble and particles are forced into one another, penetrating the film between them, attach and then released into the quiet zone where they float to the froth zone (Schubert and Bischofberger, 1998; Schulze, 1982). Koh et al. (2000), also showed, by means of CFD and applying attachment and de-attachment models, that attachment is greatest between rotor tip and stator. Secondary impacts-collision takes place in turbulent eddies further away from the rotor and to a lesser extent in the boundary layer on the walls of the flotation cell. Sliding-collision takes place further away but its contribution to collision and attachment is

limited. Even in column flotation where no rotor exists, the turbulent conditions, in terms of Reynolds number around the emerging bubble, as it is ejected from the sparger nozzle, is almost similar to those experienced on the tip of the rotor.

Figure 2 clearly shows this interaction between pulp and air on the tip of the rotor. This picture was taken by combining a digital camera and a stroboscope shining down the vortex inside the standpipe of a Wemco flotation machine.



Figure 2: The interaction between air and pulp on the tip of a rotor.

Another fact to be kept in mind is the difference between scaling up a process and scaling up a machine. In scaling up the process, the tank diameter (requirement) is normally the reference diameter and in scaling up the machine the rotor diameter (ability) is used as reference diameter. Once the requirement has been determined, then one can estimate the size of machine to deliver the required quantity.

In considering dimensionless scale-up theory, the author has attempted to provide simple, practical tools and techniques for the plant metallurgist to apply. The idea was to rely as far as possible on standard production information, instead of trying to determine difficult variables, such as surface tension, power intensity and frequency distributions of

the bubbles, all the time assuming constant mineralogy, chemistry, liberation and flow diagram.

With these issues in mind the author will consider the following hypothesis in this thesis:

Scaled-up froth flotation processes perform significantly worse than expected in the South African metallurgical industries, owing to the lack of understanding of the correct scale-up procedures. This can be improved considerably by enforcing dimensional similitude between laboratory or pilot scale experiments and industrial scale flotation plants.

The hypothesis will be examined by pursuing the following specific objectives:

- Demonstrate that scaled-up flotation plants in the South African industries perform worse than expected based on laboratory results.
- Propose a methodology based on dimensional similitude to improve the scale-up of flotation plants.
- Demonstrate the validity of the methodology via industrial case studies.

The thesis is organised as follows. First the basic concepts behind the dimensional similitude of flotation systems and the results from a literature study are considered in Chapter 2. This is followed by a full dimensional analysis of a flotation process, as well as the derivation of the transformation number for hollow stirrers, a dimensionless form of the kinetic constant and a schedule of dimensionless numbers for the characterization of flotation processes in Chapter 3. In Chapter 4, the hydrodynamics of the Wemco flotation cells are investigated by means of computational fluid dynamics. In Chapters 5 and 6, it is shown that flotation systems from a phosphate and a PGM plant perform worse than expected on the basis of laboratory-scale results and that this discrepancy in performance could be reduced substantially by improvements based on the principles of dimensional similitude. In Chapter 7 a new scale-up methodology is proposed and a discussion of the difference between literature and this thesis. The thesis ends with Chapter 8 where the conclusions of the investigation are summarized.

Appendix 1 to 5 are additional examples of the application of the schedule of dimensionless numbers, while Appendix 6 demonstrates the use of dimensionless numbers in specifying different minerals and processes. Appendix 7 gives a detail analysis of the rest of the dimensionless numbers for a flotation process and Appendix 8 shows the new scale-up algorithm.

CHAPTER 2: A LITERATURE REVIEW ON DIMENSIONAL ANALYSIS AND SCALE-UP OF FLOTATION.

2.1. Dimensional analysis and dimensionless numbers.

In studying the literature it was found that the published material can be divided into two groups and the rest of this document will be discussed under these two headings. These two groups are:

- Those that have attempted to apply the techniques of dimensional analysis to flotation, and
- Those who utilised dimensionless groups to demonstrate the relationship between these groups and flotation performance.

In engineering the application of fluid mechanics in designs make use, to a large extent, of empirical results from a lot of experiments. This data is often difficult to present in a readable form. Even from graphs it may be difficult to interpret. Dimensional analysis provides a strategy for choosing relevant data and how it should be presented. This is a useful technique in all experimentally based areas of engineering. If it is possible to identify the factors involved in a physical situation then dimensional analysis can form a relationship between them. The resulting expressions may not at first sight appear rigorous, but these qualitative results converted to quantitative forms can be used to obtain any unknown factors from experimental results. (Sleigh and Noakes, 2009).

Ruzicka (2008) stated that dimensionless numbers are useful in that:

- They reduce the number of variables needed for description of the problem thereby reducing the amount of experimental data and at making correlation.
- They simplify the governing equations.
- They produce valuable scale estimates, whence order of magnitude estimates of important physical quantities.
- When properly formed, they have clear physical interpretation and thus contribute to the physical understanding of the phenomenon under study.

2.2. Dimensions and units.

Any physical situation can be described by certain familiar properties e.g. length, velocity, area, volume, acceleration, etc. The following columns give an explanation of the difference between quantity, units and dimensions.

Quantity	Units	Dimensions
Velocity	m/s	LT ⁻¹
Force	kg m/s ²	MLT ⁻²

Dimensions are properties which can be measured. Units are the standard elements used to quantify these dimensions. In dimensional analysis we are only concerned with the nature of the dimension i.e. its quality not its quantity. All properties can be represented with L, T, M and temperature. (Sleigh and Noakes, 2009).

2.3. Dimensional homogeneity.

Any equation describing a physical situation will only be true if both sides have the same dimensions. That is it must be *dimensionally homogeneous*. (Sleigh and Noakes, 2009). For example:

The flow through a weir is:

$$Q = 0.66 \cdot B \cdot \sqrt{2 \cdot g} H_w^{1.5} \quad (3)$$

The SI units of the left hand side are m³s⁻¹. The units on the right hand side are equal to:

$$m(ms^{-2})^{1/2}m^{3/2} = m^3s^{-1} \quad (4)$$

2.4. Typical results from a dimensional analysis.

The result of performing dimensional analysis on a physical problem is a single equation. This equation relates all of the physical factors involved to one another. For example, if we want to find the force on the blade of a propeller we must first decide what might influence this force. It would be reasonable to assume that the force F_o , depends on the following physical properties:

Table 4: Physical properties for blade of propeller.

Property	Symbol / Units
Diameter	Z (m)
Forward velocity	U (m/s)
Fluid density	ρ (kg/m ³)
RPM of propeller	ω (s ⁻¹)
Fluid viscosity	μ_f (kg·m·s ⁻²)

Before we do any analysis we can write the following equation:

$$f = \phi_1(Z, \mu_f, \rho_f, \omega, U) \quad (5)$$

Where ϕ is an unknown function. It can be expanded into an infinite series which can itself be reduced to:

$$f = k'' \cdot Z^{x_1} \cdot U^{x_2} \cdot \rho_f^{x_3} \cdot \omega^{x_4} \quad (6)$$

where k'' is some constant and X_1 to X_4 are unknown exponents. From dimensional analysis one can obtain these powers and form the variables into several dimensionless groups.

The value of k'' and the function ϕ must be determined from experiments. The knowledge of the dimensionless groups often helps in deciding what experimental measurements should be taken.

2.5. Methods of performing dimensional analysis.

2.5.1. Rayleigh's indicial methods.

This alternative method is also based on the fundamental principle of dimensional homogeneity of physical variables involved in a problem. The procedure is:

- The dependent variable is identified and expressed as a product of all the independent variables raised to an unknown integer exponent.

- Equating the indices of n fundamental dimensions of the variables involved, n independent equations are obtained.
- These n equations are solved to obtain the dimensionless groups.

Example: To illustrate this method by solving the pipe flow problem.

Step 1: Write the dependent variable $\Delta p/l$ as:

$$\frac{\Delta p}{l} = \gamma \cdot U^{y_1} \cdot D_h^{y_2} \cdot \rho_f^{y_3} \cdot \mu_f^{y_4} \quad (7)$$

Step 2: Insert the dimensions of each variable in the above equation:

$$ML^{-2}T^{-2} = \gamma \cdot [LT^{-1}]^{y_1} \cdot [L]^{y_2} \cdot [ML^{-3}]^{y_3} \cdot [ML^{-1}T^{-1}]^{y_4} \quad (8)$$

Step 3: Equating the indices of M, L and T on both sides, results in:

$$y_1 + y_4 = 1$$

$$y_1 + y_2 - 3y_3 - y_4 = -2$$

$$-y_1 - y_4 = -2$$

Step 4: Solving these equations in terms of the unknown x_4 , results in:

$$y_1 = 2 - y_4$$

$$y_2 = -y_4 - 1$$

$$y_3 = 1 - y_4$$

$$\Delta p/l = \gamma \cdot U^{2-y_4} \cdot D_h^{-y_4-1} \cdot \rho_f^{1-y_4} \cdot \mu_f^{y_4} \quad (9)$$

$$\frac{\Delta p}{l} = \frac{\gamma U^2 \rho_f}{D_h} \cdot \left(\frac{\mu_f}{UD_h \rho_f} \right)^{y_4} \quad (10)$$

Or

$$\frac{\Delta p D_h^2}{l U \mu_f} = \gamma \cdot \left(\frac{UD_h \rho_f}{\mu_f} \right)^{y_4} \quad (11)$$

2.5.2. Buckingham's π -theory. (Sleigh and Noakes, 2009).

The method based on the Buckingham Pi-theorems gives a good generalized strategy for obtaining a solution. There are two theorems accredited to Buckingham which are known as his Pi-theorems.

1st π -theorem:

A relationship between m variables can be expressed as a relationship between $m-n$ non-dimensional groups of variables where n is the number of fundamental dimensions required to express the variables. If a physical problem can be expressed as:

$$\Phi_2(Q_1, Q_2, Q_3, \dots, Q_m) = 0 \quad (12)$$

Then according to the above theorem, this can also be expressed as:

$$\phi_3(\pi_1, \pi_2, \pi_3, \dots, \pi_{m-n}) = 0 \quad (13)$$

In most fluids $n = 3$.

2nd theorem:

Each π -group is a function of n governing or repeating variables plus one of the remaining ones. Both Buckingham's method and Rayleigh's method of dimensional analysis determine only relevant independent parameters of a problem, but not the exact relationship between them.

2.5.2.1. Method of repeating variables.

Let's repeat the pipe flow problem by utilizing mathematical calculations.

Step1: Compile the relevance list:

Pressure drop = Δp (Dependent variable)[ML^3T^{-2}].

Linear velocity = U [LT^{-1}].

Fluid density = ρ_f [ML^{-3}].

Fluid viscosity = μ_f [$ML^{-1}T^{-1}$].

Length of pipe = l (L).

Some reference diameter = Z_f [L].

According to dimensionless analysis the number of dimensionless numbers are equal to, the number of variables (M) and the number of physical dimensions (n), $m-n = 2$.

Step 2: Chose 3 repeating variables ($n = 3$).

Step 3: Add fourth variable and raise repeating variables to exponents and equate to 1:

$$\rho_f^{Z_1} \cdot U^{Z_2} \cdot Z^{Z_3} \cdot \mu_f = 1 \quad (14)$$

Step 4: Replace variables with dimensions:

$$[ML^{-3}]^{z_1} \cdot [LT^{-1}]^{z_2} \cdot [L]^{z_3} \cdot [ML^{-1}T^{-1}] = 1 \quad (15)$$

Step 5: Compare exponents of dimensions and set =0:

$$M: z_1 + 1 = 0 \quad (a)$$

$$L: -3z_1 + z_2 + z_3 - 1 = 0 \quad (b)$$

$$T: -z_2 - 1 = 0 \quad (c)$$

Solve for z_1 , z_2 and z_3 and substitute in (14):

$$\rho_f^{-1} \cdot U^{-1} \cdot Z^{-1} \cdot \mu_f = 1 \quad (16)$$

As Equation 16 is dimensionless, the inverse will also be dimensionless, therefore Equation 16 becomes the first π -group:

$$\pi_1 = \rho_f U Z / \mu_f. \text{ The well known Reynolds number.}$$

As L has only one dimension then:

$$\pi_2 = l/Z \quad \text{Therefore:}$$

$$\begin{aligned} \Delta p &= \gamma \cdot (\pi_1^{z_4} \cdot \pi_2^{z_5}) \\ &= \gamma \cdot [Re^{z_4}, (\frac{l}{D})^{z_5}] \end{aligned} \quad (17)$$

$$\frac{\Delta p \cdot Z^2}{\gamma} = \gamma \cdot Re^{z_6} \quad (18)$$

The constants γ and exponents z_1 - z_6 must be determined by experiment.

2.5.2.2. *Pi*-Sets by matrix transformation.

Certain authors, such as Zlokarnik (1991; 1998), prefer the method of matrix transformation where rows are the dimensions and columns are the variables. Referring to the previous example, the variables are formed into two matrices, viz. a core matrix and a residual matrix. The core matrix is transformed into a unity matrix (zero free main diagonal, otherwise zeros). When generating dimensionless numbers, each element in the residual matrix forms the numerator of a fraction, while its denominator consists of the fillers from the unity matrix. The result is the same as Equation (18).

2.6. Choice of variables.

2.6.1. List of variables.

Zlokarnik (1991) calls it the relevance list and both Zlokarnik and Ruzicka state that it must comply with the following requirements:

- They must be relevant.
- They must be independent.
- The list must be complete.

The choice is highly subjective and needs profound understanding of the problem, experience with the use of dimensionless analysis, intuition and luck. A general rule for independence is that if there are m variables then these variables will be independent, if there is no combination of these variables that will result in an additional variable with the same dimensions of any of the m variables. Examples of these dependent variables are:

$P \approx \rho \cdot \omega^3 \cdot d^5$, $v_t = \omega \cdot d/2$, $\nu = \mu_p/\rho_p$ and $q \approx \omega \cdot d^3$ therefore:

P , v_t , ν and μ_f , ρ_f , ω , and d cannot be part of a relevance list at the same time.

2.6.2. Repeating variables.

Repeating variables are those which we think will appear in all or most of the π groups and are a influence on the problem. There is considerable freedom allowed in the choice of the repeating variables although there are certain rules which should be followed. These rules are:

- From the second theorem there should be n repeating variables.
- When combined, these repeating variables must contain all the dimensions (Mass, Length and Time).
- A combination of the repeating variables must not form a dimensionless group.
- All the repeating variables do not have to appear in all π groups.
- The repeating variables should be chosen to be measurable in an experimental investigation. They should be of major importance to the designer. For example pipe diameter is more useful and measurable than roughness.

In fluid it is usually possible to choose density, velocity and some reference diameter as repeating variables. *This freedom of choice results in there being many different π -groups which can be formed - and all are valid. There is not really a wrong choice.*

2.7. Wrong choice of physical properties.

If, when defining the problem, extra unimportant variables are introduced then extra π -groups will be formed. They will play very little role influencing the physical behaviour of the problem concerned and should be identified during experimental work. If an important/influential variable was missed then a π -group would be missing. Experimental analysis based on these results may miss significant behavioural changes. It is therefore important that the initial choice of variables is carried out with great care.

2.8. Similitude.

Dimensionless numbers can be grouped into geometrical groups, kinematic groups and dynamic groups. A model is said to have similitude with the real application when the two share geometric, kinematic and dynamic similarity.

2.9. Dimensional analysis and flotation.

To demonstrate this technique in flotation it was decided to use an example by Zlokarnik (1972). Although this is a relative old example the principles and arguments are still the same. This is a very good example of the techniques, mathematics and arguments followed to eliminate certain variables in an effort to define the transformation dimensionless group.

2.9.1. Scale-up of flotation cells with stirrers and separate air intake.

Zlokarnik (1972) presented this lecture to the German expert commission on ore dressing in 1972 and is a very good example of the application of dimensional analysis on flotation. It is reproduced here to demonstrate the thinking in eliminating and combination of certain variables. Since the flow state of a flotation cell with a stirring apparatus depends largely on stirring conditions, we will select the diameter of the stirrer d , as the characteristic apparatus measurements to determine all other geometric measurements such as D/d , H/d , h/d , b/d etc, where D is the diameter of the container, H^* is the level of the liquid, h^* is the distance of the stirrer from the bottom and b is the blade height of the stirrer. The material system is completely described by the average particle size δ , the solid content of materials in suspension ϕ_s , the density of the solid and liquid ρ_s and ρ_r , the kinetic viscosity ν , and the surface tension σ . The material values of the gaseous phase may be considered as negligible. The relevant kinematic

variables are the rotational rate of the stirrer ω , the air throughput q_a and the gravitational constant g . For further analysis we will combine density and gravity such that $g\Delta\rho = g \cdot \rho_f \cdot (\rho_s - \rho_f)$. The complete function with relevant variables is:

$$f_1(d, \delta, \varphi_s, \rho_s, \rho_f, \nu, \sigma, \omega, q_a, g\Delta\rho) = 0 \quad (19)$$

The interpretation of this relationship based on the theory of similarity leads to the following set of $(10-3) = 7$ known dimensionless groups.

$$f_2(Fr, Re, We, Q_a, \rho_s/\rho_f, \delta/d, \varphi_s) = 0 \quad (20)$$

The Weber number or characteristic value is now transformed into a simple material characteristic value by a special adapted combination with Fr and Re .

$$We^* = We / (Fr' \cdot Re^4)^{0.33} = \rho_f \cdot (g \cdot \Delta\rho \cdot \nu^4)^{0.33} (\sigma \cdot \rho_f^{0.33}) \quad (21)$$

From (18) we may then derive:

$$f_3(Fr', Re, Q_a, \delta/d, We^*, \rho_s/\rho_f, \varphi_s) = 0 \quad (22)$$

The last three characteristic values in (21) are simple material variables which numeric values are not changed by a scale transformation within the same material system. The same applies to the quotient $\Delta\rho/\rho_p$ in Fr' . The following thus applies to scale transformation.

$$f_4(Fr, Re, Q_a, \delta/d) = 0 \quad (23)$$

With $\Delta\rho/\rho_p$, We^* and $\rho_s/\rho_f = \text{idem}$. (Idem indicates an identical numerical value).

Relationship (23) seems not to have been the subject of research either in flotation technology or in stirring technology. We may nevertheless assume that the flow state here differs only marginally from the flow state with automatic suction stirrers for which exhaustive research is available in terms of stirring technology (Zlokarnic M and Judat H 1969).

2.9.2. Scale-up of flotation cell with an automatic suction stirrer.

The tube stirrer is an automatic suction hollow stirrer used for adding gas to liquids, while the propeller stirrer attached to the same shaft underneath the tube stirrer was intended to churn up solid material from the bottom of the container.

For automatic suction stirrers, air throughput q_a is no longer an independent variable as it is dependent on ω and d as well as dimensions of the air channel. For a geometrically similar scale transfer the new valid function is:

$$f_5 (Fr, Re, \delta/d) = 0 \quad (24)$$

This π -space has already been investigated in the stirring technology, by Zlokarnik and Judat (1969), by determining the so called churning characteristic of the stirrer. The measurements determined the smallest rotational speed of the stirrer at which all solid particles are in motion (not floating). During these experiments these two researchers proved that the critical Reynolds and Froude number exist and can be combined into a critical Froude number:

$$Fr_{crit} = \text{const} \cdot (\Delta\rho/\rho_p) \cdot (\delta/d)^{0.33} \cdot \varphi_s^{0.33}$$

Through a process of eliminating of small ratios with low exponent numbers $(\delta/d)^{0.33}$ and for a similar scale transfer $(\Delta\rho/\rho_p, \varphi_s = \text{idem})$, Zlokarnik and Judat concluded that the transfer rule for a flotation cell with an automatic stirrer with geometrically similar shape is given by

$$Fr \sim \omega^2 \cdot d = \text{idem}. \quad (25)$$

The discovery that in the turbulent flow range ($Re > 10^4$) the flow state in a solid/liquid system without air input can also be described by Froude's number alone was confirmed by Kneule and Weinspach with extensive measurements. Zlokarnic and Judat also proved that the output P as the $We = P/\rho_p \cdot \omega^3 \cdot d^5$, and $Ne = f(Fr)$ and $Q_a = f(Fr)$, results in $Ne = f(Q_a)$. This automatically implies that the transformation is:

$$Fr = \omega^2 \cdot d/g = \text{idem} \text{ and } Q_a = q_a/\omega \cdot d^3 = \text{idem}. \quad (26)$$

2.9.3. Technical stirring conclusions derived from the transformation criterion $Fr = \text{idem}$.

Now that Fr has been identified as the relevant transformation criteria for mechanically agitated machines based on the theory of similarity, the technical stirring aspects arising from it must be discussed.

2.9.3.1. Stirring output in cells with separate air intake.

Zlokarnik(1972) continued to prove that the power output in a mechanically agitated machine with separate air intake based on the Newton number is:

$$Ne = f(Q_a)$$

This was made possible by extending the relevance list in Equation (20) by adding the Newton number and then eliminating dimensionless numbers through the following arguments:

- Experiments have shown that a volume portion solid matter in liquid containing up to 25%-30% solids in suspension, the characteristic values of ρ_s/ρ_p , δ/d and φ_s are adequately considered if Newton number is formed not with the density of the liquid but with the density of the suspension.
- In the turbulent flow range $Re > 10^4$. The Reynolds number has no effect on the Newton number. Even the surface tension and thus the Weber number barely affects the Newton number.

This means that $Ne = f(Fr, Q_a)$ and for a scaled transformation according to $Fr = idem$ and $Q_a = idem$ then $Ne = idem$.

2.9.3.2. Stirring output and gas throughput with an automatic suction stirrer.

For automatic suction stirrers both the stirring output and the gas throughput are functions of the Froude number. But as Q_a is strongly influenced by the head of liquid above the stirrer then $Q_a = f(Fr \cdot d/H^*)$. Since both Ne and Q_a are functions of the Froude characteristic value then both these functions can be represented in the so-called parameter format $Ne = f(Q_a)$ which illustrates the parallels to string output with a separate air intake.

2.9.4. Stirrer volume related output and the criterion $Fr = idem$.

Even though it is based on fluid material systems liquid/liquid and liquid/gaseous, the constant volume related stirring output $P/V = constant$ is often invoked as a standard value for dimensioning stirring chemical processes. It should not be failed to be observed that this variable is particularly ill-suited for dimensioning flotation cells. It can be shown (Zlokarnik, 2006) that when applying the scaling transformation, then:

$$(P/Q_t)_{actual} = [(P/Q_t)_{model} \cdot (S_c)^{1/2}] \quad \text{Where } S_c = \text{scale factor.} \quad (27)$$

This is because the scale-up parameter for a stirrer is the Fr number and especially $Fr^{3/2}$ which equals $(P/Q_t) \cdot d^{0.75}$. Today's experience with flotation cells show that transformation scales exceed 1:10 ratios, and therefore does not support the requirement $P/Q_t = idem$. (Zlokarnic, 1972).

2.9.5. Interpretive data of a few flotation cells.

Zlokarnik(1972) compared the data of a few industrial designs to test how far these interpretative criteria fall from practical technology and concluded that these designs did

not maintain geometric similarity with a wide variation in Froude number and aeration number. Zlokarnik found that the Wemco design is largely based on:

$$P/Q_t = \text{idem or } \omega^3 \cdot d^2 = \text{idem}$$

2.9.6. Summary of Zlokarnik and Judat's work.

A consequent analysis of flow patterns in flotation cells with stirrer based on similarity was carried out by Zlokarnic and Judat. A comparison of the resulting relationships with the recent findings of mixing research lead to the scale-up conditions:

$Fr = \omega^2 \cdot d/g = \text{idem}$ and $Q_a = q_a / \omega \cdot d^3 = \text{idem}$. Identical materials and geometric similitude supposed.

Consequently, the stirrer has to be dimensioned according to $\omega^2 \cdot d = \text{idem}$ and not as previously on the basis of constant tip speed $v_t = \omega \cdot d$.

The air throughput has to be scaled up according to:

$$Q_a \cdot Fr^{1/2} = q_a \cdot (d^{2.5} \cdot g^{0.5}) \sim q_a / (A_c \cdot d^{1/2}) = \text{idem.} \quad (28)$$

Not as previously thought on the condition of constant surface throughput q_a/A_c . For the power input, these conditions $Fr, Q_a = \text{idem}$ have the consequence that in scale-up the power number $Ne = \rho_p \cdot \omega^3 \cdot d^5$ retains its numerical value. In the case of automatic suction stirrers, the condition $Fr = \text{idem}$ leads to $Q_a = \text{idem}$.

A further consequence of $Fr = \text{idem}$ as scale-up criteria is that the power per unit volume, P/Q_t increases with the square root of the scale.

Dimensional analysis either works or fails. When it works it gives good or bad results. When it gives good results, either the choice of variables is correct or the extra variables are eliminated. When it fails, it is either by logical contradiction (dimension of left hand side not equal to right hand side) or by insolubility, since extra variables bring more equations but not new dimensions (Ruzicka, 2008)

2.10. Flotation performance and dimensionless numbers.

Many publications are available on researchers such as Deglon et al. (1999; 2000) and Rodrigues et al. (2001), who produced very interesting results of flotation performance based on dimensionless numbers without performing dimensionless analysis or scale-up analysis, but have chosen these specific numbers based on their knowledge of the flotation process.

- Rodriques et al. (2001) probably produced the best evidence that recovery in a mechanically agitated flotation process is a function of Reynolds number, Froude number and power number. Rodriques's results were based on very small laboratory scale experiments with very low Reynolds numbers and power numbers. These results showed distinct maximums in recovery at Reynolds number = 10000, Froude number = 1 and power number > 0.55.
- Deglon et al. (2000) evaluated industrial machines in the South African platinum industry and also found a large variation in rotor tip Reynolds number, aeration numbers, power numbers and Froude numbers. Deglon et al. (2000) did not try to give an explanation for these large variations.
- Mavros (1992) suggested that these variations are functions of rotor aspect ratio, which is not considered in the determination of the power number and aeration number, and the large variations in rotor tip Reynolds number is a function of the ratio of particle size to tank diameter between designs.
- Newell and Grano (2006; 2007) found that the scale-up of the flotation rate constant can be achieved by maintaining a constant bubble surface area flux as well as maintaining $\omega^3 d$. A constant $\omega^3 d$ enable the measurement of mean energy dissipation (W/kg). The problem with these experiments is that they were all executed on relative small cells.
- Gorain et al. (1996) showed that a linear relationship exists between kinetic constant and bubble surface area flux and that it is independent of the type of impellor. This finding does have potential as a scale-up tool. Gorain et al. (1997) also developed very useful tools for bubble surface flux:

$$S_b = 134 (\cdot v_t)^{0.33} \cdot (J_g)^{0.75} \cdot (\dot{A}R_a)^{-0.12} \cdot (P_{80})^{-0.4}$$

Looking at experimental and predicted results then this model predicts very accurate results. These variables are also easy measureable factors.

2.11. Summary.

The results from this literature study can be summarized as follows:

- 2.11.1. Dimensionless analysis for scale-up in flotation is limited to a few authors, while the use of dimensionless numbers to describe flotation performance is more common.

2.11.2. While Deglon et al. (2000), Gorain et al. (1996), and Rodriques et al. (2001) concentrated on energy dissipation, rotor tip velocity and Reynolds number, Froude number, aeration and power number to prove a relationship between these variables and recovery or kinetic constant, only Zlokarnik (1972) attempted to derive the transformation number, for mechanism scale-up, with dimensional analysis.

2.11.3. Both Zlokarnic, Deglon et al. (2000) and Gorain et al. (1999), concluded that industrial designs, both external and self-aerated, do not comply with the basic Froude number as transformation scale-up number but rather a combination of Reynolds and Froude in the form: $Re \cdot Fr^{0.5} = idem$. For self-aerating machines the parameters $Q_a = idem$ and $Ne = idem$ also apply.

Interesting to note that the scale-up number $Re \cdot Fr^{0.5} = \rho_p \cdot \omega^3 \cdot d^5 / \mu_p \cdot \sqrt{g \cdot \omega \cdot D^{2.5}}$ is a special form of the power number.

2.11.4. Very little information is available on actual application and success of the scale-up numbers from pilot plant to full scale plant as well as the identification of deficiencies and prediction of improvements.

In the following chapter the author will perform a dimensional analysis with all the possible macro hydrodynamic variables and with the emphasis on a new transformation equation, a dimensionless kinetic constant and a schedule of dimensionless numbers as a simple tool for the plant metallurgist to analyze and identify deficiencies in his/her plant.

CHAPTER 3: DIMENSIONAL ANALYSIS OF A FLOTATION PROCESS.

3.1. Dimensional analysis.

In this analysis the flotation process will be divided into the following characteristic operations:

- Machine characteristics.
- Kinetic characteristics.
- Process characteristics.

During this analysis the author will endeavour to define the transformation numbers for machine scale-up, the kinetic model in dimensionless form for performance prediction and a schedule of dimensionless numbers to characterize the process with mechanical agitated machines.

Fundamentally, dimensional similitude, by way of the π -theory, offers the only means of dealing with problems that cannot be formulated mathematically and that two processes may be considered completely similar if they take place in similar geometrical space and if all the dimensionless numbers necessary to describe them, have the same numerical values (Zlokarnic, 1991). This fundamental approach forms the basis for the rest of this thesis.

From §2.5.3 the arguments state that if a variable y' , depends upon a number of independent variables $Q_1, Q_2, Q_3 \dots Q_n$, then they may be arranged in the following generic functional form:

$$y' = f_1(Q_1, Q_2, Q_3 \dots Q_n) \quad (29)$$

If all n variables can be expressed by m fundamental dimensional units, then they may be grouped in $(n-m)$ dimensionless π -terms. To compile these dimensionless groups for a froth flotation system, the variables indicated in Figure 3 and summarised in Table 6 were defined.

3.2. Relevance list and linear independence.

To compile the relevance list one must have a clear understanding of what one wants to achieve. This will help in identifying unwanted and unnecessary variables that will complicate the experimental setup. In this case the relevant list will include all the variables that can be identified and the rules for the selection of variables (§ 2.6.1) will be applied for each characteristic operation.

Table 6: Descriptive variables in mechanically agitated froth flotation systems.

Var	Description	Unit	Var	Description	Unit
	Machine Parameters			Process Parameters	
P	Power	kW	q_p	Volume Feed rate	m^3/s
ω	Rotor rotational speed	rad/s	P_{80}	Screen size@80% pass	m
q_a	Aeration rate	m^3/s	F_d	Froth depth	m
q_c	Machine circulation	m^3/s	η	Conditioning time	min
D	Cell diameter	m	σ	Surface tension	N/m
H	Cell height	m	ξ	Froth retention time	min
h	Rotor submergence	m	ρ_p	Pulp density	kg/m^3
b	Rotor height	m	μ_p	Pulp viscosity	kg/ms
d	Rotor diameter	m	θ	Conditioner tank turn around	min^{-1}
	Process Parameters			Constants	
S_g	Material specific gravity	-	k	Kinetic constant	min^{-1}
T	Retention time	s	g	Gravity	m/s^2

3.3. Buckingham π -Theorem based on repeating variables.

To describe the system shown in Figure 3 in terms of dimensionless numbers the following steps should be followed:

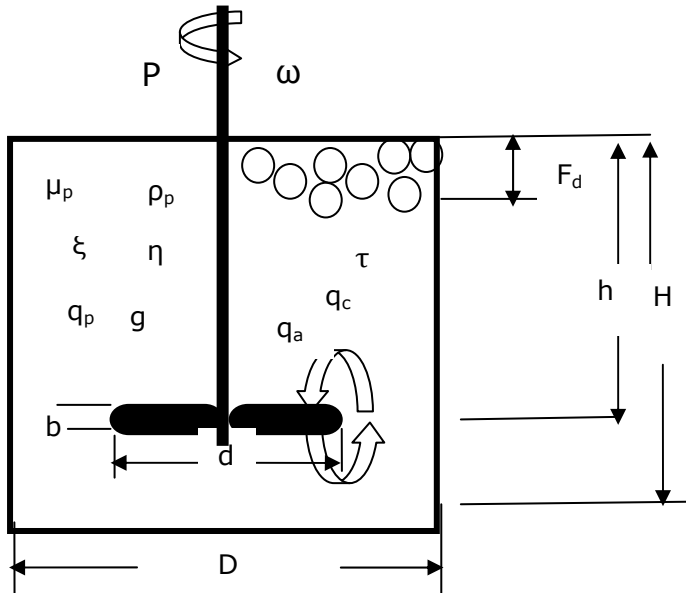


Figure 3: The model of a flotation cell with all the variables identified.

Step 1: List all relevant variables. (See Table 6)

Step 2: Choose three repeating variables.

Three, because there are three fundamental dimensions, viz. mass, distance and time, $m = 3$. In this case it was decided on $\rho_p =$ Pulp density, $[\text{kg}/\text{m}^3]$, $\omega =$ Rotor rotational speed (s^{-1}) and $D =$ Cell diameter $[\text{m}]$.

Step 3: Create a dimensionless π -group by adding a fourth variable and adding exponents to the repeating variables and equate to 1.

$$\pi_1 = \rho_p^x \cdot \omega^y \cdot D^z \cdot \mu_p = 1 \quad (30)$$

Step 4: Decompose Equation (3) into its basic dimensions.

$$\pi_1 = [M/L^3]^x [1/T]^y [L]^z [M/LT] = 1 \quad (31)$$

Step 5: For the π -number to be equal to 1, then the exponents associated with each fundamental dimension must be equal to zero. Therefore, generate three algebraic equations by comparing basic dimensions and equate to zero:

$$\text{For M : } x+1 = 0 \quad 31(a)$$

$$\text{For L : } -3x+z-1 = 0 \quad 31(b)$$

$$\text{For T : } -y-1 = 0 \quad 31(c)$$

Solve Equation (a), (b) and (c) for exponents x, y and z:

$$x = -1, y = -1 \text{ and } z = -2$$

Step 6: Substitute back into (30).

$$\pi_1 = \mu_p / (\rho_p \cdot \omega \cdot D^2) \quad (32)$$

As the group is dimensionless, it is allowable to invert the group, so:

$$\pi_1 = (\rho_p \cdot \omega \cdot D^2) / \mu_p \quad (33)$$

Equation 33 is the well-known Reynolds number.

Step 7: Repeat for all variables and group into geometrical (geometry), kinematic (velocity), and dynamic (force) groups. This gives the following list of dimensionless groups for a flotation cell.

Geometrical groups.

$$\pi_1 = \text{Diameter ratio (DR}_a) = d/D.$$

$$\pi_2 = \text{Relative particle size (}\check{R}p_s) = P_{80}/D.$$

$$\pi_3 = \text{Tank slenderness ratio (T}_a\text{SR}_a) = H/D.$$

$$\pi_4 = \text{Relative froth depth (}\check{R}F_d) = F_d/D.$$

$$\pi_5 = \text{Submergence ratio (Su) = } h / D.$$

$$\pi_6 = \text{Rotor height (R}_h) = b/D.$$

Kinematic groups.

$$\pi_7 = \text{Aeration number (A}_e\text{N) = } q_a / \omega D^3.$$

$$\pi_8 = \text{Circulation number (CN) = } q_c / \omega D^3.$$

$$\pi_9 = \text{Dimensionless Conditioning time (C}_{oT}) = \omega \eta.$$

$$\pi_{10} = \text{Conditioner tank turn around (}\theta) = \theta / \omega.$$

$$\pi_{11} = \text{Dimensionless Froth retention time (F}_{RT}) = \omega \xi.$$

$$\pi_{12} = \text{Superficial Reynolds number (Re}_s) = \rho_p \omega D^2 / \mu_p.$$

$$\pi_{13} = \text{Froude No (Fr) = } \omega^2 D / g.$$

Dynamic groups.

$$\pi_{14} = \text{Tank power number } (T_a PNo) = P/(\rho_p \omega^3 D^5).$$

$$\pi_{15} = \text{Weber number } (We) = \rho_p \omega^2 d^3 / \sigma.$$

3.4. Combination of some groups.

The Buckingham π -theory allows one to multiply and divide groups with each other to generate new groups that might be more tangible and easier to compare or interpret, although the original number still stays the scale-up number.

3.4.1. Volumetric ratio (VR_a).

$$\begin{aligned} \pi_{16} &= VR = \pi_1^{-1} \cdot \pi_3^{-1} \cdot \pi_5^{-1} \\ &= D^3/d \cdot h \cdot H \end{aligned} \quad (34)$$

3.4.2. Rotor Tank volume ratio ($\acute{R}T_a VR_a$).

$$\begin{aligned} \pi_{17} &= \pi_1^2 \cdot \pi_3 \cdot \pi_6^{-1} \\ &= d^2 \cdot b / D^2 \cdot H \end{aligned} \quad (35)$$

3.4.3. Rotor tip Reynolds number (Re_t).

$$\begin{aligned} \pi_{18} &= \pi_{11} \cdot \pi_1^2 \\ &= \rho_p \cdot \omega \cdot d^2 / \mu_p \end{aligned} \quad (36)$$

3.5. Dimensionless numbers and transformation equations.

The relevant function for the transformation equation for stirrers with separate and automatic air intake from Equation (23) and (24) is:

$$f_{t1}(Re_t, Fr, We, A_e N, \check{r}p_s) = 0 \quad (37)$$

From Chapter 2 the term P_{80}/D can be neglected as being very small and the Weber number can be replaced by a simple relationship between Re and Fr according to Equation (19). Therefore:

$$f_{t2}(Re_t, Fr, Q_a) = 0 \quad (38)$$

Accept for $Q_a = idem$ it is clear from Table 7 that the transformation equation does not follow the scale-up equation $(Re, Fr) = idem$, but more like:

$$f_{t3}(Re_t, Fr, \dot{A}R_a, G) = 0 \quad (39)$$

Where G represents the ratio between full scale plant P_{80} and tank diameter and pilot plant P_{80} and tank diameter. A comparison of industrial designs are shown in Table 7.

Table 7: Comparison of transformation equation for industrial installations.

Machine	Dim.	Denver PP	Wemco 21m ³	Metso 20m ³	O/K 20m ³	BQR 50m ³	O/K 130m ³
Mineral processed	NA	Phos.	Phos.	PGM UG2	PGM UG2	PGM UG2	PGM Mer
Tank Volume	M ³	0.08	20	20	20	50	130
Tank Diameter	m	0.43	3.6	3.25	3.2	4.3	6
Tank Height	m	0.41	2.4	3	3.45	4.2	5.2
Submergence	m	0.25	0.3	2	2.45	2.7	3.7
Rotor Diameter	m	0.22	0.76	0.79	0.75	0.99	1.3
Rotor Height	m	0.03	0.76	0.54	0.47	0.645	1.23
RPM	r/s	90	18.5	18	19.3	14	10.3
(FSP) _{p80} :(PP) _{p80}	μm	250:250	350:250	150:100	150:100	150:100	150:100
Circulation	m ³ /s	0.003	0.53	1.1	1.16	2.7	3.5
Aeration	m ³ /s	0.0006	0.1	0.167	0.116	0.167	0.33
Power	kW	0.56	60	55	65	110	144
Re _t	-	1.75E6	4.6E6	4.36E6	4.2E6	5.34E6	6.77E6
Fr _D	-	45.5	6.7	6.5	7.1	4.95	3.5
Fr* = Re _t · (Fr _D) ^{0.25} (10 ⁶)	-	4.5	9.2	7	6.8	8	9.26
Fr* · $\dot{A}R_a^{-0.2}$ · G ^{0.45} (10 ⁶)	-	3.1	3.3	3.4	3.3	3.4	3.4

According to the result in Table 7 the transformation Fr=idem was not followed and even though the application was for the same mineral, it seems that the designs complied to a combination of Re_t, Fr^{0.25}, $\dot{A}R_a^{-0.2}$ and G^{0.45}. It seems that the designs average around Fr_{RGA} = Re_t · Fr^{0.25} · G^{0.45} · $\dot{A}R_a^{-0.2}$ = 3.5x10⁶. Here again the Wemco design did not follow the theoretical transformation equation of Fr=idem but also Fr_{RGA} = idem. In Table 7 the designs, from the different suppliers, different sizes and different minerals, followed

(Fr_{RGA}) = 3.5×10^6 and in Table 8 from the same supplier, different sizes but same mineral, it followed the same Fr_{RGA} .

Table 8: Showing a comparison between different machine sizes for the Wemco design.

Size (m ³)	PP	8.5	21	42
D (m)	0.22	0.67	0.76	1.09
$\dot{A}R_a$	7	1.4	1	1
ω (r/s)	90	23	19	13
(FSP) _{P80} (PP) _{P80} (μm)	250:250	350:250	310:250	350:250
D (m)	0.43	2.9	3.6	4.2
$Re_t(10^6)$	1.75	4.2	4.6	6.25
Fr_D	45.5	9.1	6.7	4.8
$Fr^* \cdot G^{0.45} \cdot \dot{A}R_a^{-0.2}(10^6)$	3.1	3.7	3.3	3.9

3.6. Dimensionless kinetic constant.

The kinetic constant in Equation (1) can be rewritten as:

$$k = f_3(VR_a, \dot{A}T_a VR_a, A_e N, CN, T, \theta, Fr_D, Re_s, \check{R}F_d, \dot{A}PN_o, Re_t, \check{R}p_s). \quad (40)$$

According to Gorain et al.(1999) the kinetic constant $k = F_p \cdot S_b \cdot R_f$.

Where: F_p = Floatability parameter, S_b is the bubble surface area flux, R_f the froth recovery factor.

For this reason the kinetic constant will be replaced by the three target numbers that constitute the kinetic constant.

3.6.1. Empirical prediction model for kinetic constant in mechanically agitated flotation machines based on dimensionless numbers: Model development and construction.

Various empirical models have been developed for F_p , S_b and R_f (AMAIR P9L, Vol 2) with varying levels of success, as these models always entail the estimation of some constant.

3.6.1.4. Froth recovery factor.

To develop the froth recovery factor (R_f) the same reasoning is followed in that R_f is:

- Inversely dependent on volumetric ratio: The bigger the volumetric ratio means that the rotor is smaller and is positioned higher up in the tank closer to the froth zone.
- Inversely dependent on rotor tip Reynolds number: The higher the Reynolds number, the higher the agitation and therefore a higher probability of disturbing the froth zone resulting in increased drainage.
- Inversely dependent on froth depth: The bigger the froth depth means longer froth retention time with higher probability for particle drainage.
- Directly dependent on air dispersion: Higher aeration represents higher superficial gas velocity which means shorter froth retention time with less change of losing the recovered particle.

Based on above reasoning, the following equation applies:

$$R_f = f_6 (VR_a, A_e N, \check{R}F_d, Re_{t,r}) \quad (41)$$

From Marco Vera's paper on "Methodology for the froth Zone Recovery determination" in the AMIRA P9L report 1999, a mass balance between feed, tails, concentrate, collection zone and froth zone, produced the following equation for the froth recovery factor:

$$R_f = [1 - (\check{R}F_d / \{\check{R}F_d\}_{k=0})] \quad (42)$$

Applying this to the present production statistics of a phosphate mine, the range of R_f was calculated on average to be between 0.6 - 0.88 over 5 to 8 number of cells. The absence of a drainage factor made equation (42) insensitive to disturbances of the quiet and froth zone.

From Barun Gorain's paper on "The calculation of Froth Recovery from k-S_b Data" in the AMIRA P9L project report 1999, the froth recovery factor for external aerated and self aerated machines based on froth residence time, is equal to:

$$R_f = i \cdot e^{j\tau_g} \quad (43)$$

Combining (41) and (43) and the results of the phosphate plant and through a process of trial and error, resulted in R_f in dimensionless terms:

$$R_f = 1.1 \cdot e^{-(\Delta\xi)} \quad (44)$$

Where:

$$\Delta = [(Re_t)^{0.2} \cdot (VR_a)^{0.1}]/1000 \quad \text{and} \quad \xi = [\check{R}F_d \cdot 1000]^{0.6} \cdot (A_e N)^{-0.2}.$$

In the above equation the factor Δ represents the drainage component and ξ represents the dimensionless froth residence time. The volumetric ratio fixes the position of the rotor in the tank while the Reynolds number represents the agitation level. The combined effect impacts on the stability of the quiet and froth zones.

3.1.1.1.1. Validation of froth recovery factor.

To validate the froth recovery factor the constants α and β are compared with the results of the Scuddles test results in the AMIRA P9I project.

Table 9: Comparing the constants i and j with the AMIRA P9L results.

Constant	AMIRA P9 Scuddles	This Thesis
i	0.25	1.1
j	0.012-0.26	0.02-0.032
R_f^*	0.5-0.7	0.6-0.66

*Phosphate

The AMIRA results seem to have a higher upper and lower limit for 'j' but a lower value for 'i'. The reason is probably that the AMIRA model utilises a "specific" froth retention time while this thesis utilises a "dimensionless" froth retention time. Values calculated for R_f seem to correspond well.

3.6.1.3. The bubble surface flux.

Gorain et al.(1999) developed a very elegant model for bubble surface flux:

$$S_b = 134(v_t)^{0.33} \cdot (J_g)^{0.75} \cdot (\check{A}R_a)^{-0.02} \cdot (P_{80})^{-0.4} \quad (45)$$

This model does not exhibit a maximum as demonstrated by Vera et al. (1999) who showed that:

$$S_b = S_{bmax} \cdot \alpha \cdot \beta \cdot j_g^{\beta-1} \cdot e^{j_g^\beta} \quad (46)$$

Where $0 < \alpha < 1$ and $1 < \beta < 4$.

The first step is to rewrite Equation (46) in dimensionless form by replacing J_g with the equivalent dimensionless number. By adding J_g to the relevant list will result in an additional dimensionless number.

$$\pi_x = J_g/\omega \cdot D \quad (47)$$

Replacing J_g in Equation (47) with q_a/D^2 results in:

$$\pi_x = q_a/\omega \cdot D^3 \quad (48)$$

Equation (48) is the aeration number based on tank diameter and to a certain extent it also represents the air hold-up. The next step is to find a suitable replacement for S_{bmax} in Equation (46). By studying the work done by Degner and Treweek (1976) and Nelson and Lelinsky (2000), it is evident that self aerating designs, such as the Wemco machine, exhibit some threshold rotational speed at which the circulation increases marginally while the aeration increases almost exponentially (Figure 4). Apparently this is the point where the air starts to replace so much pulp in the rotor that an increase in rotational speed does not result in an increase in circulation.

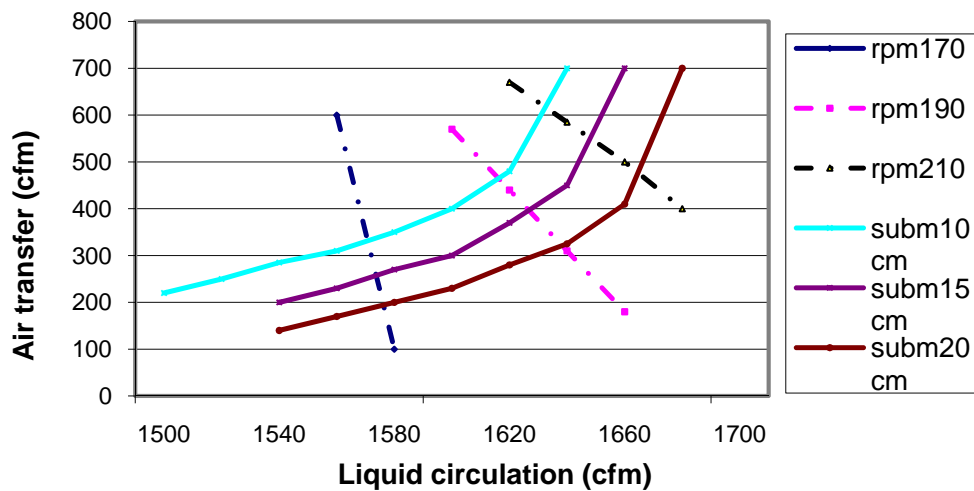


Figure 4: Showing the exponential increase of aeration with RPM for the Wemco machine.

From Degner and Treweek (1976) the circulation is equal to:

$$Q_a = d^x \text{Ln } \omega \quad (49)$$

$$\therefore \frac{\partial^2 Q_a}{\partial \omega^2} > 1 \text{ (For } Q_a \text{ to exhibit a maximum).}$$

$$\therefore \frac{-d^{x'}}{\partial \omega^2} > 1 \text{ (For } Q_a \text{ to exhibit a maximum).}$$

From Figure 4 the critical rotational speed is equal to:

$$\therefore \omega_c \geq \frac{14}{\sqrt{d^{2.4}}} \quad (50)$$

This is similar to the model for critical speed for rotating equipment where:

$$N_c = \frac{188}{\sqrt{y''}} \text{ where } y'' = \text{some maximum deflection.}$$

Equation (51) and (52) were fitted to the Wemco information in figure 4.

$$q_a = \frac{1.25d^3}{\sqrt[3]{h \cdot \dot{A}R_a}} \cdot \left(\frac{\rho_w}{\rho_p}\right)^2 \cdot \left(\frac{\omega}{\omega_c}\right) \cdot (1 - 0.588d) \quad (51)$$

Where h = submergence, and:

$$q_c = \frac{856 \cdot h}{\rho_p \cdot \dot{A}R_a^2} \cdot d^{2.4-n'} \cdot \text{Ln } \omega \quad (52)$$

where $n' = 0.85$ for $d < 0.76$ and $n' = 0$ for $d > 0.76\text{m}$.

From the work done by Vera et al. (1999) it seems that the maximum occurs at $J_g \sim 1$ cm/s. For the 100^3 O/K machine in Gorain et al.'s (1999) test work at Broken Hill concentrator with $J_g=1$ cm/s, requires a $q_a = 0.245$ m³/s and with $J_g = 2$ requires a $q_a = 0.59$ m³/s. From Equation (51) this will correspond with $\omega = 22\text{r/s}$. Thus for maximum S_b , the following variables are substituted in Equation (45):

$$v_t = 15 \text{ m/s.}$$

$$J_g = 1 \text{ or } 2 \text{ cm/s.}$$

$$\dot{A}R_a = 1.$$

$$P_{80} = 75\mu\text{m or } 100\mu\text{m.}$$

The maximum for an external aerated machine is calculated by selecting an equivalent self aerating machine, with the same dimensions and then determine the rotational speed that will produce the required aeration rate according to Equation (50) and (51).

The reason for utilising Equation (45) is because it corresponds very well with measured results according to the AMIRA P9L reports. Based on the above reasoning, the following equation was developed for external aerated machines:

$$S_b = 1.07 \times 10^{-6} \cdot S_{b\max} \cdot \left(Re_t^{1.1} \cdot \frac{\dot{R}_{ps}^{-0.5}}{2} \right) \cdot \left[(\dot{R}_T V R_a)^{0.25} \cdot (\dot{A} R_a)^{-0.02} \right] \cdot (A_e N)^{0.85} \cdot e^{-\alpha (A_e N \cdot 9 \times 10^3)^\beta} \quad (53)$$

For self aerating machines the equation becomes:

$$S_b = 0.012 \cdot S_{b\max} \cdot \left(Re_t^2 \cdot \frac{\dot{R}_{ps}^{-0.5}}{2} \right) \cdot \left([\dot{R}_T V R_a]^{0.25} \cdot \dot{A} R_a^{-0.02} \right) \cdot (A_e N)^{0.85} \cdot e^{-\alpha (A_e N \cdot 9 \times 10^3)^\beta} \quad (54)$$

3.1.1.1.2. Validation of bubble surface area flux.

A comparison of Equation (53) and (54) with Equation (45) based on the same Pasmenco Mining Broken Hill Concentrator results, on which Gorain et al. (1999) developed the constants and exponents for Equation (45), is given in Figure 5 & 6.

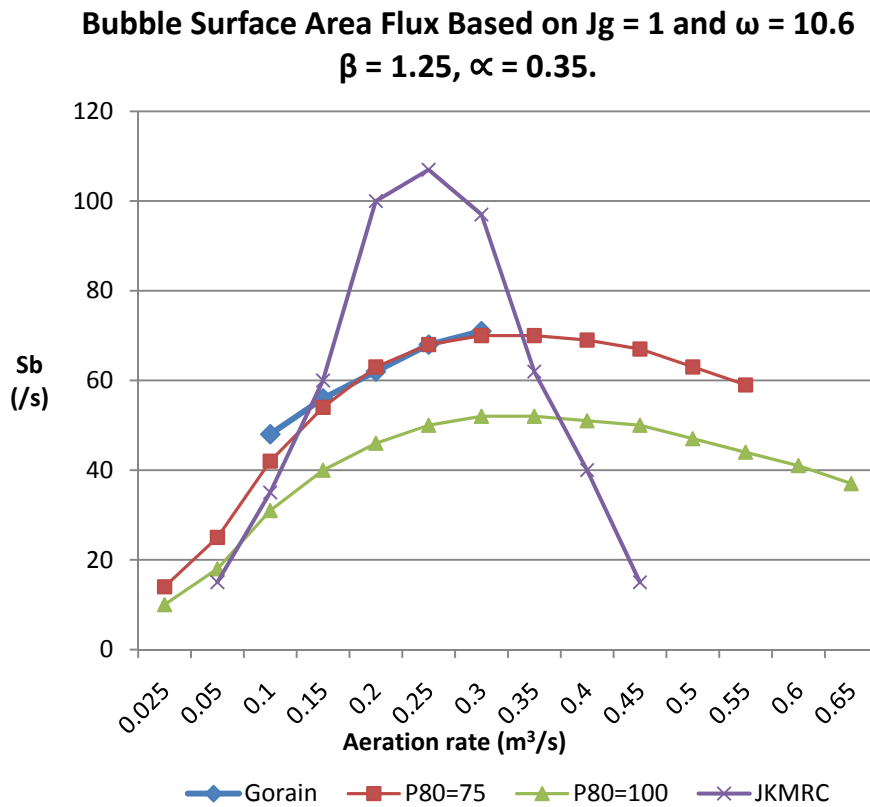


Figure 5: Bubble surface area flux as a function of aeration rate.

In Equation (53) and (54) the terms $Re_t \cdot VR_a$ represent the bubble break-up mechanism, while the other terms represent the aeration component. It is interesting to note that the aspect ratio in Equation (45) has been replaced by the volumetric ratio and P_{80} by Reynolds number. In this case the VR_a can be manipulated by multiplying the VR_a with b/D which results in $VR_a = (D^2 / \dot{A} R_a \cdot h \cdot H)$. In the results of Gorain et al. (1999) on the Pasmenco concentrator the superficial gas velocity was measured as $J_g \sim 2$ cm/s and $P_{80} = 100 \mu m$, and Figure 6 therefore is the best comparison. Figure 7 shows that the dimensionless model predicts a lower kinetic constant at higher bubble surface area flux

compared with Gorain et al. and it may have something to do with the way the floatability parameter is constructed in handling particle size.

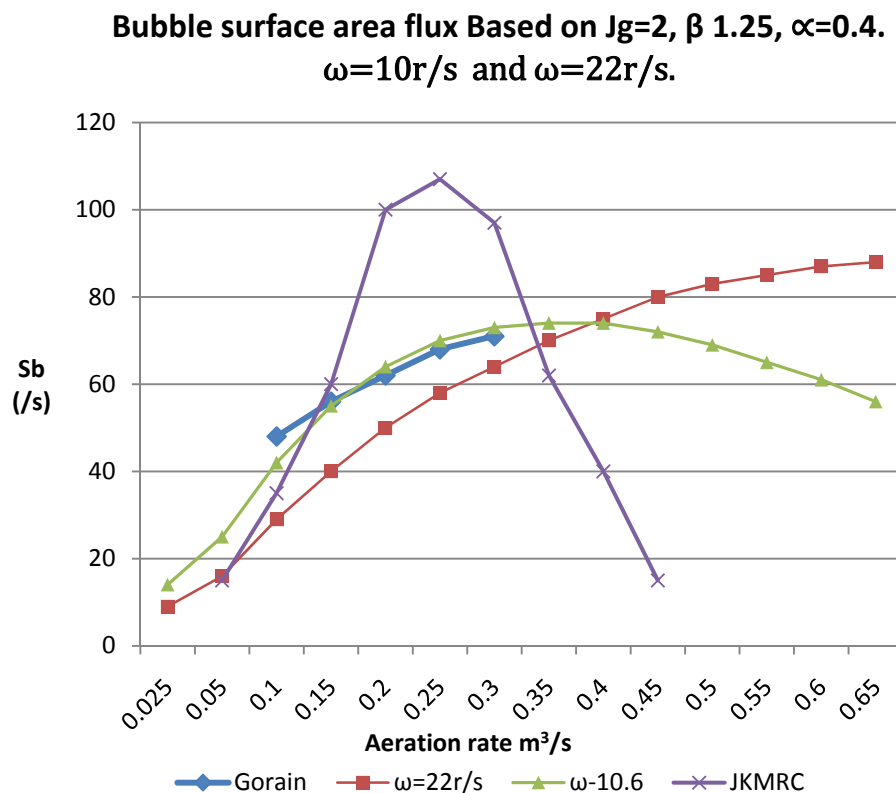


Figure 6: New bubble surface flux model with $P_{80} = 100\mu m$.

3.6.1.1. Floatability parameter.

Gorain et al. (1997) showed that there is a linear relationship between the kinetic constant and bubble surface area flux for different particle sizes and that the slope of this model represents the floatability parameter.

$$F_p = k/S_b \tag{55}$$

Deglon et al. (1998) proved by combining attachment and de-attachment rate constant models with a bubble population balance model that the kinetic constant is not linearly dependent on bubble surface area flux but rather that it exhibits a maximum.

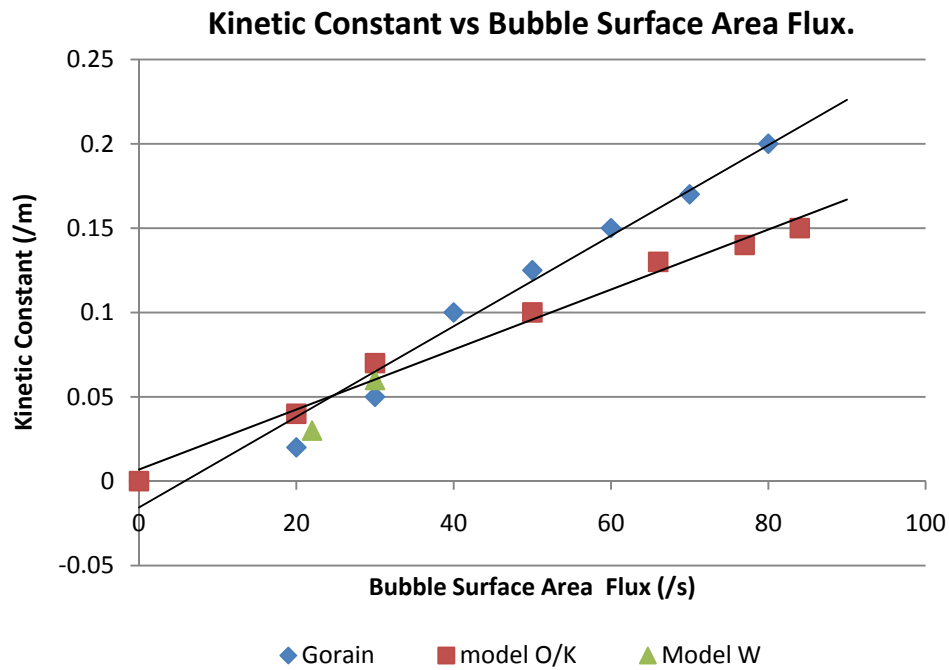


Figure 7: Comparison between the results obtained by Gorain and the dimensionless model.

Deglon et al. (1998) proposed:

$$k = \frac{k_a}{1 + k_d \tau_g} \quad (56)$$

where

$$k_a = f(\epsilon^{0.91}) \quad (57)$$

and

$$k_d = f(\epsilon^{1.64}) \quad (58)$$

Deglon's approach, where the kinetic constant and therefore floatability is a function of energy dissipation rate, is more in line with the reasoning that floatability is a function of mineral and machine properties, therefore the floatability parameter is:

- Inversely dependent on particle size: The bigger the particle the more difficult it is to suspend.
- Directly dependent on circulation and Froude number: The higher the pumpability the better the chance of exceeding the settling velocity. Analysing the power number resulted in a special combination of the rotor tip Reynolds number and Froude.

- Directly dependent on rotor tip Reynolds number or agitation.
- Directly dependent on conditioning time and tank turn around: Surface preparation.
- Directly dependent on volumetric ratio: The lower the rotor in the tank the better the ability to suspend.

Therefore:

$$F_p = f_4 (VR_a, Fr, CN, C_oT, \theta, Re_t, \check{R}p_s) \quad (59)$$

Kym Runge (AMIRA P9L report, 1999) reported in her paper on the "Conservation of Floatability around Industrial Flotation Cells", based on size-mineralogical-liberation classes, that the overall circuit can also be treated as a node. In circuits where no reagent addition and regrinding occurred, Runge stated that ore floatability was a conserved property and did not change significantly during the residence time in the flotation circuit. Runge, Harris and Savassi used a reverse calculation method based on equation (1) and equation (62). By measuring variables such as bubble surface area flux, froth depth, superficial gas velocity, particle sizes, entrainment parameters, froth recovery factor, overall recovery, feed rates and cell dimensions, the overall kinetic constant is estimated based on equation (1). With the kinetic constant known the estimation of floatability parameter is based equation (62). With Barun Gorains's results from the Mount Isa copper process, equation (59) and through a process of trial and error, the following model was established:

$$F_p = 2 \cdot 10^{-11} \cdot [\{\check{R}p_s\}^{-0.2} \{VR_a\}^{-0.01} \{Re_t\}^{0.5} \{CN \cdot Fr\}^{0.5} \{\eta \cdot \theta\}^{0.2}]^{0.37} \quad (60)$$

In equation (60) the tip Reynolds number represents the bubble generator while the tip Reynolds number combined with the volumetric ratio represents the drainage factor. The circulation number and Froude number represents solid suspension while the conditioning parameters θ and η represents the surface preparation entrainment factor

This model seems to hold for external aerated and self aerating machines.

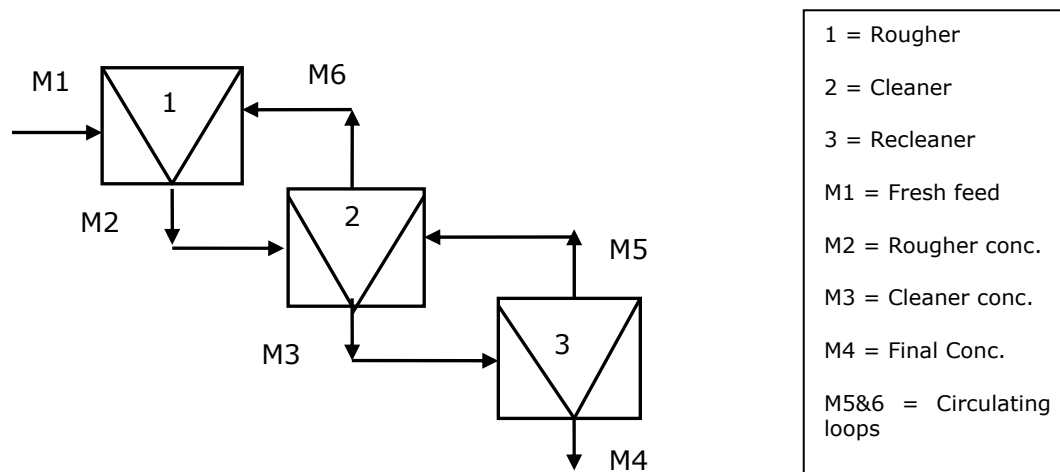
3.6.1.2. Validation of floatability parameter.

No specific tests have been performed to produce data of floatability but the AMIRA P9L test results for galena and various other minerals and for different particle size and feed rates seems to concentrate around 1×10^{-4} while the floatability parameter based on dimensionless numbers according to Equation (60), for nickel and phosphate, vary between 1×10^{-4} to 5×10^{-5} .

3.6.1.3. Dimensionless kinetic constant.

3.6.1.3.1. Effect of Volumetric Capacity.

The volumetric capacity is the ratio of cleaner and recleaner volumes to rougher and scavenger volumes. The change in performance of the cleaner and recleaner circuit influences the circulating load and grade of material returning to the rougher and scavenger circuit.



- Any additional capacity reduces circulating load and therefore increases retention time, which in turn will increase recovery.
- If the removal of additional mass is because of an improvement in the kinetic activity, of the cleaners and recleaners, then the removal of more product from the circuit will impact on the upgrading of the head grade to the first rougher which will reduce the probability of collision and in turn will reduce the kinetic constant in the roughers. At the same time it will increase the overall kinetic constant by increasing the total recovery.
- Referring to Figure 8, the effect of an increase in volumetric capacity results in the modification of rougher or cleaner retention time at steady state as follows:

$$T_{\text{Rougher}} = \text{Rougher Tank Volume}/(M1 + M6) \quad (61a)$$

$$T_{\text{Cleaner}} = \text{Cleaner Tank Volume}/(M2 + M5) \quad (61b)$$

$$T_{\text{Recleaner}} = \text{Recleaner Tank Volume}/(M3) \quad (61c)$$

- To determine the volume of the circulating loads require a good mass balance which will also require the hydrodynamics of roughers, cleaners and recleaners such that:

$$M2 = (M1 + M6) \cdot [(1 - e^{-kT})]_{\text{Roughers \& Scavenger}} \quad (61d)$$

And

$$M3 = (M2 + M5) \cdot (1 - e^{-kT})_{\text{Cleaners}} \quad (61e)$$

And

$$M4 = M3 \cdot (1 - e^{kT})_{\text{Recleaners}} \quad (61f)$$

- From Equations (61d) to (61f) it is clear that these equations are all interconnected and that Equation (60), (53), (54) and (44) must be analysed to determine the impact on the overall kinetic constant.

From the mass balance in Figure 8 the overall recovery is therefore defined as:

$$R = R_m [1 - (e^{kT})_{\text{Roughers}} - (e^{kT})_{\text{Cleaner}} - (e^{kT})_{\text{Recleaners}}] \quad (61g)$$

3.6.1.3.2. Adjusted kinetic constant.

To accommodate the cleaner and recleaner components the overall kinetic constant according to Equation (40) is now defined as:

$$|k| = (F_p \cdot S_b \cdot R_f) \quad (62a)$$

To provide for the interlocking of kinetic constant and volumetric capacity according to Equation (61a) to (61g) the following modification of Equation (62) is proposed.

$$|k'| = |k| \cdot 6.5 \cdot (VC)^{0.28} \quad (62b)$$

3.6.1.3.3. Validation of dimensionless kinetic constant.

Equations (62a) and (62b) have been calibrated utilising available practical results from a nickel plant and a phosphate plant. The author utilised these equations in optimizing and maximizing a nickel (Table 10) plant and to compare four different streams at the phosphate plant (Table 11) to determine which one is lacking in kinetic activity, with a high degree of success. As both these plants utilised self aerating machines, the kinetic constant and recovery were calculated by:

- Varying the plant throughput and calculating particle size by utilizing Bond Working Index.

- Estimated retention time by dividing Q_t/q_p .
- Calculate froth recovery factor, bubble surface area flux and floatability by utilizing Equations (44), (53), 54 and (60).
- Estimated k and k' by Equation (62a) and (62b).
- Estimated recovery by utilizing Equation (1).

The dimensionless floatability parameter and bubble surface area flux change with particle size as expected. Aeration and froth depth were kept constant and therefore the dimensionless froth recovery factor remained constant. In this experiment the maximum nickel units coincided with 55 tph, but as a 40% loss of product was not acceptable the plant was set at 40-45 tph.

Table 10: A comparison between measured and predicted recoveries for a nickel plant.

Feed tph	$P_{80}(\mu\text{m})$ Calculate	$S_b (s^{-1})$ Model	F_p Model	R_f Model	k' min^{-1}	τ min	R (%) Model	R (%) Actual
35	130	45	9×10^{-4}	0.565	0.081	52	82	82
45	201	35	8.7×10^{-4}	0.564	0.061	42	72	73
55	282	28	8.3×10^{-4}	0.562	0.046	34	65	62
65	370	23	8×10^{-4}	0.562	0.036	26	50	49

The phosphate plant also utilised self aerating machines installed in three banks to process three different mineral combinations. The modified E-bank was an actual improved installation where the improvements were suggested and implemented after analysing plant deficiencies by utilising the schedule of dimensionless numbers. The predicted recovery was calculated by utilising Equations (44) to (60) and (62b) and (1). Although extension-8 performed better than the original E-bank and F-bank, Table 11 shows clearly that something was drastically wrong with its kinetic activity. The dimensionless model showed that the problem lies with aeration, bubble surface flux, Froude number and volumetric ratio.

Equation 40-62 need to be calibrated and refined with every application as a result of unusual modifications experienced in certain plants. Small flotation machines would be fitted with the next size rotor modified to operate within the installed power and these secondary changes are not covered by equations 40-62.

Table 11: The kinetic deficiencies between the different phosphate streams.

Plant	PP	E-Bank (O)	Ext-8	F-bank	E-Bank (M)
Feed (Tph)	0.5	600	600	1200	480
Pulp specific gravity	1.4	1.35	1.35	1.4	1.35
Rougher & Scavenger Volume (m ³)	0.4	336	672	544	336
Retention time (min)*	19	12	28	10	12
Actual recovery (%)	95	72	75	55	83
Overall kinetic constant (/min)	0.35	0.16	0.055	0.09	0.18
Predicted recovery (%)	94	0.79	71	53	83
Predicted kinetic constant (/min)	0.22	0.15	0.055	0.082	0.18

(*Assumed 65% circulating load, except for pilot plant where circulating load is 50%).

3.7. Characterization of plant deficiencies based on a schedule of dimensionless numbers.

This methodology has been developed to facilitate the plant metallurgist to analyse for deficiencies and to decide on what steps to take to improve performance based on dimensionless numbers. A demonstration of the application of this schedule is demonstrated in Chapters 5 & 6.

Table 12 shows the dimensionless numbers which have been selected to populate the schedule. These numbers have been selected on the bases of practicality and in a certain sense it is a reflection of all the variables of the kinetic constant.

3.7.1. Dimensionless parameters influencing flotation.

3.7.1.1. Dimensionless numbers and field of influence.

Table 12 shows the dimensionless groups which represents the most important and easy measurable groups. This section describes the methods of determining the numerical values and highlights the pitfalls and difficulties in determining these numbers.

3.7.1.2. Fundamental zones in flotation and dimensionless groups.

Mavros (1992) suggested that a flotation machine can be divided into three very distinct zones, viz. the agitation zone, the quiet zone, and the froth zone and that each of these zones has a very specific requirement in terms of turbulence.

Each zone has a specific function in the flotation process and therefore specific requirements and each zone has been characterized in terms of dimensionless numbers.

3.7.1.2.1. Agitation Zone.

This is the zone where solid particles are kept in suspension and the air is dispersed into small bubbles. Here intense blending between solids, chemicals, liquid and air take place. This is also the region where the bubbles and mineral are trapped for a sufficiently long period in a highly turbulent and agitated environment to enhance the probability of collision and selective attachment of minerals to bubbles (Yoon, 2000). To ensure that this occurs without disruption of the separation zone, the rotor must be low enough in the flotation cell and the rotor aspect ratio must be of a certain size. There are specific conditions that must be met to ensure sufficient agitation and power and to enable the machine to create a hydrodynamic barrier between these two zones automatically.

The requirements for the agitation zone in terms of turbulence and rotor position is:

Rotor tip Reynolds number $4 \times 10^6 < Re_t < 7 \times 10^6$ and Volumetric ratio $4 < D^3/dhH < 10$. These numbers have been obtained from industrial machines operating successfully.

Table 12: Dimensionless parameters and field of influence on flotation.

PI NO.	Dimensionless parameter	Dimensionless Group	Field of influence
π_1	Relative particle size*	P_{80}/D	Grind and Solid suspension
π_4	Relative froth depth	F_d/D	Froth recovery and concentrate grade
π_8	Aeration number	$q_a/\omega d^3$	Gas hold-up and bubble surface area flux
π_9	Circulation number	$q_c/\omega d^3$	Solid suspension
π_{10}	Conditioning time*	$\omega\eta$	Hydrophobicity and floatability
π_{11}	Froth retention time*	$\omega\xi$	Drainage
π_{12}	Conditioner tank turn around	θ/ω	Hydrophobicity and floatability
π_{13}	Tank Power number*	$P/\rho_p\omega^3D^5$	Solid suspension
π_{14}	Volumetric ratio*	D^3/dhH	Relative position of rotor in
π_{15}	Rotor tank volume ratio*	d^2e/D^2H	Relative size if rotor
π_{16}	Rotor tip Reynolds number	$\rho_p\omega d^2/\mu_p$	Agitation level.
π_x	Froude number Fr_{RGA}^*	$Re_t Fr_D^{0.25} G^{0.45} AR^{-0.2}$	Transformation number

High agitation requires high rotor tip velocity and it will be shown later that this is also a requirement for good bubble formation and bubble surface flux. Schubert and Bischofberger, (1998) concluded that micro-processes are turbulence driven and that this happens in the turbulent stream behind the rotor.

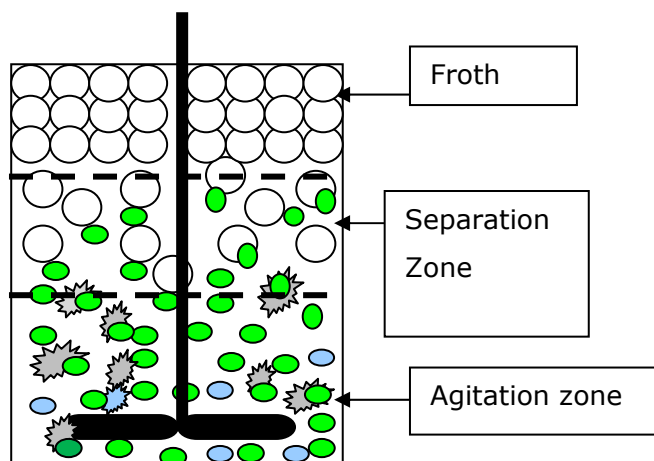


Figure 9: The classical model with the different macro-zones for a flotation machine.

Rodrigues et al. (2001) demonstrated that recovery is dependent on rotor tip Reynolds number, Froude number and power number and that a maximum exist for each variable. They concluded that the reason for these maxima were probably due to the destruction of bubble/particle aggregates at too high dimensionless numbers. The values reported by Rodrigues et al. (2001) are significantly lower than the practical values experienced in industrial applications and Rodrigues et al. (2001) suggested that this might be because of the big difference between particle size to tank diameter ratio. Unfortunately Rodrigues et al. (2001) did not provide information on pulp densities, retention time and froth depth.

3.7.1.2.2. Separation Zone.

Flow conditions with a Reynolds number below 2000 to 2300 are generally considered to be laminar (Fox et al., 2008), while flow conditions with a Reynolds number above 3000 are generally considered to be turbulent where $2000 < Re < 3000$ are called the transition range. The separation zone protects the fragile froth zone from the turbulence created by the rotor. It can therefore be visualised as a safe haven into which the bubble, with its mineral package, can escape from the agitation zone. It should therefore be protected from excessive turbulence as such turbulence will either destroy the bubble or strip the bubble from its mineral package. The specification for this zone is low or suppressed turbulence, which can be characterized by the superficial Reynolds number:

$$Re_s = \rho_p J_p D / \mu_p < 100000 \quad (63)$$

The turbulence level in the separation zone is determined by two factors, namely the rotor speed and the position of the rotor in the cell. The superficial Reynolds number is determined by the superficial flow through the tank and is best visualised by removing the mechanism (rotor & stator assembly) from the cell.

The value of $Re_s < 100000$ has been determined by CFD analysis and practical investigation of industrial machines and it seems to represent a good economical level of turbulence. Pilot plants normally operate in the laminar range ($Re_s < 2000$), but full scale cells, which have been tested and found to perform well, operated at a superficial Reynolds number equal to $Re_s = 100000$.

By studying the mixing theory of continuous stirred tank reactors, Wittrup (2007) showed that the number of tanks in series required to approach the RTD of an impulse is:

$$n'' = \frac{\tau^2}{\psi^2} \quad (64)$$

Where τ is the average residence time and ψ is the variance of the distribution function $E(t)$ where:

$$E(T) = \frac{1}{\tau} e^{-t/\tau} \text{ The probability that a certain element will still be in the tank at time } t.$$

The variance is:

$$\psi^2 = \int_0^{\infty} (t - \tau)^2 e(t) dt \quad (65)$$

From Equation (64) it is clear that n is a dimensionless number and therefore Equation (62) can be transformed into a dimensionless number:

$$n'' = (Re_s)^2 \cdot \left(\frac{\mu \cdot T P H.}{\omega \cdot \psi \cdot \varphi_s} \right)^2 \quad (66)$$

Equation (66) shows that the number of tanks in series can be expressed as a function of superficial Reynolds number. This indicates that the superficial Reynolds number can be used to determine the number of parallel units in a bank. As indicated in Figure 10, the value of the superficial velocity is determined by:

$$J_p = q_p / D \cdot H \quad (67)$$

It is generally accepted that there will be some sort of velocity profile through the tank and that this number represents a superficial horizontal velocity. In the case of so-called

smart cells one will have to rely on computational fluid dynamics analysis (See Chapter 4) or on potential flow patterns to determine the velocity profile through the cell, such as indicated in Figure 10 & 11, showing streamlines and velocity potential profiles. By comparing different process lay-outs, the author discovered that the superficial Reynolds number is also a good criterion to determine the number of parallel banks. If the superficial Reynolds number is above 20000, then the number of parallel banks is increased to reduce the velocity and the superficial Reynolds number.

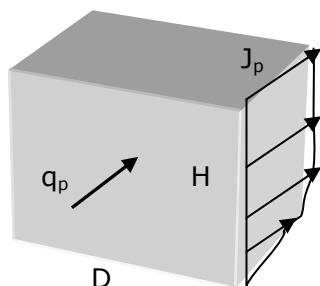


Figure 10: A model for the calculation of the superficial pulp velocity.

The first problem is to decide on the velocity profile in the feed channel. For the purpose of this analysis it is assumed to be:

$$v_r = v_o(1-r_c^2/r_o^2) \quad (68)$$

According to the theory of potential flow, the volume flow between streamlines a and b, and a' and b' in Figure 11, should be the same throughout the flow pattern (Fox et al., 2008). With this knowledge the velocity v_o and v_r can be calculated and the Reynolds number throughout the cell is then known. V_r calculated with the requirement of constant volume flow corresponds very well with the average velocity based on the projected area. After ensuring that the rotor tip Reynolds number is below $Re_t 7 \times 10^6$, the position of the rotor and size of the rotor must also comply with certain requirements. The rotor must be installed low enough in the cell and must stay well clear of the separation zone. The position of the rotor is determined by the volumetric ratio. From Equation (34) follows:

$$VR_a = D^3/d \cdot h \cdot H, < 10$$

The size of the rotor is determined by the diameter ratio ($DR_a = 0.2- 0.5$) and aspect ratio ($\hat{A}R_a > 1$). Most industrial machines have been designed with $4 \leq VR \leq 6$.

The following three criteria will ensure that the design will create a natural hydrodynamic barrier between agitation zone and separation zone.

- $Re_t < 7 \times 10^6$.
- $VR_a < 10$.
- $Re_s < 10000$.

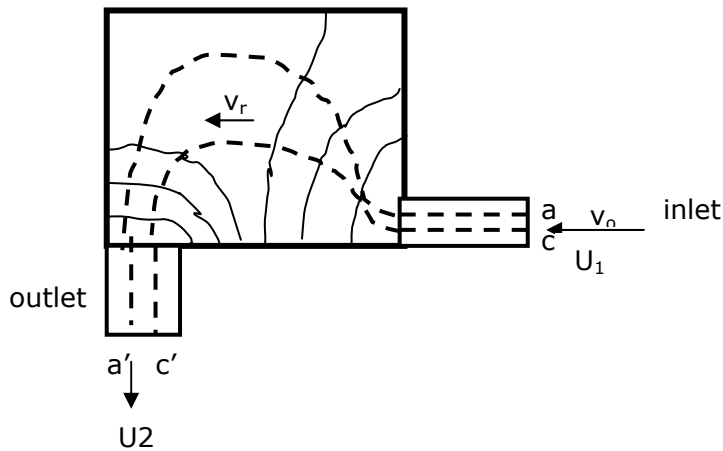


Figure 11: Flow pattern in a smart cell.

3.7.1.2.3. Froth Zone.

The requirement for the froth zone is no turbulence, i.e. $Re < 500$. Any turbulence in this zone will destroy the bubble integrity and will cause the bubbles to drop their mineral packages. This phenomenon is called drainage. It is also not good practice to allow the froth to stay in the froth zone for too long, as it increases the drainage potential. High aeration rates and low froth depth will reduce this risk.

3.7.1.2.4. Aeration Requirement, Circulation number and Volumetric flow.

The aeration number $A_e N = q_a / \omega \cdot D^3$ represents the air distribution requirements based on cell diameter.

As this number is based on tank diameter it is also an indication of gas hold-up, i.e. the distribution of air through the pulp. The relative aeration $\check{R}A_e = Q_a / Q_p$ is a more tangible number for quick comparison between two flow processes and represents the aeration requirements based on pulp flow. These numbers must be kept constant when scaling-up.

The circulation number $Q_c = q_c / \omega \cdot D^3$, together with the agitation requirements, represent the ability of the rotor to suspend solids.

Therefore this number must be kept the same when scaling up. Similarly, the relative circulation $\check{R}Circ = Q_c / Q_p$ is a quick indication of whether sanding-up problems can be

expected. Tank Turn Around (the number of times the mechanism can turn the tank volume around in one minute) is also a valuable number for quick reference. The volumetric flow $Q_p = q_p/\omega \cdot D^3$ is a good indication of whether the cell or bank is overloaded and represents to a certain extent a dimensionless retention time.

3.7.1.2.5. Froude number.

The Froude number is the primary dimensionless group when considering "partially submerged objects". Some researchers (Zlokarnic, 1991) have shown that the gas hold-up in columns is a function of the Froude number. This is a bit contentious as there are no partially submerged objects present in a flotation unit. Although air bubbles and particles are present, they are all totally submerged. With the presence of gravity in the Froude number, solid suspension might be a function of the Froude number and this in turn might influence the gas hold-up capabilities in the flotation unit. Rodrigues et al. (2001) have demonstrated with glass and quartz particles, that recovery is a function of the Froude number and in fact that a maximum recovery exists.

3.7.1.2.6. Rotor Power Number and Tank power number.

Discussions with project managers and plant metallurgists and a study of a number of pilot plant reports indicated that they rely on specific power consumption as an indication of the energy requirement for a cell, but the power number indicates that there is not a cubic relationship between cell diameter and energy requirement. After one has decided on the pulp density for best conditioning, ω and d for best aeration, circulation and agitation, then the power scale-up becomes a simple numeric calculation by keeping the power number constant. It is interesting to compare power requirements, calculated with the tank power number, with that calculated from kW/m^3 . Rodrigues et al. (2001) have found that recovery is dependent on the power number and that a maximum recovery exists.

Deglon et al. (1999) have proved that a maximum relationship exists between power intensity, expressed as kW/kg , and the flotation kinetic constant, and that this maximum appears at reduced intensity with increased tank size.

3.6.1.3.4. Summary of requirements for each zone based on practical experience.

To ensure that the machine will be able to create the required macro environment, then the following practical specifications should be adhered to:

Geometrical requirements.

- Rotor tank volume ratio; $\dot{R}T_a VR_a = 1.2\%$.
- Volumetric ratio: $VR_a = <10$.

Kinematic requirements.

- Rotor tip Reynolds number: $4 \times 10^6 < Re_t < 7 \times 10^6$.
- Superficial Reynolds number: $Re_s < 100000$.
- Circulation number: $Q_c = 4.2 \times 10^{-4}$.
- Aeration number: $Q_a = 4.2 \times 10^{-4}$.

Dynamic requirements.

- Tank power number: $4 \times 10^{-5} < T_a PNo < 5 \times 10^{-5}$.

These stated numbers have been derived from successful flotation plants in the South-African Industry and do not vary significantly with mineral type.

3.8. Partial similarity.

Several 'rule of thumb' techniques exist for dimensioning different type of parameters and are in fact scale-up rules based on partial similarity (Zlokarnic, 1991). These rules include the so-called volume related mixing power (kW/m^3) widely used for dimensioning mixing vessels. Another partial rule for solid suspension is tank turn around per time unit.

This is a very useful number when sizing conditioners and other mixing vessels. The energy dissipation parameter (kW/kg) is covered by the dimensionless Froude number and Weber number.

Newel and Grano, (2006), concluded that the energy dissipation rate is independent of cell diameter and a function of the impeller diameter. Energy dissipation is a requirement and not an ability, and is therefore a function of tank diameter, such that Equation (69) is a dimensionless number.

$$\pi = \frac{\epsilon}{\omega^3 \cdot D^2} \quad (69)$$

3.8.1. Surface tension of the pulp.

Most of the metallurgists on the plant do not have the ability or tools to determine surface tension and hence to determine the Weber number. According to Schubert and Bischofberger (1998), the capillary pressure over an air bubble is $\partial p = 4\sigma/d_b$. Where d_b = bubble diameter and σ = surface tension. Substituting this in the Weber number, gives:

$$We = \frac{g \cdot d_b}{\omega^2 \cdot D^2} \quad (70)$$

This equation proves that it is possible to reduce dimensionless numbers such as the Weber number to simpler variables, such as a modified Froude number which is easier to measure in practice.

3.8.2. Viscosity of the pulp.

This is probably one of the most difficult variables to determine. Although the Roscoe model (Roscoe, 1952) is widely used, it is not clear whether this model includes the effect of reagents and it was therefore decided to produce a viscometer from a hand held drill modified as shown in Appendix 6. The current drawn is related to the torque which in turn depends on the viscosity of the fluid. Very good correlation with Roscoe's method was found between in the range of pulp densities found in flotation.

3.9. Practical plant measurements.

To ensure some level of consistency the author tried to indicate in the following sections where this information could be found and how to analyse and evaluate this information. The author did not try to involve statistics but rather come up with a generic solution for every variable. Information on conditioning, retention time and froth depth are demonstrated graphically and pit falls are highlighted where possible. To complete the range of information, flow diagrams are also shown as various types are encountered in practice. Although flow diagrams are not dimensionless items it is also required that they should stay the same between pilot plant and full scale plant, as is required for mineralogy and reagent dosage. It is imperative to start any flotation process by studying the mineralogy as it indicates problem minerals and secondary minerals of value that must be stockpiled separately and this might put extra requirements on the design of the plant. Pre-extraction of these secondary minerals might benefit the flotation process by increasing the head grade and under certain conditions reduce and simplifies the reagent suite and consumption.

3.9.1. Mineralogy.

3.9.1.1. Phosphate.

It is important to make sure we are dealing with the same mineral and liberation characteristics used during the laboratory and pilot test trials.

Table 13 shows the different geological combinations for the Phalaborwa mineral complex. Looking at the Phalaborwa phosphate minerals, one must take cognisance of the following when designing the main plant:

- The presence of diopside requires high line velocities in pumping systems and high pumpability in flotation cells to ensure solid suspension, as diopside tends to break into little cubes, which do not flow easily.
- The presence of magnetite poses grinding problems, as well as suspension problems, and requires careful engineering to ensure successful handling. It might also require separate tailings disposal routes as it has a secondary value.
- Phlogopite and calcite absorb the same collector as apatite and require special depressants.

Table 13: The main phosphate bearing minerals of the Phalaborwa geological complex.

Mineral	Apatite	Diopside	Phlogopite	Magnetite	Calcite	Dolomite
Pyroxenite	18	60	22	-	-	-
Foskorite	18	-	50	20	12	-
Carbonotite	20	-	-	-	70	10

3.9.1.2. A copper ore.

Table 14: Mineralogy of a copper deposit (Palaborwa Mining Co.).

Item	Chalcopyrite	Cubanite	Bornite	Chalcocite	Valleriite	Magnetite
Past	52%	2.4%	40%	0.45%	3.3%	29%
Present	62%	11%	20%	2.2%	3.1%	21%
Future	46%	9%	25%	8%	12%	16%

Table 14 shows general change in mineralogy over the last 40 to 50 years. The change in valleriite from 3% to 12% is significant in the sense that valleriite is a sulphide wrapped in a hydroxide layer and does not respond to the standard chemistry. It also tends to contaminate other minerals and render them difficult to float.

3.9.2. Liberation (P_{90}).

One of the most important tools of the metallurgist is to understand the behaviour of the mineral under certain milling and liberation conditions. This is the factor that indicates whether the valuable mineral has been separated from the gangue.

3.9.2.1. A Phosphate mineral.

Figure 12 shows the recovery vs. particle size for phosphate obtained from Foskor's production statistics. This information is generated by sampling the feed, tails and concentrate every two hours for a week and then composite the three categories, screening them and then analysing them. The recoveries per fraction are then calculated by utilising the "FATCAT" method. This is valuable metallurgical information, as it shows that the optimal recovery (blank bar) lies between +38 μ m and -200 μ m and that the maximum concentrate grade is associated with the coarse fraction, +150 μ m (solid bar). This means that the apatite has almost been completely liberated up to 300 μ m. It also shows that the grinding process does not comply with the +38 μ m and -200 μ m requirement, as almost 50% of the apatite (dotted bar) falls outside the limits for maximum recovery.

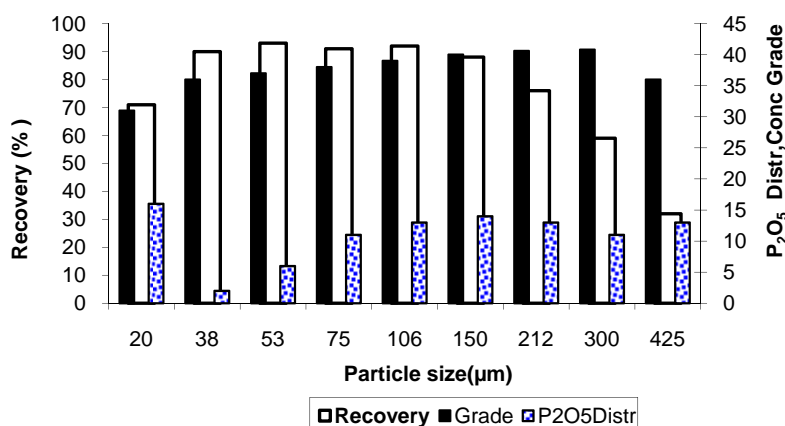


Figure 12: Foskorite recovery, grade and apatite distribution as a function of particle size.

From Figure 11 the P_{80} for phosphate based on recovery should be about 150 μ m while the distribution of P_2O_5 is unacceptable as almost 40% of the P_2O_5 reports outside this limit.

3.9.2.2. A Copper mineral.

Figure 13 shows the recovery of a copper mineral (blank bar) where the liberation has been optimised for a phosphate float (black bar). It is clear that the copper recovery is mostly associated with a particle size below 100 μm . P_{80} should be about 75 μm .

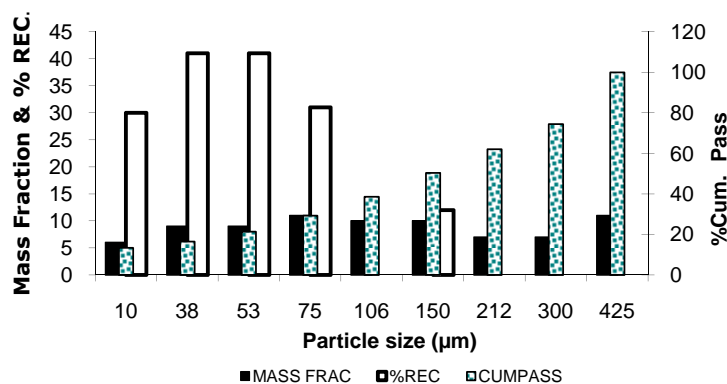


Figure 13: The liberation and recovery of a copper float (Foskor production statistics).

3.9.3. Chemistry.

Reagents consist of collectors, frothers, depressants and modifiers. Each reagent has a very specific purpose and needs to be dosed in much the same quantity as on the pilot plant, taking into account the variation in geology, liberation, short-circuiting and circulating loads. Most of this information is available in the log suites of the pilot plant. It is also available in laboratory bench tests but the pilot plant information is more realistic as it includes the circulating loads.

3.9.4. Conditioning.

During the conditioning phase, the reagent is allowed time to prepare the surface of the mineral prior to getting into contact with the air, to allow the hydrodynamics to perform its purpose. To ensure this, the conditioning is characterised by a certain conditioning time and agitation level represented by the pump ability of the stirrer. Pump ability is defined as tank turn around (θ). θ is the number of times the stirrer can turn around the tank volume in one minute. During scale-up the conditioning time (η) and tank turn around (θ) must be kept constant.

The conditioning times for a few industrial minerals, are briefly indicated below, based on experimental work done by the author. These conditioning models are normally for the collector dosage.

3.9.4.1. Phosphate.

Figure 14 shows the behaviour for a phosphate mineral. The conditioning time in this case should be about $\eta = 8$ minutes for a recovery of more than 80%. This should be combined with a conditioner tank turn around $\theta = 9\text{min}^{-1}$. For fine grained $P_{80} < 100\mu\text{m}$, θ should be about 7min^{-1} .

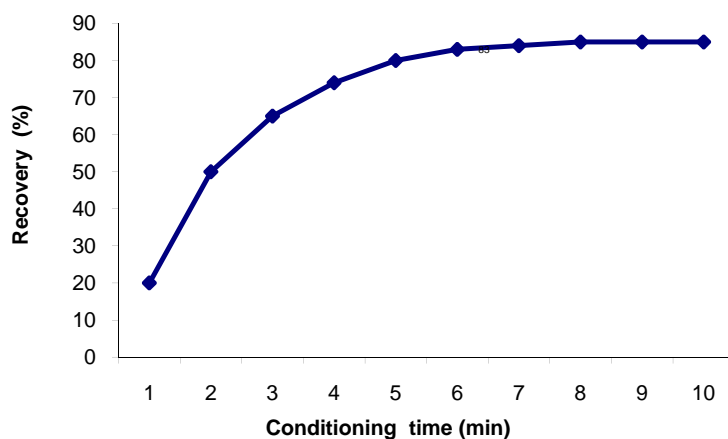


Figure 14: Effect of conditioning time on the recovery of a phosphate mineral.

The design of the conditioner must be such that the discharge from the conditioner is at the top of the conditioner. When no sanding up occurs then the value of θ should be acceptable. Theta should be increased stepwise until no sand up occurs. This would prevent theta to be too high. (See paragraph 3.9.6 for more detail). Accept for the stirrer at the bottom, good conditioner design includes a small impeller at the top where it creates a little vortex which is the dosage point. With such a design the reagents are sucked into the stirrer circulating zones.

3.9.4.2. Conditioning model for a copper mineral.

Figure 15 shows the conditioning time for the Palabora copper mineralogy. Palabora mine does not condition, although the model clearly shows about a five minutes conditioning is required for a recovery of more than 90% ($\eta = 5\text{min}$). The rationale behind the decision not to condition is unknown and has probably something to do with cost during the initial design stage. This model shows that all models have similar shapes and need careful analysis before making decisions. The irregular shape of the second and third graphs is a result of oxidising during the preparation stage of the sample. The tests were done over three consecutive days although all the grinding has been done on day1.

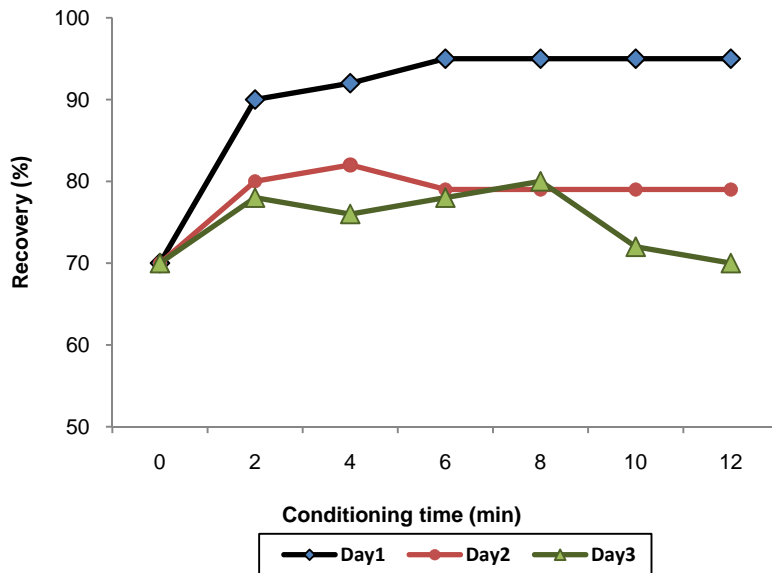


Figure 15: Effect of oxidation on conditioning time on the recovery of copper at Palabora.

3.9.4.3. Antimony conditioning model.

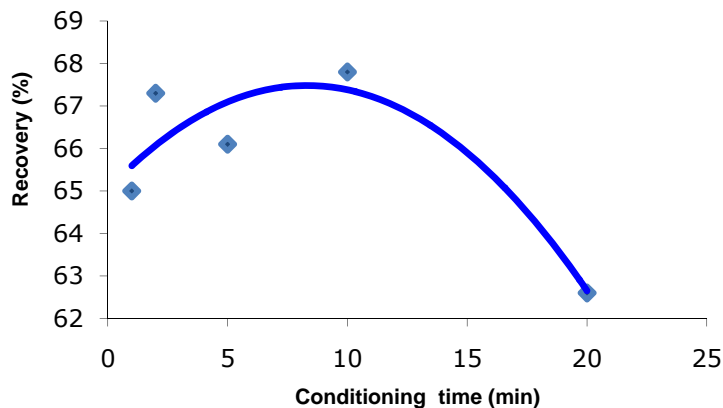


Figure 16: Effect of conditioning time on the recovery of antimony.

The conditioning time for antimony in Figure 16 shows a maximum at $\eta = 10$ minutes. Prolonged conditioning time can have a negative effect because of double layering, oxidation etc. In this case pH adjustment was required and this also might have had an effect on the maximum.

3.9.4.4. Conditioning model for copper slag.

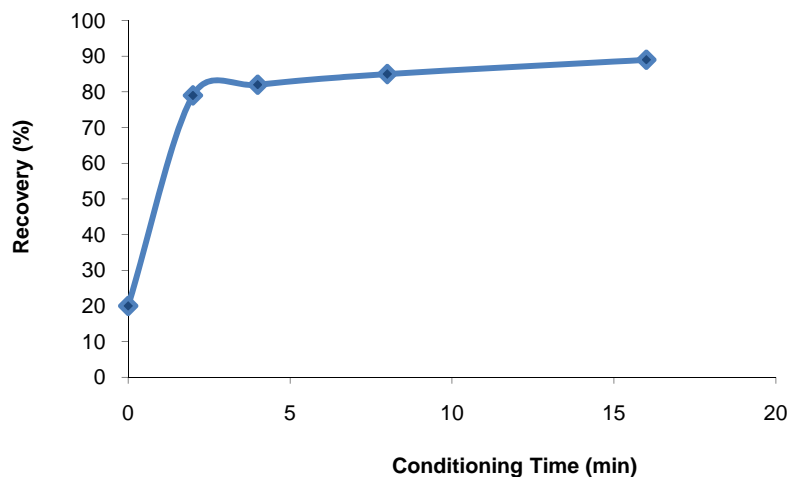


Figure 17: Effect of conditioning time on the recovery of copper slag.

Figure 17 shows that copper slag can also be characterised with standard metallurgical processes. Some of the copper is attached to silica and laboratory analysis needs to be done with hydrofluoric acid to dissolve all copper. The conditioning curve shows that very long conditioning is required for copper slag, $\eta > 15\text{min}$.

3.9.4.5. Conditioning model for Nickel and Copper combination.

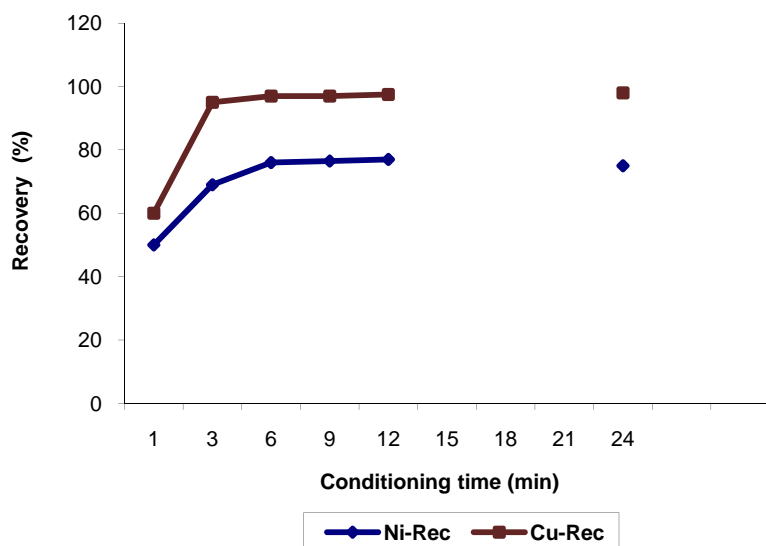


Figure 18: Effect of conditioning time on the recovery of Ni and Cu in a differential float.

From Figure 18 it is clear that both Copper and Nickel require 6-9 minutes conditioning time.

Differential flotation means that one mineral will be floated first while both minerals are present and then the float will be adjusted to float the second mineral. Normally pH adjustment is done with lime, to suppress the second mineral.

3.9.4.6. Conditioning Tank Turn-around.

The tank turn-around capability (θ) ensures intimate mixing between solids and therefore requires a high level of turbulence. In certain cases as high as 9x tank turn-around is required. This requirement is a function of the sinking velocity of the mineral particle. Assuming Stokes flow $C_d = (64/Re)^{0.5}$ then the following force system applies:

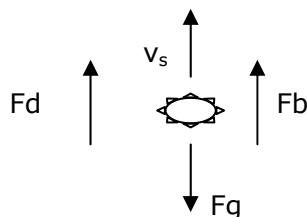


Figure 19: Model of a particle settling under gravity.

$$F_b - F_g - F_{cd} = 0 \quad (71)$$

It can be shown under Stokes flow assumptions, that the sinking velocity is:

$$V_s = \frac{g \cdot (\rho_s - \rho_p) \cdot d^2}{18\mu} \quad (72)$$

3.9.5. Average retention time.

3.9.5.1. Retention model for a phosphate mineral.

Retention time and conditioning time go hand-in-hand and one needs to study the interaction between these two parameters to find the most beneficial condition as the adsorption of reagents can create the windows within which one has to condition or retain. Normally this model is done on logarithmic scale but for simplicity has not been done on linear scale. Figure 20 shows that pyroxenite requires about 20 minutes retention time for a recovery of more than 80%. This is done in a laboratory and confirmed in the pilot plant. Care must be taken to keep the froth depth at the same level.

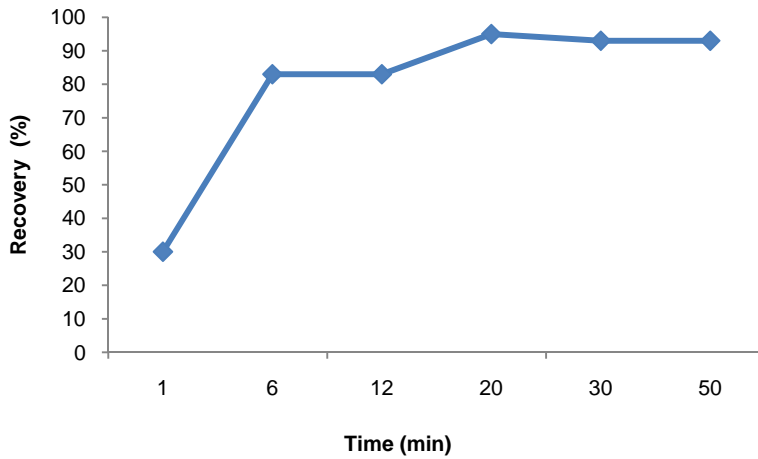


Figure 20: Recovery vs. retention time for pyroxenite ore.

3.9.5.2. Retention time model for Copper and Zinc.

Figure 21 shows a typical recovery vs. retention time for a copper and zinc ore. The high recovery is a result of very high head grades and the lower zinc recovery is due to the suppression of zinc as part of the differential flotation requirements. Retention time of 18 minutes for both copper and zinc are required

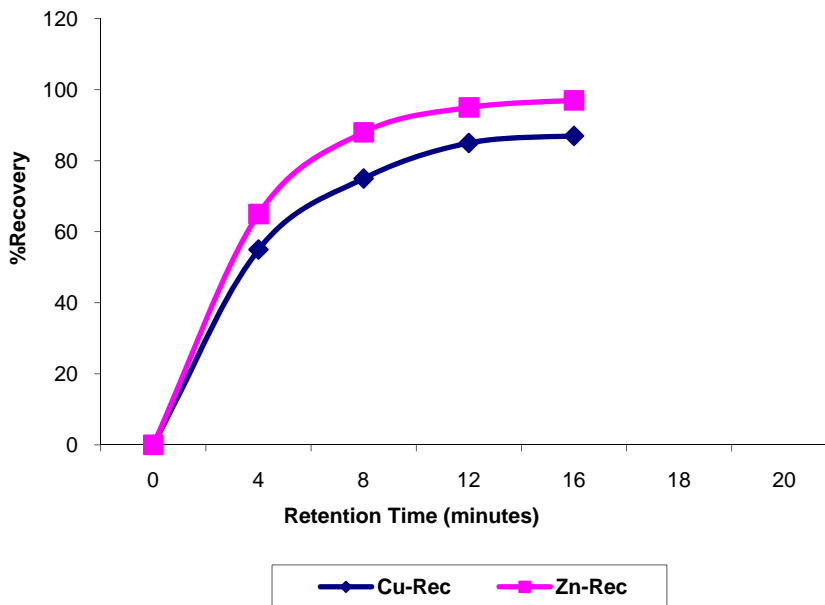


Figure 21: Recovery vs. retention time for copper and zinc.

3.9.5.3. Calculating average retention time in flow circuits.

During scale-up, the retention time must stay the same and this parameter determines the rougher and scavenger volumetric size. The definition for average retention time is:

$$\tau = (\text{Rougher} + \text{Scavenger volume}) / (\text{Pulp feed rate}) \text{ [min]} \quad (73)$$

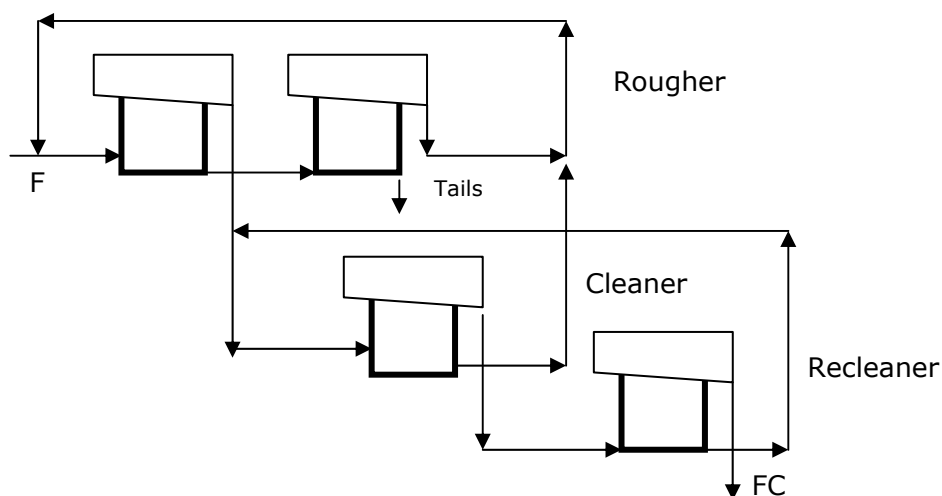
In a classical flotation circuit flow diagram the circulating loads should be added to the feed rate and could in some instances be as much as 70% of the feed rate. As the recovery improves the mass removed will increase and this will reduce the circulating load in practice to as low as 30% of the feed rate.

$$\text{Pulp feed rate} = [(\text{Feed tons} + \text{circulating tons}) / (S_{gp} \cdot \phi_s \cdot 3600)] \quad (74)$$

3.9.6. Flow diagrams.

3.9.6.1. Classical flow diagram.

At first it might seem that the flow diagram does not have an influence on flotation, but it determines the retention time, mass balance as well as circulating loads, which do have an influence on flotation. Almost all flotation plants use the classic flow diagram of milling, conditioning, rougher, scavenger, cleaner and recleaner (Figure 22).



(F = Feed; Tails = Tailings; FC = Final concentrate).

Figure 22: The classical flotation flow diagram.

3.9.6.2. Double grind diagram.

The platinum industry prefers to primary milling, float and secondary milling and float (Figure 23). The two industries also use a different scavenging / recycle diagram and the

prominent feature of the platinum flow diagram is the scavenging cycle in every phase. The classical flow diagram focuses on the enrichment of the feed, and thereby increases the probability of a collision and recovery. The problem is that both seem to work well.

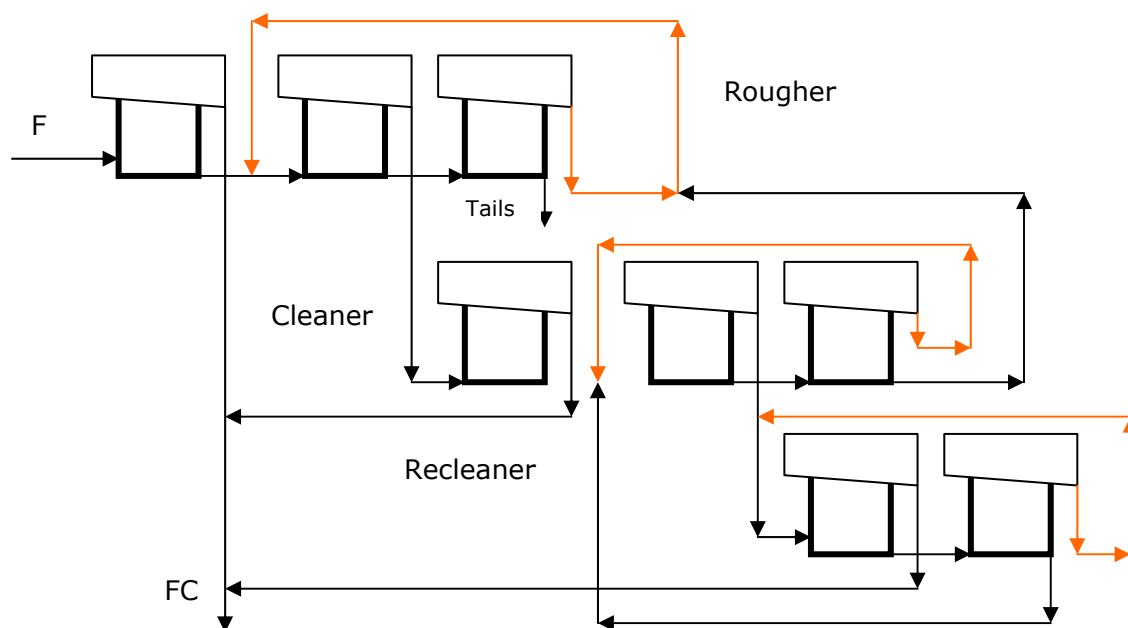


Figure 23: The platinum flow diagram.

3.9.7. Volumetric capacity.

With a fixed flow diagram the volumetric capacity is defined as:

$$VC = (\text{Cleaner \& Recleaner Volume.}) / (\text{Rougher \& Scavenger Volume.}) \quad (75)$$

The recleaner capacity is defined as:

$$R_{CLC} = (\text{Recleaner volume}) / (\text{Cleaner volume}) \quad (76)$$

These two numbers must be confirmed by performing a proper mass balance. Simple generic models based on the first order kinetic model seem to work well. These two capacities determine the circulating load and thus the retention time.

3.9.8. Froth Depth.

Figure 24 shows the classical froth depth model for mineral and gangue. To produce the froth depth model, one needs a transparent container with froth depth markings measured from the lip of the container. There are two basic approaches to produce a froth depth model, based on the average depth and the constant depth.

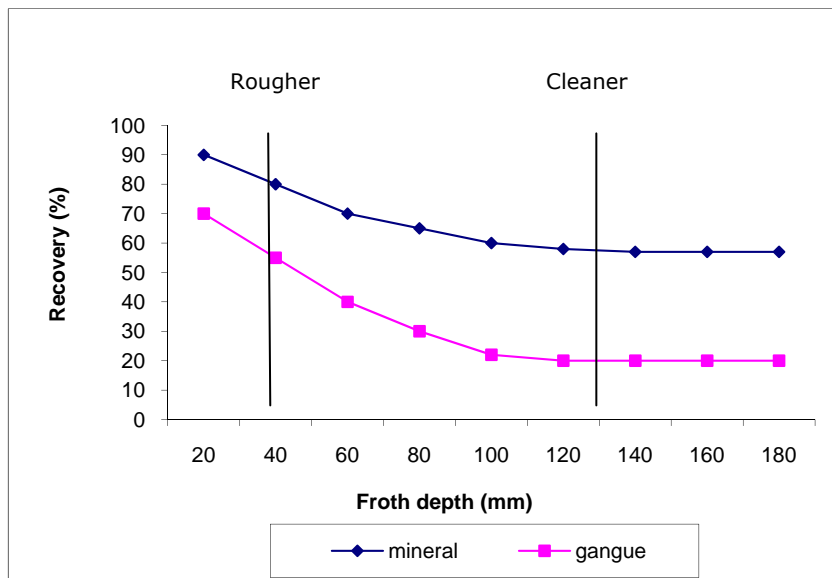


Figure 24: A classical model for recovery versus froth depth.

3.9.8.1. Average depth.

The experiment starts at a certain depth and end at a certain depth after keeping the retention time constant. The average of the froth depth is calculated with its corresponding recovery. The problem is that in keeping the retention time constant, one has to start at different depths which will impact on the final result.

3.9.8.2. Constant depth.

In this case the water level is kept constant at a certain depth by adding water, and the float runs for a certain retention time. With this method the pulp density changes all the time and will certainly impact on the final result.

The accuracy of these models are of secondary importance, but the profiles of the recovery vs. froth depth curves are important.

3.9.8.3. Interpretation of froth depth models.

The diverging model is called the classical model, where the rougher will run with a shallow froth, while the cleaner will run with a deep froth and is typical for sulphide minerals. In the case of the converging model, both the rougher and cleaner will run with a shallow froth. This was found with copper slag and the inverse reaction might have something to do with the copper trapped in silica. The parallel model represents the most difficult one and the froth depth is determined by trial and error or by the secondary gangue minerals in the main plant.

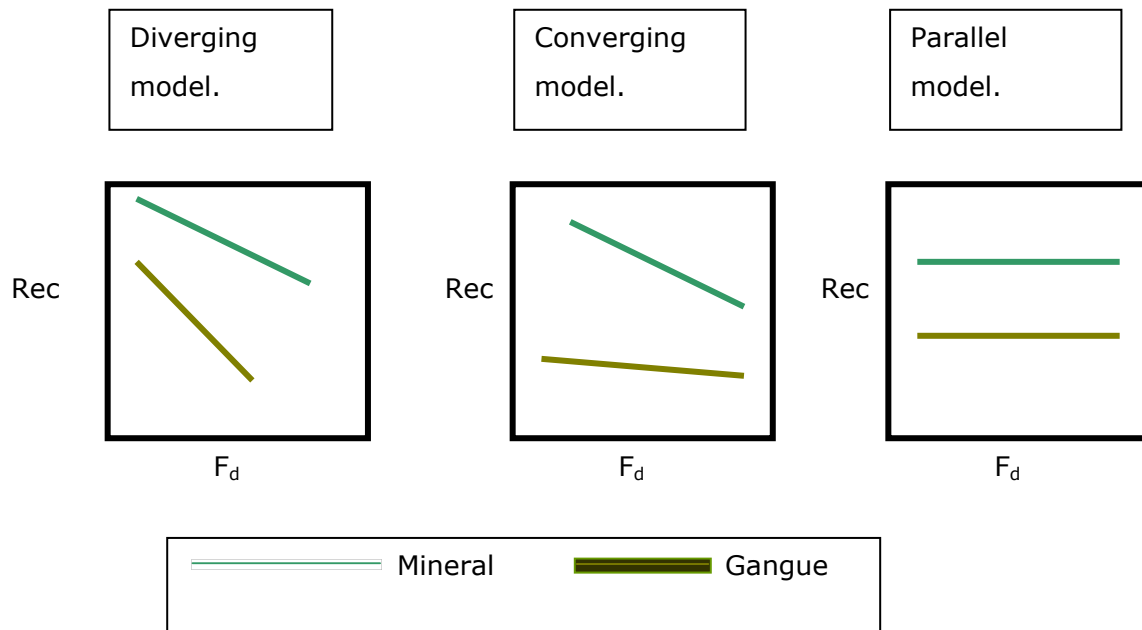


Figure 25: Three types of froth depth models with different profiles.

The phosphate model (Figure 25) is a typical parallel one and both rougher and cleaners run at shallow depth to reduce magnesium and potassium recovery. Froth depth and superficial gas velocity (J_g) represents the time that the mineral will spend in the froth phase. To long time will increase the probability of drainage. This parameter appears in the equation for the froth recovery factor, Equation (41). To make the froth depth more universal and comparable, it should be expressed as a percentage of diameter or tank height, thus making it dimensionless.

3.10. Deficiencies in industrial plants based on the schedule of dimensionless parameters.

The application of the schedule of dimensionless numbers on several mining sites revealed the result in Table 15. When comparing the main plant with the process specification, all plants showed almost the same deficiencies.

Not only did the deficiencies occur in the hydrodynamic variables but also in the normal standard metallurgical parameters such as grinding, conditioning time and retention time. In certain cases the process specification did not even exist and had to be generated in the same time.

Table 15: Comparison of some industrial designs.

Factor	Phosphate	Copper	Platinum	Zinc	Antimony	Nickel
Liberation						
Condition						
Tank Turn Around						
Retention						
Flow Diagram.						
Volumetric Cap.						
Froth Depth						
S_b						
Volumetric Ratio						
Re_s						
Re_t						
A_eN						
CN						
T_aT_u						
$T_aPNo.$						

Dark= Compliance; Light= Non-compliance

In other cases operators would use aeration to control pump sump levels. Finally an inspection of the flotation pump floor must be conducted to ensure that no pump sump is overflowing because that is a sure indication that the recoveries recorded are not accurate. This condition must be rectified before any measurements are taken.

These deficiencies and the non-compliance to the transformation equation based on Froude number led to the conclusion that metallurgist, engineers and suppliers do not understand the basic scale-up requirements. These deficiencies represent about R7 billion revenue loss in South Africa. This represents the salaries of about 150000 employees in South Africa.

3.11. Dimensionless comparison of industrial designs.

Figure 26 demonstrates the design criteria of some well known industrial designs and the domain of the pilot designs (Denver and Tornado). The low tank power number and bubble surface area flux of the industrial machines might be the reason for most of the deficiencies in full scale plants.

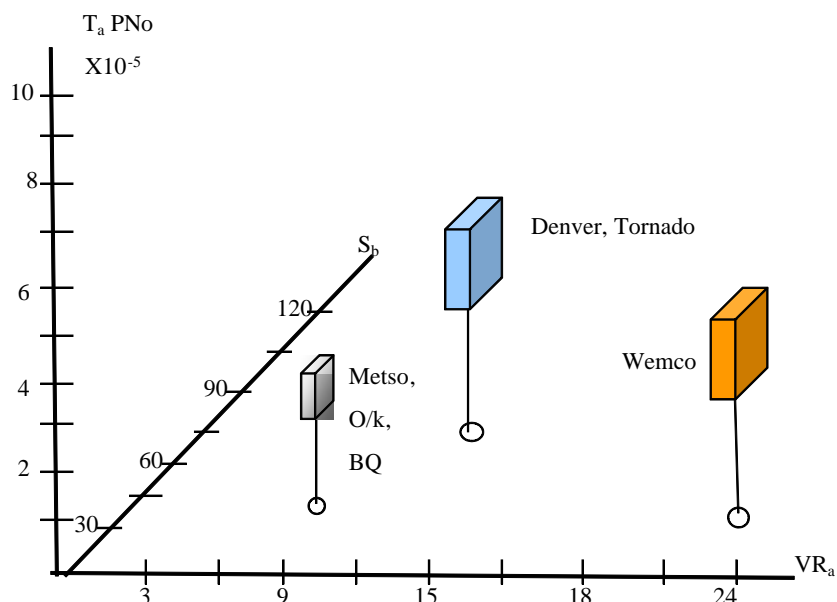


Figure 26: Graphical presentation of the design domain of some industrial and pilot plant designs.

3.12. Summary for the application of the schedule of dimensionless numbers.

From the previous discussion the key variables and dimensionless numbers required to describe flotation processes can be summarised as follows:

- **Mineralogy:** To be studied in detail to determine problematic minerals or minerals with secondary economic potential and to be kept the same during scale-up.
- **Reagent suite:** Collectors, frothers, depressants, activators, modifiers, pH agents and dosage rate to be kept the same between pilot plant and full scale plant.

- **Liberation:** Recovery vs. particle size is a useful tool to determine milling requirements. The characterisation process is based on laboratory scale experiments and pilot plant results.
- **Conditioning:** Determine conditioning time from laboratory experiments and confirm on pilot plant. Maintain same energy input (Tank Turn Around) and conditioning time between pilot plant and main plant.
- **Retention:** Determine retention time on laboratory scale and confirm on pilot plant. Combine with flow diagram configuration. Both retention time and flow diagram to be kept the same for pilot and main plant.
- **Rotor tank volume ratio (d^2b/D^2H):** Maintain same Ratio in full scale plant.
- **Volumetric ratio (D^3/dhH):** Position of rotor in tank to protect quiet and froth zones. Maintain same ratio in full scale plant depending on basic design.
- **Rotor tip Reynolds number ($\rho_p v_t d / \mu_p$):** Agitation level on tip of rotor. To be combined with relative particle size ratio and to be the same for pilot plant and main plant.
- **Superficial Reynolds number ($\rho_p UD / \mu_p$):** To be investigated taking cognisance of the requirements of the mixing theory.
- **Rotor aspect ratio (d/b):** Shape of rotor. Maintain same ratio in full scale plant depending on basic design.
- **Aeration number ($q_a / \omega D^3$):** Required aeration. Maintain same dimensionless number in full scale plant.
- **Circulation number ($q_c / \omega D^3$):** Solid suspension requirement. Maintain same dimensionless number in full scale plant taking into account the multiple rotor effect.
- **Froude number ($\omega^2 d^2 / gD$):** Additional requirement for solid suspension. Combine with Re_t , aspect ratio and relative particle size ratio to produce Fr_{RGA} and maintain same dimensionless number in full scale plant.
- **Tank power number ($P / \rho_p \omega^3 D^5$):** Power requirements. Maintain same dimensionless numbers in full scale plant.

- **Mechanism power number ($P/\rho_p\omega^3d^5$):** Mechanism size. Maintain scale-up ratio taking into account the multiple rotor effect.

Finally, a complete set of parameters are combined, in a process specification sheet (Schedule of dimensionless numbers) to assist in the identification of plant design deficiencies.

Although the main aim is to maintain the same dimensionless ratios in the full scale plant design, Deglon et al. (2000) and Zlokarnic (1975) have shown that present-day industrial designs do not comply with these objectives and varies over a large range in almost every respect.

The next Chapter presents the results of a computational fluid dynamics analysis which was done to get a better understanding of the hydrodynamic parameters, such as circulation, aeration, eddies and turbulent levels in a Wemco flotation machine. The reason for choosing the Wemco machine is that it does not represent the standard design approach, as its volumetric ratio is very large and being a self-aerating machine, with a low aspect ratio rotor, it requires special physical barriers to protect the separation and froth zone.

In the following Chapter the CFD analysis presented a unique opportunity to study the effects of these barriers and design contradictions. The dimensionless parameters such as aeration number, $A_eN = q_a/\omega D^3$, rotor tip Reynolds number, $Re_t = \rho_p\omega d^2/\mu_p$ and velocity profiles will be of particular interest.

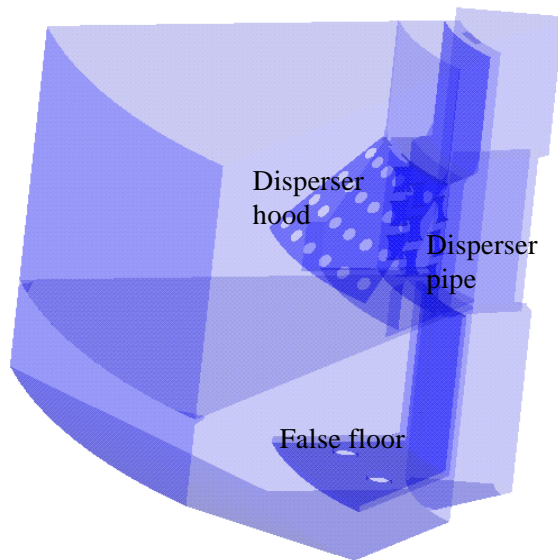
CHAPTER 4: INTERPRATIVE RESULTS OF A COMPUTATIONAL FLUID DYNAMIC ANALYSIS OF FLOTATION CELL HYDRODYNAMICS.

Computational fluid dynamics (CFD) has been widely used in the analysis of complex flow and thermal problems but very little work has been done by applying this technique to flotation processes and flotation machine design. The WEMCO flotation machine is a self-aerating machine utilising a low aspect ratio rotor which has been positioned high up in the flotation tank to improve aeration ability. To protect the quiet zone from the agitation zone, certain mechanical barriers were assembled around the rotor in the shape of dispersers and hoods which again resulted in very complex flow patterns. To improve circulation and solid suspension the design also features a unique false bottom/draft tube combination which further complicates flow patterns and predictability (See Figure 29). For this reason Megchem, represented by Beyers (2002), was contracted to perform a CFD analysis of the Wemco machine. The client was responsible for supplying design and process data and for the interpretation of results in terms of dimensionless parameters. CFD analysis, based on CFX software and Perspex modelling, have been utilised to contribute towards a better understanding of these complicated flow patterns. As it is very difficult to undertake research on a full scale plant, this approach provided the research team with an unique opportunity to do “what if” studies and to eliminate expensive experimental set-ups. The objective of the study was to quantify turbulent levels, aeration levels, solids suspension and conditions which would support a high probability of successful recovery. As similarity is based on flow conditions where the dimensionless groups have the same numerical value, the CFD analysis either supported the standard analytical calculations or improved the accuracy of the numerical values.

4.1. Design data.

4.1.1. Geometry.

The present multiphase simulations were done with the cell geometry modelled with actual perforated disperser plates and not with porous regions. An axi-symmetric cylindrical wedge model, with included angle of 36° , is utilised. The modelled geometry included the as-built perforated plates is shown for clarity in Figure 27.



CFX

Figure 27: Modelled geometry for the multiphase CFD simulation.

4.1.2. Fluid properties.

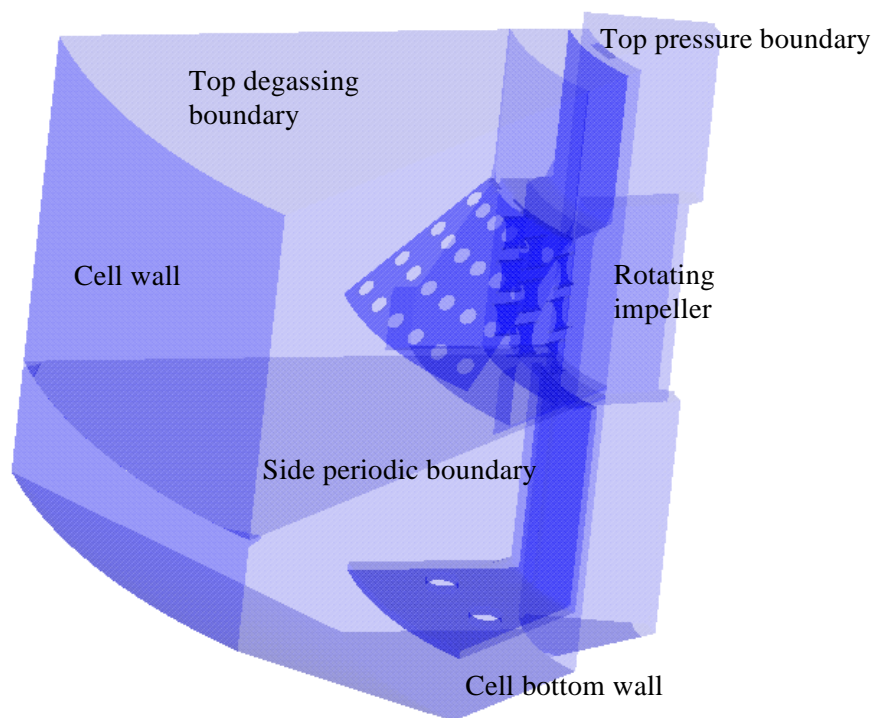
Table 36: Fluid properties for the CFD model.

Phase description	Property	Value	Units
Water: Continuous fluid phase	Density	998.0	kg.m ⁻³
	Viscosity	1X10 ⁻³	Pa.s
Air: Dispersed phase	Density	1.18	kg.m ⁻³
	Viscosity	1.8X10 ⁻⁵	Pa.s
	Bubble diameter	1.0	Mm
Solids: Dispersed particles	Density	3100	kg.m ⁻³
	Particle diameter	0.2	mm

The fluid properties shown above remain constant during the course of the simulation.

4.1.3. Boundary conditions.

Boundary conditions were selected to ensure accurate physical modelling of the flotation cell as shown in Figure 28.



CFX

Figure 28: Boundary conditions employed.

The inlet of the stand pipe was set as a constant pressure boundary to ensure that the induced suction generated by the impeller is not influenced by an inlet boundary but rather implicitly calculated during the solution of the flow field. A degassing boundary condition was assigned to the top section of the flotation cell on the outside of the stand pipe. This type of boundary is essentially a simplified free surface that allows air to escape through the boundary surface. Since the model consists of a 36° angle axi-symmetric cylindrical wedge it was required to include periodic boundaries on each of the two side planes. No other inlets or outlets were specified, thus ignoring the limited effects of the actual inflow and outflow of the pulp. This simulation includes no inlet mass flow boundary conditions for any of the three phases. It was established in earlier work that the inlet boundary conditions do not greatly influence the overall flow characteristics. It would however be beneficial to establish some inlet pulp flow condition in the future for the axi-symmetrical wedge modelled here.

An additional boundary condition was applied to ensure that only air enters the impeller stand pipe. This required volume fraction values for each phase as described by Table 17.

Table 17: Additional volume fraction boundary conditions.

Boundary	Phase description	Pressure	Volume fraction
Top pressure	Continuous liquid	0.0	1×10^{-10}
	Dispersed air	0.0	1.0
	Dispersed solids	0.0	1×10^{-10}

Since the model contains no inlet boundary conditions it was important to specify constant initial volume fraction values to each phase through the computational domain. The initial values employed used are shown in Table 18.

Table 18: Initial volume fraction conditions.

Phase description	Initial value
Continuous liquid	0.729
Dispersed air	0.1
Dispersed solids	0.1711

4.2. CFD model.

The CFD model represents the WEMCO flotation cell as per the information from the engineering drawings received from the client. The 36° included angle of the cylindrical wedge was selected based on the included angle between adjacent impeller blades. The impeller rotational speed was set at 22 r/s as per specifications. A sliding grid method was employed to model the impeller rotation. The mathematical models included in the CFD simulation, consists of the following:

- Three-dimensional flow in cylindrical coordinates.
- Transient flow analysis.
- Unmatched sliding grid interfaces for rotation of the impeller.

- Unmatched surfaces for complex grid configurations for the perforated plate simulation.
- Turbulence modelling with the standard $k-\varepsilon$ turbulence model for the continuous phase only. Laminar flow conditions were applied to the two dispersed phases.
- Multiphase flow with three phases was included with:
 - One continuous phase (liquid) and two dispersed phases (bubble and particle).
 - Particle drag for dispersed phases.
 - Buoyancy.
 - Constant fluid properties.
 - Inter-phase momentum coupling between air bubbles and liquid and between solid particles and liquid.
- User Fortran coding was employed to calculate various flow parameters from the simulation results including, pulp Reynolds number, bubble Reynolds number, interpolated recovery rates potential, volume averaged recovery rate potential, bubble-particle collision frequency and recovery rate potential from bubble particle collision theory among others.

For the purpose of this report the x-coordinate is taken along the impeller axis, y-coordinate in radial outward direction from this axis and the z-coordinate representing the tangential direction.

4.3. CFD RESULTS.

Figure 30 clearly shows the air intake and circulating flow patterns. The unique feature of the Wemco design is the utilisation of a false bottom to improve solid suspension and the use of a disperser and hood assembly to protect the quiet zone.

4.3.1. Standard Wemco design.

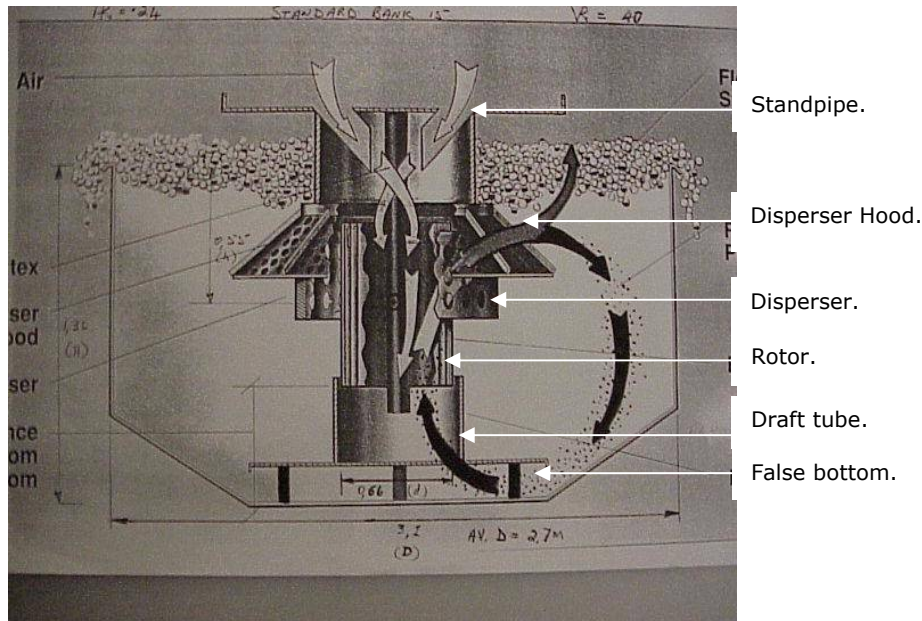


Figure 29: Standard Wemco design with simplified flow pattern.

4.3.1.1. One Phase flow (Water only).

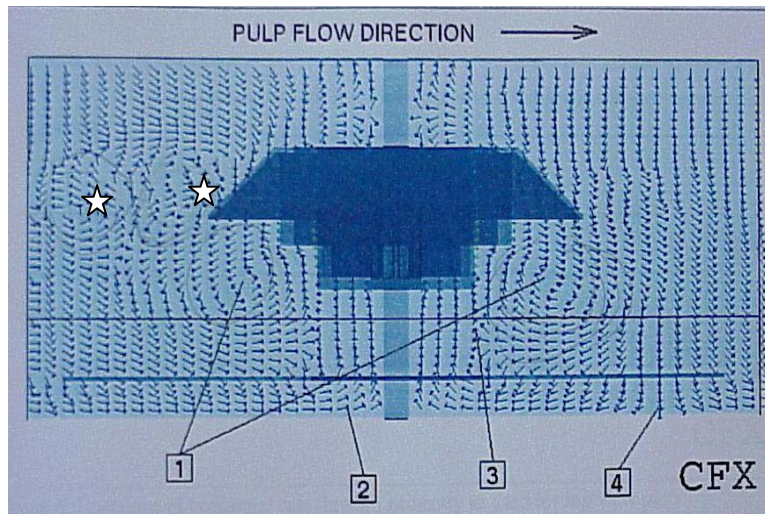


Figure 30: Shows the first water only model.

The eddies above the hood (Stars) were worrying as these eddies will certainly agitate the quiet zone.

4.3.1.2. Two-phase flow (Water and air).

Figure 31 shows the first water air model and clearly shows the stripping of air by the hood and one can assume that this stripping also meant the stripping of its mineral package and would therefore enhance the de-attachment of mineral and air and the loss of recovery.

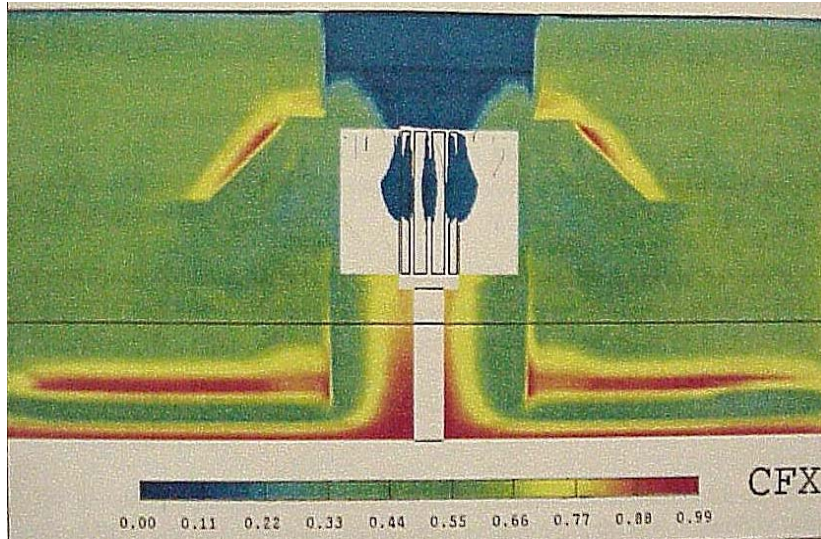


Figure 31: Showing lack of aeration above the hood and below false bottom.

Figure 32 shows the Perspex model of the standard Wemco that was built by the author to study the flow patterns and was operated at about 500 RPM so as to produce just enough air to allow visual observation and photography.

(1 = Standpipe: 2 = Hood; 3 = disperser; 4 = Draft tube; 5 = False bottom).

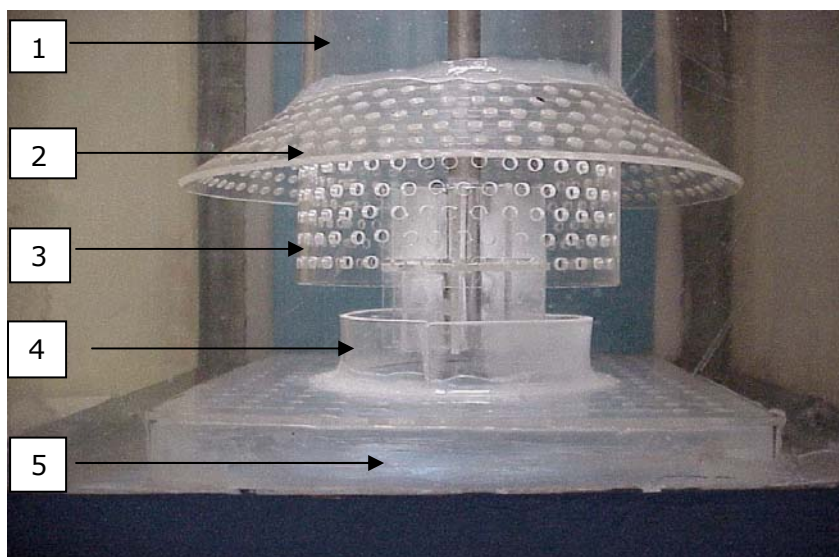


Figure 32: Detail of the Perspex model of standard design.

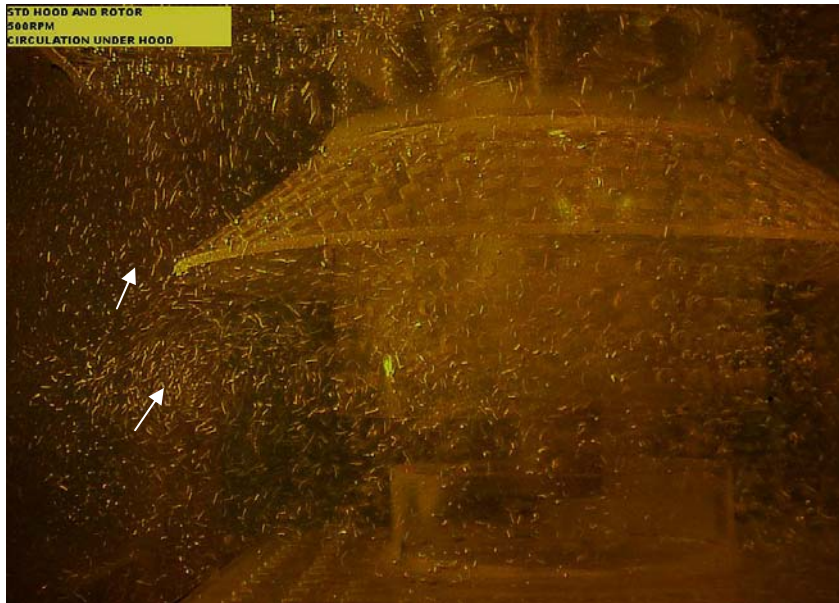
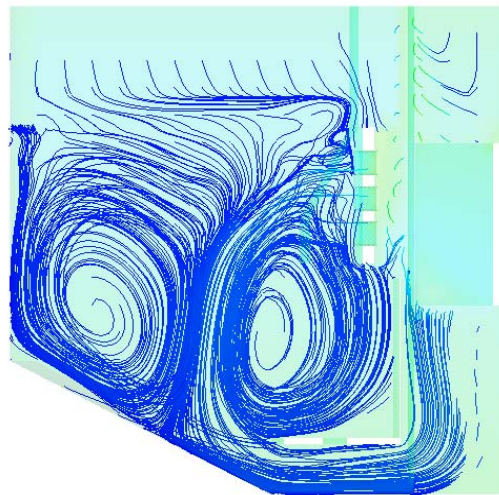


Figure 33: Shows the Perspex model in operation.

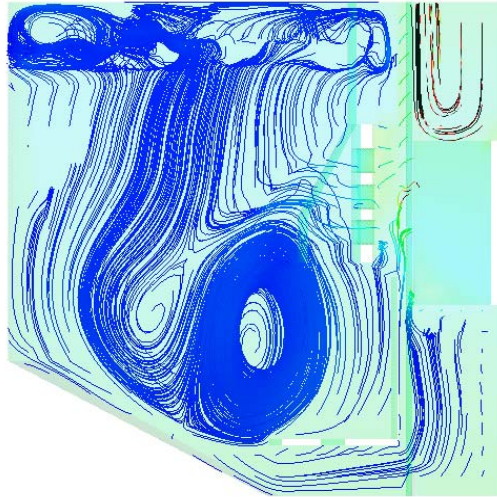
The eddies below and above the hood (white arrows in figure 33) and also the lack of air flow through the hood are clearly visible. The eddies and lack of air through the hood, indicated that the CFD analysis was giving reliable results as far as flow patterns were concerned and based on this results the three phase flow analysis (water, air and solids) was initiated.

4.3.2. Multiphase results.



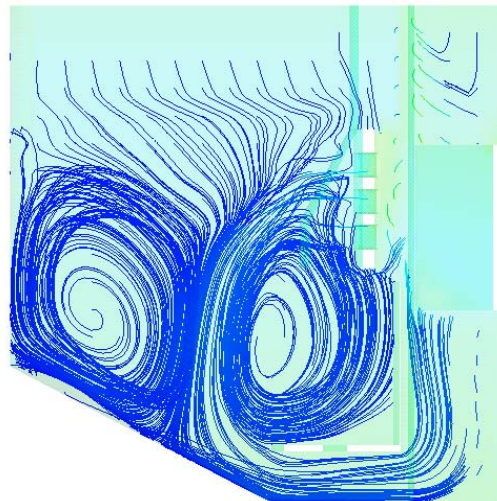
CFX

Figure 34: Streamline plot for phase 1.



CFX

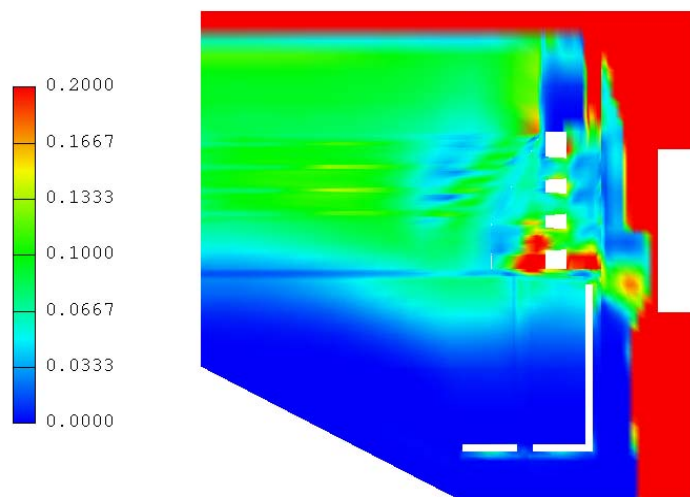
Figure 35: Streamline plot for phase 2.



CFX

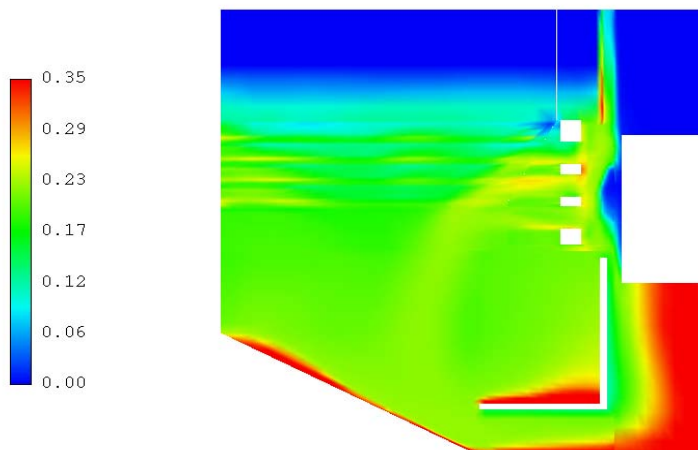
Figure 36: Streamline plot for phase 3.

4.3.3. Hydrodynamic and metallurgical results.



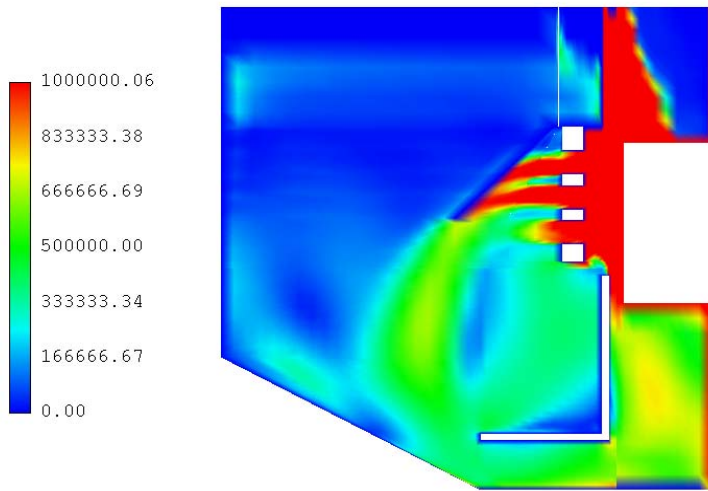
CFX

Figure 37: Scaled contour plot of phase 2 volume fraction distribution.



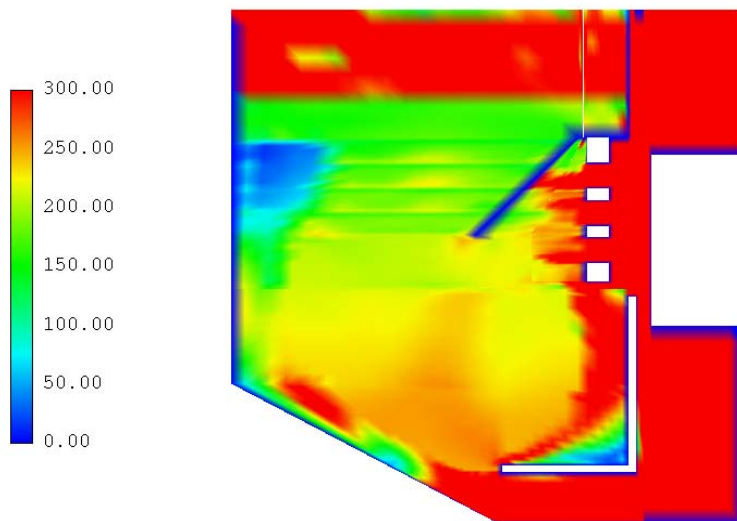
CFX

Figure 38: Scaled contour plot of phase 3 volume fraction.



CFX

Figure 39: Scaled contour plot of the pulp Reynolds number.



CFX

Figure 40: Scaled contour plot for controlled volume Reynolds number.

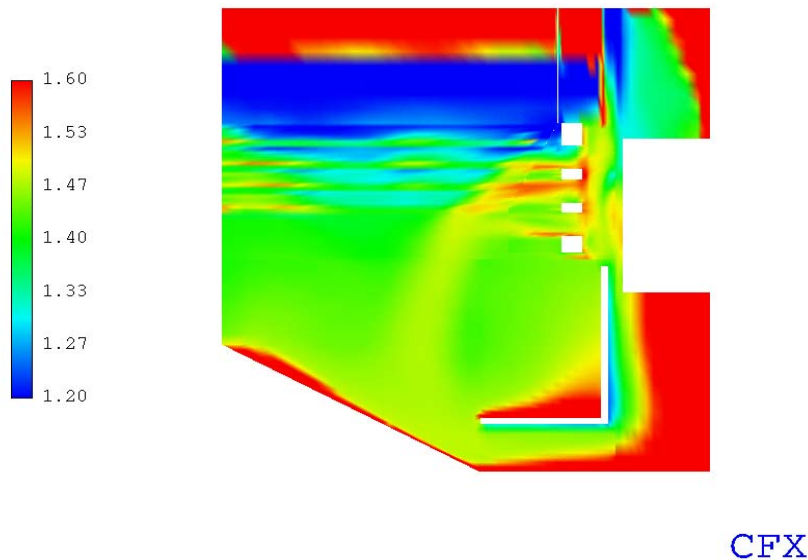


Figure 41: Scaled contour plot of pulp density.

4.4. Mathematical procedure to calculate the mineral recovery rate potential.

This section describes the mathematical procedure incorporated into the CFX Fortran user subroutines to calculate the potential or possibility of mineral recovery inside a WEMCO 120 mineral flotation cell. The method is applied during the multiphase flotation cell CFD simulations.

Tabulated data (Table 19) provided by the client of the mineral recovery potential is used to calculate the recovery potential at control volume centres in the computational domain. This data includes the recovery rates potential as a function of a few global parameters namely Reynolds number, relative aeration rate and pulp density number. The application and implementation of each of the parameters given by the client is discussed below.

4.4.1. Continuous fluid vs. discrete flow element.

The fluid parameters applied in the mineral recovery potential calculations include Reynolds number, pulp density and relative aeration rate. These parameters, given in the form presented by the client, are calculated using the global flotation cell characteristics. Since we obtain detailed local field results from the CFD simulations it is important to recalculate these fluid parameters for a local control volume scale but in the process ensuring that their original global scale remains relevant. Once this is done, we

may assume that the fluid properties and conditions as given by the client data will remain relevant and applicable although they are applied to the control volume scale.

4.4.2. Pulp density.

The client defines a pulp density number as:

$$S_{gp} = \frac{\rho_p}{\rho_w} \quad (77)$$

For calculation of fluid parameters, the local pulp density at control volume centres is calculated for the CFD simulation from:

$$\rho_{cv} = \frac{\alpha_f \cdot \rho_f + \alpha_m \cdot \rho_m}{\alpha_f + \alpha_m} \quad (78)$$

The pulp density number at control volume centres then becomes:

$$\rho_{p_{cv}} = \frac{\rho_{cv}}{\rho_w} \quad (79)$$

4.4.3. Reynolds number.

The Reynolds number given and calculated by the client is based upon the impeller tip speed, the impeller tip diameter as well as pulp density and viscosity i.e.:

$$Re = \frac{\rho_p \cdot v_t \cdot d}{\mu_p} \quad (80)$$

Where the subscripts p_p denotes the pulp phase and subscript t denotes the impeller tip position. At each control volume in the CFD computational domain, the local speed and volume fraction for each phase is available from the simulation results. For the calculation of the local control volume Reynolds number a new Reynolds number is defined as:

$$Re_{cv} = \frac{\rho_{cv} \cdot v_{cv} \cdot d}{\mu_{cv}} \quad (81)$$

Where

$$\mu_{cv} = \mu_f \quad (82)$$

and

$$V_{cv} = \frac{V_f \cdot \alpha_f + V_m \cdot \alpha_m}{\alpha_f + \alpha_m} \quad (83)$$

The subscript 'cv' denotes control volume scale and subscript 'f' and 'm' denote continuous fluid and mineral particle respectively. The viscosity value represented by equation (80) should strictly speaking be the pulp viscosity but are maintained at the initial fluid viscosity for simplicity. The new Reynolds formulation equation (81) ensures that if fluid properties at local control volume centres are similar to flow conditions represented by a Reynolds number based on Equation (80), then the local Reynolds numbers calculated with equation (79) will give a similar value. Subsequently the tabulated client data will remain relevant and applicable.

4.4.4. Relative aeration rate.

The relative aeration rate as provided by the client is based on the ratio of volume flow rate of air at the impeller inlet draft tube to the volume flow rate of pulp in the flotation cell i.e.:

$$\frac{q_a}{q_p} = \frac{v_a \cdot A_{si}}{v_p \cdot A_c} \quad (84)$$

where v_a is the average impeller inlet air velocity and v_p is the average outlet pulp velocity. A_{si} denotes the impeller air standpipe diameter and A_{cell} denotes the outlet area for pulp flow. For the calculation of the local relative aeration rate at control volume centres Equation (84) becomes:

$$\frac{q_{acv}}{q_{pcv}} = \frac{v_{acv} \cdot A_{si}}{v_{pcv} \cdot A_c} \quad (85)$$

The local airflow speed is denoted by v_{acv} and the local pulp speed denoted by $v_{pcv} = v_{cv}$. Since Equation (85) is also based on the draft tube area and pulp outlet area similar values will be found compared to values from Equation (84) if the air/pulp velocity ratio is similar. Again, this ensures that the tabulated client data remains relevant and applicable.

4.5. Interpolation of Recovery rate potential data supplied by client.

4.5.1. Interpolation method.

The mineral recovery rate potential data provided by the client is shown in Table 19. The data given for recovery rate potentials are tabulated against specific values of pulp density, flotation cell Reynolds number, relative aeration rate and chemical composition. Since chemical composition is not included in the CFD simulation it was excluded from the analysis. In order to use the recovery rate potential data at local control volume

centres in the computational domain, it is necessary to interpolate recovery rate potential values at pulp density, relative aeration rate and Reynolds number values that lie between the given tabulated values. In order to achieve this, a three-dimensional bilinear interpolation was employed. This method allows one to find interpolated values of recovery rates potential at different pulp densities, Reynolds numbers and relative aeration rate than those tabulated. Should any of the independent variables fall outside the tabulated range then the subsequent interpolated recovery rate potential values are discarded.

Table 19: Recovery rate potential based on plant data.

Q_a/Q_p	$S_{gp} = 1.6$				
0.21	75	70	60	50	40
0.17	85	80	70	60	50
0.13	95	85	75	65	45
0.08	95	85	75	65	45
0.04	85	80	60	50	35
	500	1000	10^4	10^6	10^9

Reynolds Number

Q_a/Q_p	$S_{gp} = 1.4$				
0.21	80	75	65	55	45
0.17	90	85	75	65	55
0.13	100	95	90	70	50
0.08	100	95	90	70	50
0.04	90	85	70	60	40
	500	1000	10^4	10^6	10^9

Reynolds Number

Q_a/Q_p	$S_{gp} = 1.2$				
0.21	70	65	55	45	35
0.17	80	75	65	55	45
0.13	90	80	70	60	40
0.08	90	80	70	60	40
0.04	80	70	50	40	30
	500	1000	10^4	10^6	10^9

Reynolds Number

4.5.2. Sample calculation for control volumes.

4.5.2.1. Flotation cell characteristics.

Impeller diameter: $d = 0.66\text{m}$

Impeller standpipe inlet diameter: $d_i = 0.795\text{m}$

Flotation cell diameter: $D = 3.02\text{m}$

Standpipe inlet area: $A_{si} = \pi \frac{d_i^2}{4}$ $A_{si} = 0.496\text{m}^2$

Actual cell projected area: $A_c = \pi \frac{D^2}{4}$ $A_c = 7.163\text{m}^2$

4.5.2.2. cal fluid properties at control volume centre.

Liquid phase volume fraction: $\alpha_f = 0.65$

Liquid phase density: $\rho_f = 998.0\text{kg.m}^{-3}$

Liquid phase velocity magnitude: $U_f = 0.55\text{m.s}^{-1}$

Liquid phase viscosity: $\mu_f = 1.003 \cdot 10^{-3}\text{kg.m}^{-1}\text{s}^{-1}$

Air phase volume fraction: $\alpha_a = 0.13$

Air phase density: $\rho_a = 1.18\text{kg.m}^{-3}$

Air phase velocity magnitude:	$U_a = 0.6\text{m}\cdot\text{s}^{-1}$
Air phase viscosity:	$\mu_a = 1.8\cdot 10^{-3}\text{kg}\cdot\text{m}^{-1}\text{s}^{-1}$
Air bubble diameter:	$d_b = 1\cdot 10^{-3}\text{m}$
Solid phase volume fraction:	$\alpha_m = 0.22$
Solid phase density:	$\rho_m = 3100\text{kg}\cdot\text{m}^{-3}$
Solid phase velocity magnitude:	$U_m = 0.52\text{m}\cdot\text{s}^{-1}$
Solid particle diameter	$d_m = 2\cdot 10^{-4}\text{m}$

4.5.2.3. Calculation of interpolated recovery rate.

Pulp density:	$\rho_p = \alpha_f \cdot \rho_f + \alpha_m \cdot \rho_m$	$\rho_p = 1330.7\text{kg}\cdot\text{m}^{-3}$
Pulp density number:	$S_{gp} = \frac{\rho_p}{\rho_f}$	$S_{gp} = 1.33$
Pulp viscosity:	$\mu_p = \mu_f$	
Pulp velocity magnitude:	$U_p = \frac{U_f \cdot \alpha_f + U_m \cdot \alpha_m}{\alpha_f + \alpha_m}$	$U_p = 0.542\text{m}\cdot\text{s}^{-1}$
Local cell Reynolds number:	$Re_{cv} = \frac{\rho_p \cdot U_p \cdot d}{\mu_p}$	$Re_{cv} = 475767$
Local cell air volume flow rate number:	$q_{acv} = U_a \cdot A_{si}$	$q_{acv} = 0.298\text{m}^3\cdot\text{s}^{-1}$
Local cell pulp volume flow rate number:	$q_{pcv} = U_p \cdot A_c$	$q_{pcv} = 3.89\text{m}^3\cdot\text{s}^{-1}$
Local cell relative aeration rate:	$q_{ra} = q_{acv}/q_{pcv}$	$q_{ra} = 0.077$

Thus from the pulp density number, the relative aeration rate and Reynolds number we find from Table 19 and bi-linear interpolation, the value for the mineral recovery rate potential is 72%.

The interpolation of recovery rate potential values is carried out during the simulation in the Fortran user coding. The results are shown below. The interpolated recovery rate potential values provide firstly a mechanism to evaluate the existing recovery characteristics of various areas within the flotation cell.

From the predicted values one may determine whether a change in design or design specifications is actually increasing the efficiency of the mineral flotation. Furthermore, it provides a tool to establish and evaluate a new recovery rate potential CFD model based on the bubble-particle collision frequency. This model is described below.

4.6. Bubble particle collision frequency.

The efficiency of the flotation characteristics of a flotation cell depends on the probability of bubble-particle attachment during bubble-particle collisions. Therefore the probability of bubble-particle collisions is an important parameter in evaluating flotation cell efficiency. Schubert and Bischofberger (1998) applied an expression proposed by Abrahamson (1975) and as presented by Schwarz et al. (2000) of the collision rate of bubbles and particles to flotation cells. This expression reads:

$$Z_{pb} = 5 \cdot N_m \cdot N_a \left\{ \frac{d_m + d_b}{2} \right\} \cdot \{U_m^2 + U_a^2\}^{0.5} \quad (86)$$

where N_m and N_a is the mineral particle and air bubble number concentration respectively and d and d_b denotes the mineral particle and air bubble diameter respectively. U_m is the relative velocity between the mineral particle and the continuous phase and U_a is the relative velocity between the air bubble and the continuous phase.

When this expression is used in conjunction with the interpolated recovery rate potential data, a new function may be established which gives the mineral recovery rate potential as a function of bubble-particle collision. This may be done since the interpolated recovery rate potential values in the cell follow the collision frequency trend as shown in the superimposed plot in Figure 48. By plotting the interpolated recovery rate potential data described above against the bubble-particle collision frequency at the same location in the flotation cell, and fitting a curve through the data one finds a new function for the mineral recovery rate potential as a function of collision frequency. The resultant function is,

$$Q_{rrp} = A \{Z_{pb}\}^2 + B \{Z_{pb}\} + C \quad (87)$$

Where $A = -2.04 \times 10^{-22}$, $B = 2.84 \times 10^{-10}$ and $C = -0.1851$, determined from the curve fit.

4.7. Streamline plots.

Figure 34 to Figure 36 show the streamline distributions for each of the three phases. The streamline plots clearly supports the above arguments further. The plots indicate the circulation zones inside the flotation cell also shown by the velocity vector plots. The liquid phase sets up two strong circulation zones arising from the channelling of the flow downwards from the disperser hood. The solid particles are entrained in these circulation zones. The bubbles are also circulated in the inner circulation zone closest to the impeller bottom draft tube. The bubbles however leave the outer recirculation zone since the buoyancy force dominates their trajectory.

4.8. Volume fraction distribution.

Figure 37 and Figure 38 show the volume fraction predictions for phases two and three. The liquid phase is relatively equally dispersed throughout the flotation cell except at the impeller top inlet area and the outer top surface. Air is sucked in through the top of the impeller and leaves the flotation cell through the top de-gassing boundary. The induced air suction of the impeller seems to be accurately simulated. The scaled distribution plot of the air phase volume fraction indicates that the distribution of air bubbles through the remainder of the flotation cell is of the order of 1%. Although this volume fraction seems low, it still corresponds to approximately 19×10^6 bubbles per cubic metre. The solid particles are also distributed relatively equally throughout the internal area of the flotation cell. Since the solid particles are heavier than the liquid phase it is expected to settle on the bottom surfaces. This is clearly shown in the scaled volume fraction plot of the solid phase. Particles tend to concentrate on the bottom floor as well as the false floor. Particles also concentrate near the impeller bottom shaft section.

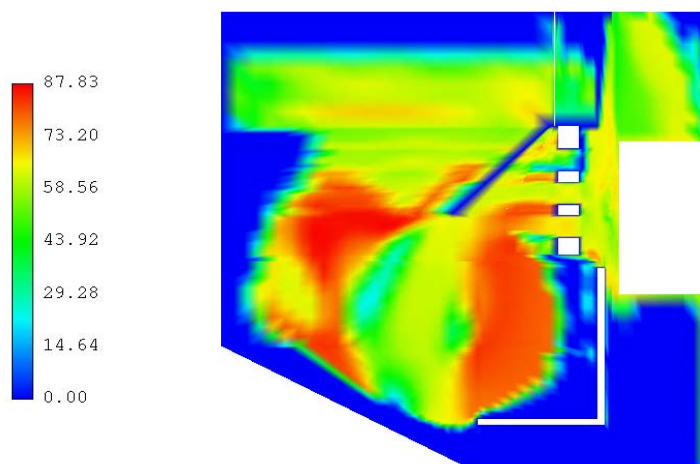
4.9. Pulp Reynolds number.

Figure 39 shows the pulp Reynolds number plot for the flotation cell. Figure 40 shows the control volume Reynolds number as per Equation (81). The plots show that the pulp Reynolds numbers are high in the agitation zone and become progressively less towards the collection zone.

4.10. Pulp density distribution.

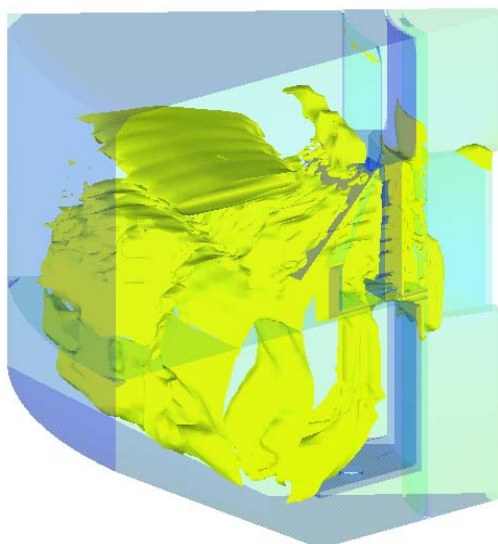
Figure 41 show the contour plot of the relative density as defined by Equation (76). These are shown to indicate the areas where the Foskor recovery rate data and subsequently the interpolated recovery rate values are applicable namely $1.2 < S_{gcv} < 1.6$.

4.11. Bubble particle collision frequency and probability for successful recovery.



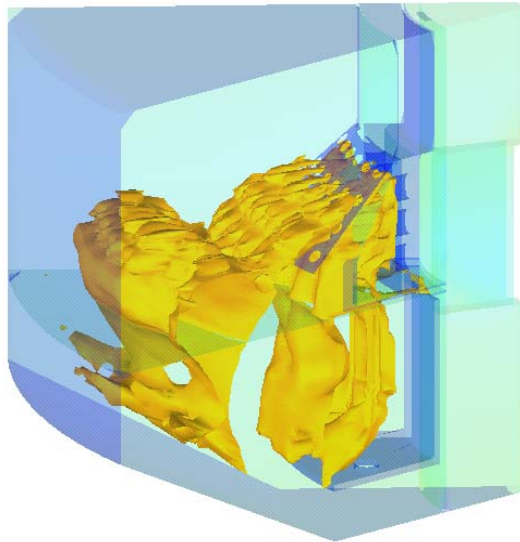
CFX

Figure 42: Showing the contour plot for the interpolated mineral recovery success rate.



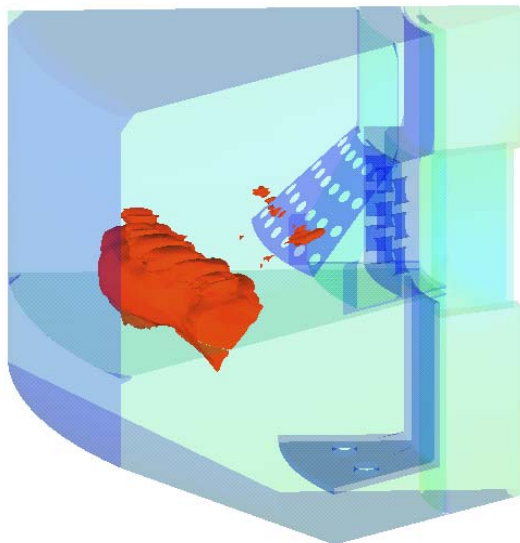
CFX

Figure 43: Iso-surface plot for a 65% interpolated mineral recovery success rate.



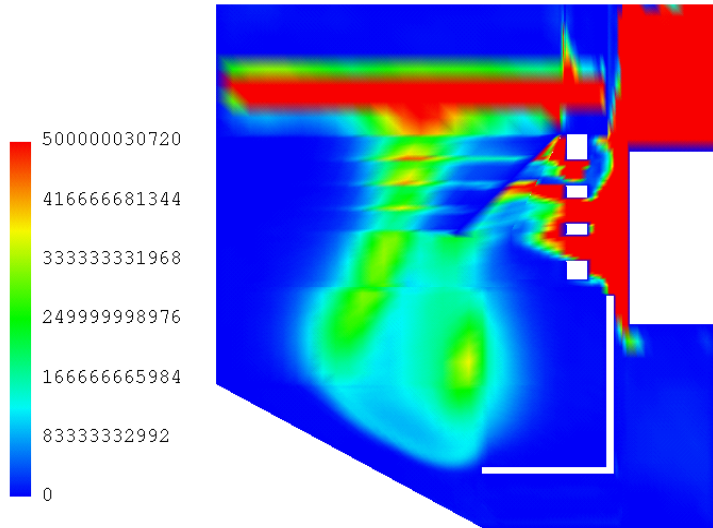
CFX

Figure 44: Iso-surface plot for a 75% interpolated mineral recovery success rate.



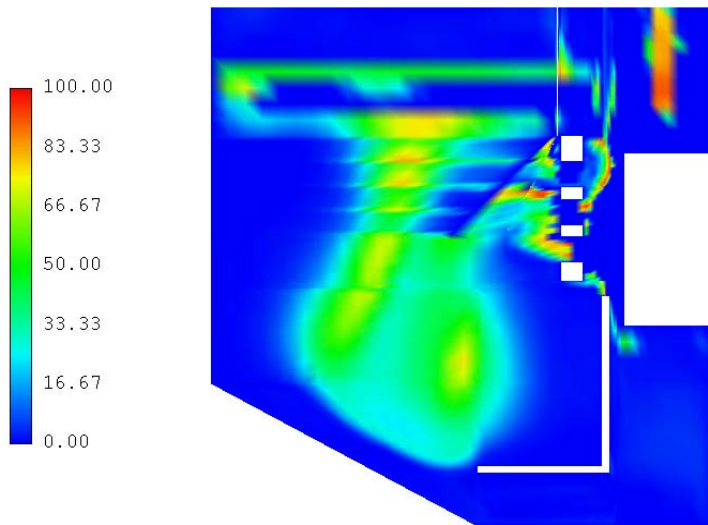
CFX

Figure 45: Iso-surface plot for a 85% interpolated mineral recovery success rate.



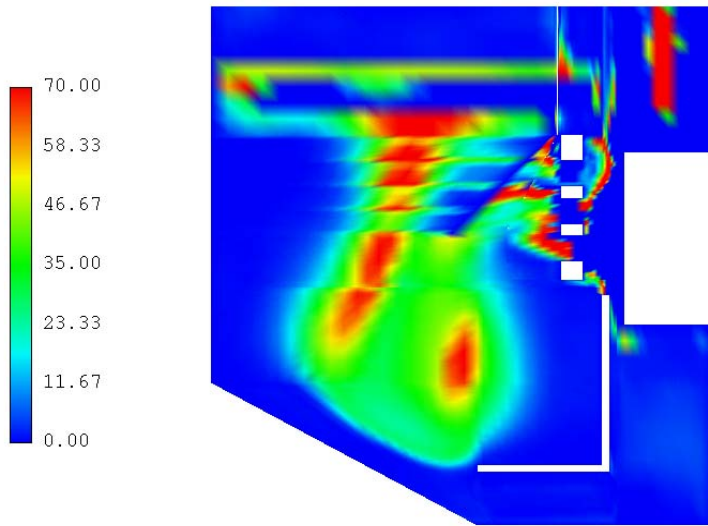
CFX

Figure 46: Contour plot of bubble-particle collision frequency.



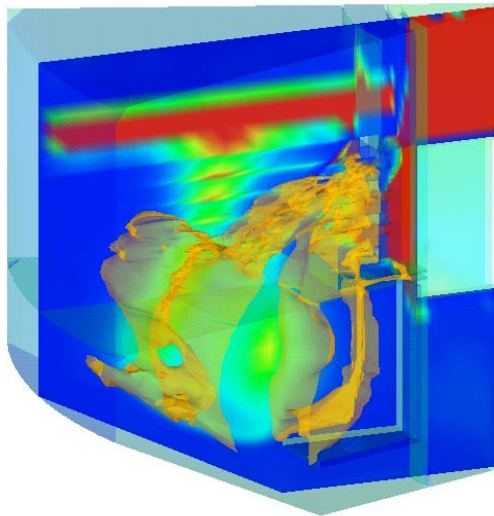
CFX

Figure 47: Recovery success rate based on bubble particle collision frequency.



CFX

Figure 48: Scaled recovery success rate based on bubble-particle collision frequency.



CFX

Figure 49: Iso-surface of 75% interpolated recovery success rate mapped to bubble-particle collision frequency.

4.12. Interpolated mineral recovery rate potential.

Figure 42 shows the contour plot for the interpolated mineral recovery success rate distribution for the flotation cell. These values were found from interpolation of the data supplied by the client and as discussed earlier. The plot shows that the mineral recovery rate is highest below and to the left of the disperser hood area. This is also the area where the bubble Reynolds numbers are smaller than 300. The bubble Reynolds number and the interpolated recovery rate show the same trends. It seems that high bubble Reynolds numbers ($Re_b > 250$) corresponds to low recovery probably due to continued agitation. The particles will probably not remain attached in this zone under such high slip velocities. However, for bubble Reynolds numbers smaller than 250, it is evident that the contours of interpolated recovery rate closely match the shape of the contours of bubble Reynolds numbers.

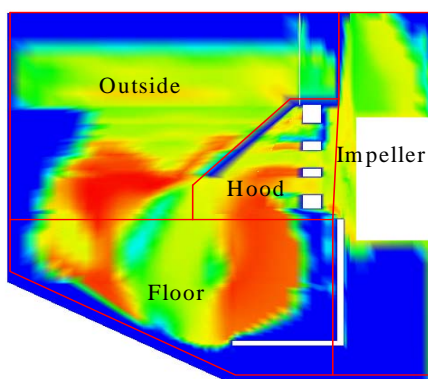
The pulp Reynolds number does not show the same significance or trend. It is therefore believed that the bubble Reynolds number may be a better evaluation parameter for CFD simulation.

Figure 43 to Figure 45 show the iso-surface plots of the interpolated recovery success rate. It shows a good and even distribution of recovery success rates of 65% throughout the flotation cell. The higher recovery success rates (85%) are predominantly located outside the disperser hood area. This corresponds to the collection zone, where the high recovery success rate area also has highest volume fraction of air bubbles inside the flotation cell and a bubble Reynolds number of smaller than 250 and an even pulp density distribution.

Figure 46 shows the bubble-particle collision frequency as calculated from Equation (82). This plot shows clearly the same contour trend as the interpolated recovery rate contour plot. It is clear that this parameter is an important one to add to the relevant parameters required for efficient recovery of solid particles. Not only does the general trend follow the area where the highest recovery rates area found.

Figure 47 and Figure 48 show the recovery rate values found from using Equations (86) and (87). These recovery rates do show the same trend as the interpolated recovery success rates shown in Figure 42. The importance and relevance of the bubble-particle collision rate in determining the recovery success rate is shown again in Figure 49. Here the iso-surface plot of 75% interpolated recovery success rate is plotted on top of the slice plot of the bubble-particle collision contours. This shows that the areas of high actual recovery success rate found from the client data do match the areas of the theoretical bubble-particle collision frequency.

From the present CFD simulation it is also possible to calculate the volume averaged interpolated recovery rate values for four different zones. The volume averaged values from the CFD simulation is shown in Table 20. The location of each of the zones is shown in Figure 50. The impeller zone includes the top and bottom inlet impeller draft tubes as well as the impeller, the hood zone includes the area within the perforated hood towards the impeller, the floor zone is the cell volume below the perforated hood zone and the outside zone includes the area outside of the perforated hood but above the floor zone.



CFX

Figure 50: Flotation cell zone description.

Table 20: Volume average recovery.

Zone description	Volume averaged recovery rate (%)
Impeller zone	28.32
Hood zone	65.81
Floor zone	42.17
Outside zone	42.15

These values indicate that, although the highest recovery rates area found outside to the left of the disperser hood area, as per Figure 50, the most effective recovery in terms of effective volume is found within the disperser hood zone.

4.13. Summary of CFD results.

- The possibility exists that the disperser and hood in the standard Wemco design may strip the pulp from its air and indirectly stripping it from its mineral package too. By modifying the hood and disperser slots, plus adding a separation disc on the rotor displaced the eddies towards the false bottom thereby improving the conditions required for quiet zone protection. Further analysis of the recovery rate potential also indicated a marked improvement in the 75% iso-surface.
- Perspex modelling is a useful tool to study aeration, air dispersion, streamlines, eddies and vortex stability.
- Deglon et al. (2000) and Nelson and Lelinski measured and calculated the air hold-up for the Wemco to be between 7%-12%. Figure 29 shows a 3%-17% air hold-up which compares very favourable with the published results. Therefore the aeration number of $Q_a = q_a/\omega d^3 = \text{idem}$ is an acceptable scale-up number. A aeration number of $Q_a = 4.6 \times 10^{-4}$ is equal to an air hold-up of $4.6 \times 10^{-4} \cdot \omega = Q_a/D^3 = 10.6\%$.
- Figure 39 shows a rotor tip Reynolds number in the agitation zone to vary between 7×10^6 to 9×10^6 . These numbers were calculated with water density (1000kg/m^3) and viscosity ($1 \times 10^{-3} \text{kg/ms}$). When adjusted with a pulp density of 1300kg/m^3 and a viscosity of $1.6 \times 10^{-3} \text{kg/ms}$ then the Reynolds numbers reduce to 5×10^6 to 7×10^6 which corresponds very well with practical calculated results.
- The relatively low bubble Reynolds number can have a favourable effect on bubble particle attachment as this Reynolds number is in the laminar range.
- Figure 39 also shows a very sharp dissipation of the Reynolds number, which corresponds well with the observations done by Deglon et al. (2000) and Newel and Grano(2007). This is substantially higher than the superficial Reynolds number calculated. It seems that the numerical value for superficial Reynolds number should be increased by about 50% for scale-up purposes.
- The favourable comparison between the interpolated recovery rate potential and the bubble particle collision frequency was a surprising discovery as practical results in the plant were rearranged by swapping 100% probability of a 60% recovery to a 60% probability of a successful recovery.
- The threshold RPM in the Perspex models corresponds with the Wemco hydrodynamic information.

CHAPTER 5: APPLICATION OF SCHEDULE OF DIMENSIONLESS NUMBERS TO A PHOSPHATE PLANT.

5.1. Background.

The Phalaborwa complex is an igneous complex that was discovered by Dr Hans Merensky in the 1940's. Foskor was established shortly after this discovery in 1952. The ore is predominantly Ca-Mg-combinations with chlorides and fluorides as problem process components. The plant started with two 50 tons per hour rod mills and a flotation plant equipped with 1.5m³ Denver cells. Being removed from the South African Industrial hub the management established one of the best equipped laboratories and pilot plants north of Pretoria. During the 1960's the mill plant was extended to 12 x 50 tons per hour rod mills and the flotation plant was also extended to include about 150 x 1.5m³ Denver cells. In the 1970's the mill plant was extended again to include another 12 x 100 tons per hour rod mills and the flotation plant to about 180 x 8.5 m³ Wemco units. The plant was divided into three sections as each section processed a different ore combination. The three types of ore are shown in Appendix 6 specification sheet 1 to 3. The reason was that the three types of ore required three different types of reagent suites. This pushed the throughput to about 3000 tons per hour and at 7.5% P₂O₅ head grade produced 3 million tons concentrate at 37% P₂O₅.

The rest of the plant consisted of thickeners, filters, drying, dispatch and tailings handling. In this case study the focus was on the pyroxenite section. From its inception the plant operated at 75% recovery and 37% concentrate grade, while the pilot plant performed at a 95% recovery and 40% concentrate grade with the same mineralogy. The performance of the main plant stayed the same irrespective of ore type, machine type and machine size. This represented about R100m/a revenue loss at that stage. In 2002 the plant was analysed according to the principles and technique described in this thesis and the results are described in the rest of this Chapter.

In order to develop some methodology to accumulate all the relevant information, a specification sheet was used that prompts the metallurgist to enter the information in such a way as to facilitate the comparison of the various scale-up factors between pilot plant and full scale plant. The specification column is normally pilot plant information. To demonstrate how to compile the specification sheet, a phosphate mineral in a Denver pilot plant will serve as an example.

5.2. Geology.

The outcrops of the Phalaborwa complex belong to rocks of the plutonic origin. No volcanic equivalents are found, which means that great volumes of this complex have been eroded away. This complex consists predominantly of pyroxenite (igneous) rocks, with intruded granites and gneisses. Three prominent pipe-like features with concentric structures flow into one another, forming lobes, named the Northern pyroxenite, Loolekop and Southern pyroxenite. The Loolekop lobe is an old volcanic structure and contains approximately 0.8% copper, 20% magnetite, 5% apatite, phlogopite and small amounts of Gold, Silver and Thorium.

5.3. Pilot plant conditions.

5.3.1. Pilot plant lay-out.

The pilot plant was established to provide Foskor with the ability to develop a unique process with unique reagents as the industrial circumstances were such that no information was available to the Foskor at that stage and had to develop the process from what was available in the country in 1952. Denver equipment was available and a standard lay-out was established and configured as shown in Figure 50. Reagents were much different then and had to be prepared on site sodium silicate, guar and the process was also heated because of the availability of access steam as Foskor generated its own electricity in the 1950's and 60's.

5.3.2. Mineralogy.

The mineralogy of this complex is shown in Appendix 6. The mineralogy is important in the scale-up phase as it indicates the type of reagents to target and also provides valuable information for plant pump systems and milling circuit design. In this case the magnetite and diopside require a line-velocity of more than 3m/s to prevent settling and also require special milling conditions. The phlogopite and Calcite compete with the apatite for fatty acid and therefore special suppressants will have to be developed for these minerals.

5.3.3. Operational Information and flow diagram.

5.3.3.1. Operational conditions.

The pilot plant is equipped with continuous pulp density meter and mass flow meter and feed, tails and concentrate are sampled every hour. Analysis are done on every sample and a composite is prepared at the end of every day and analysed by a second

accredited laboratory. This laboratory is the laboratory responsible for final analysis of all plant samples before dispatch.

Table 21: Summary of pilot plant operational conditions.

Parameter	Value	Units
Pulp density	1460	kg.m ⁻³
Pulp viscosity	1.8x10 ⁻³	kg.m ⁻¹ .s ⁻¹
Feed rate	700	kg.h ⁻¹
Milling (P ₈₀)	250	m ³ x10 ⁶
Cell Volume	85	m ³ x10 ³
Conditioner volume	118	m ³ x10 ³
Power input	500	kW

5.3.3.2. Flow diagram.

The flow diagram in this case is the classical single row rougher (3 x Denver#8), scavenger (2 x Denver#8), cleaner (2x Denver#8) and recleaner (1 x Denver#8) circuit as indicated in Figure 51. The Denver design is typical with weir overflow and high aspect ratio rotor. A high T_aT_u conditioner is employed with inline pulp density meter.

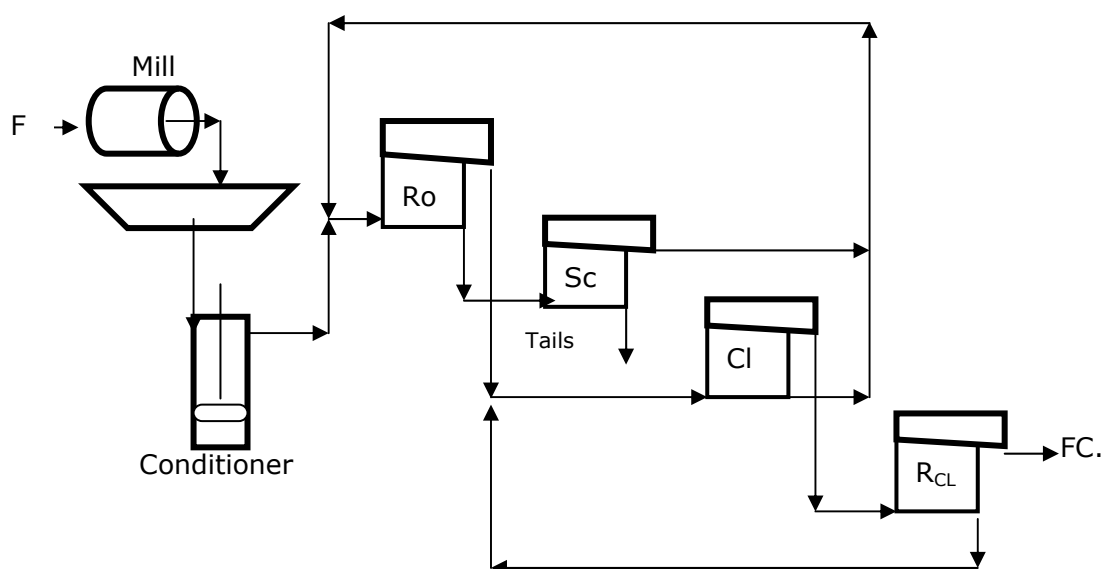


Figure 51: Flow diagram for pilot plant.

5.3.4. Reagent dosage.

The log sheets from the pilot plant operator will give the information as in Table 22.

Table 22: Typical pilot plant log sheet.

Time	FA(g/t)	SA(g/t)	TPH	S _{gp}	Feed	Conc. %	Tails %	Rec. %
8H	292	167	.72	1,46	7.0	40.4	0.3	96.4
9H	333	167	.72	1,45	6.7	40.3	0.5	93.7
10H	329	164	.73	1,46	6.8	40.0	0.1	98.8
11H	333	167	.72	1,46	7.4	40.3	0.1	98.9
12H	329	164	.77	1,45	7.2	40.2	0.5	94.2
13H	329	164	.72	1,46	7.0	40.1	0.7	91.6
14H	333	167	.72	1,45	6.7	39.8	0.3	96.3
15H	329	164	.73	1,46	7.0	40.7	0.5	94.0
Average	326	166	.73	1,46	7.0	40.2	0.4	95.5

FA = Fatty acid : SA = Sulphonic Acid.

This log sheet represents 8 hours operation where samples were taken every hour. Feed (tons per hour), pulp specific gravity (S_{gp}), feed grade (F), concentrate grade C, and tailings grade (T) were determined. Recovery was calculated according to the formulae $R = C(F-T)/F(C-T)$. The pyroxenite ore does not contain diopside or magnetite and therefore does not require depressants, such as poly-glycol ether and sodium silicate. In this case the Fatty Acid is the collector and the sulphonic acid is a depressant for phlogopite.

5.3.5. Liberation.

Samples from the feed are screened to determine the full particle size distribution and the percentage of product per fraction. This model will be compared with the recovery model at a later stage to determine whether the milling circuit is producing a particle

size, which is conducive to maximum recovery. Figure 52 gives an indication of what this models looks like for pyroxenitic ore.

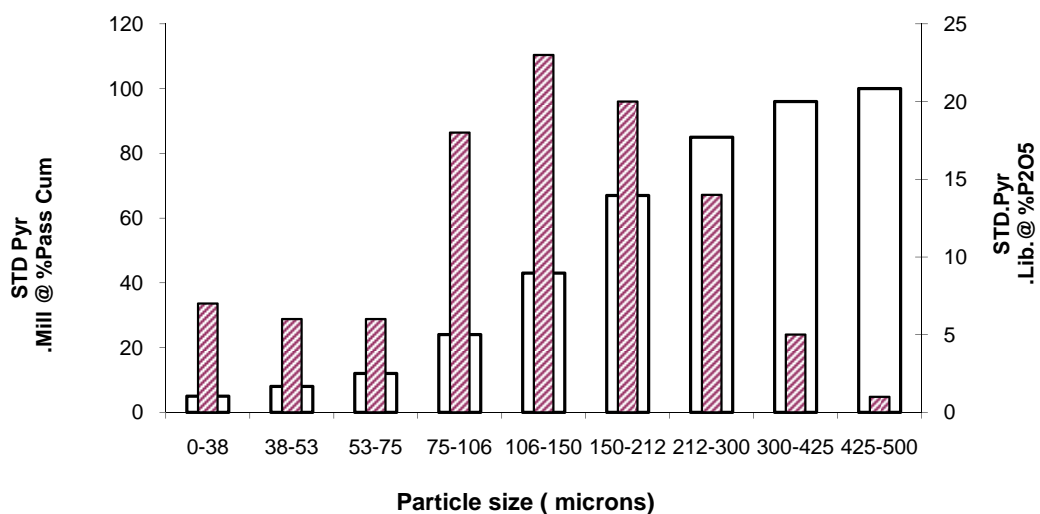


Figure 52: Particle size distribution (blank bars) and P₂O₅ distribution (dashed bars) in the feed to flotation.

Figure 52 clearly shows a P₈₀ of about 250µm and that most of the valuable mineral, about 94%, reports in the -300µm fraction.

5.3.6. Conditioning model.

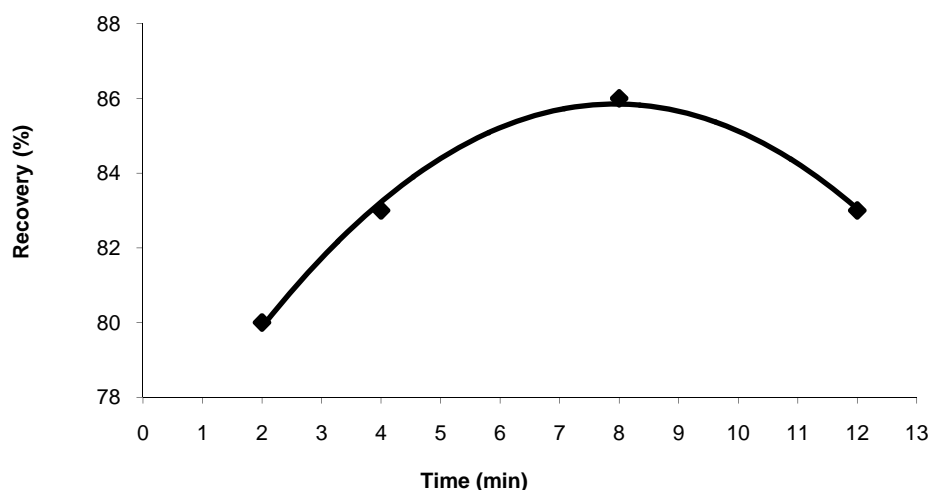


Figure 53: Laboratory model for recovery vs. conditioning for pyroxenite ore.

The mass fraction of the solids at 1460 kg/m^3 is equal to:

$$\begin{aligned}\Phi_s &= (S_{gm}/S_{gm}-1) \cdot (S_{gp}-1/S_{gp}) \\ &= 1.5 \cdot (0.46/1.46) \\ &= 0.472\end{aligned}$$

The total fresh feed volume flow (without circulating load) is equal to;

$$\begin{aligned}q_p &= \text{Feed}/(\phi_s \cdot S_{gp} \cdot 3600) \\ &= 0.700/(0.472 \cdot 1.46 \cdot 3600) \\ &= 3 \times 10^{-4} [\text{m}^3/\text{s}]\end{aligned}$$

Therefore the average conditioning time (η) is:

$$\begin{aligned}C_0T &= (\text{conditioner Volume})/q_p [\text{s}] \\ &= 0.118/3 \times 10^{-4} \\ &= 393 [\text{s}] \text{ (6.6 min)}\end{aligned}$$

Conditioner mechanism $\theta = 7$. As the model in Figure 53 was generated in the laboratory the practical calculation of 6.6 minutes corresponds very well with the maximum of 8 minutes.

5.3.7. Retention Time model.

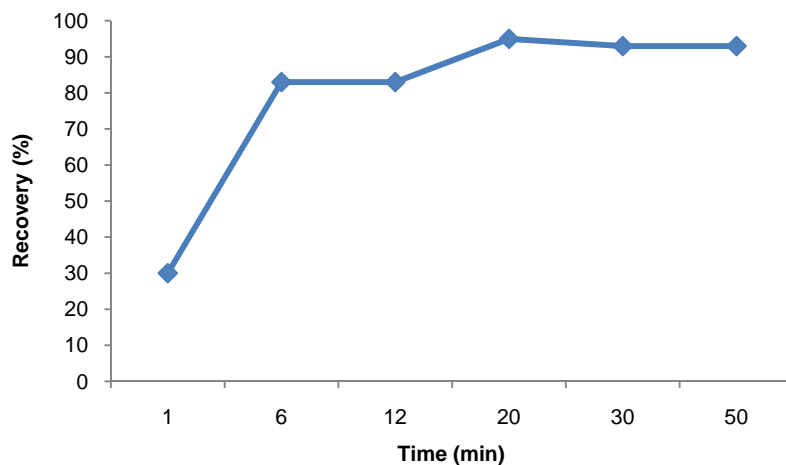


Figure 54: Laboratory model for Recovery vs. Retention time for pyroxenite.

Retention time is calculated in the cells where the initial recovery takes place, that is the roughers and scavengers plus circulating load equal to 30% fresh feed:

$$\begin{aligned}\tau &= (\text{Rougher \& Scavenger volume})/q_p \\ &= (5 \cdot 0.085)/(3 \times 10^{-4} \cdot 1.3) \\ &= 1089[\text{s}] (18.1\text{min})\end{aligned}$$

It is sometimes necessary to make an estimation of the circulating load by consulting the pump system curves and that must be included in the feed. Again in this case the practical calculated value corresponded very well with the laboratory results of 20 minutes.

5.3.8. Volumetric Capacity.

The volumetric capacity is defined as:

$$\begin{aligned}\text{VC} &= (\text{Cleaner \& Recleaner volume})/(\text{Rougher \& Scavenger volume}) \\ &= 3 \cdot (0.085)/[5 \cdot (0.085)] \\ &= 0.6\end{aligned}$$

This value needs to be verified by mass balance calculations. Simple generic models based on one of the kinetic models produce acceptable results.

5.3.9. Froth Depth.

Figure 55 shows the laboratory results for a pyroxenite mineral and gangue. An interesting discovery was the behaviour of magnesium and potassium with the two inflection points at 5% and 10% cell depth. The pilot plant trials showed that the roughers were running at 10% cell depth and the cleaners were running at 5% cell depth. This is contradictory to the classical froth depth model and it stresses the point to analyse for mineral, gangue and secondary gangue. The behaviour of the magnesium and potassium could not be explained at the time of the experiment. The value of this discovery was that the contradiction to the classical model could be explained.

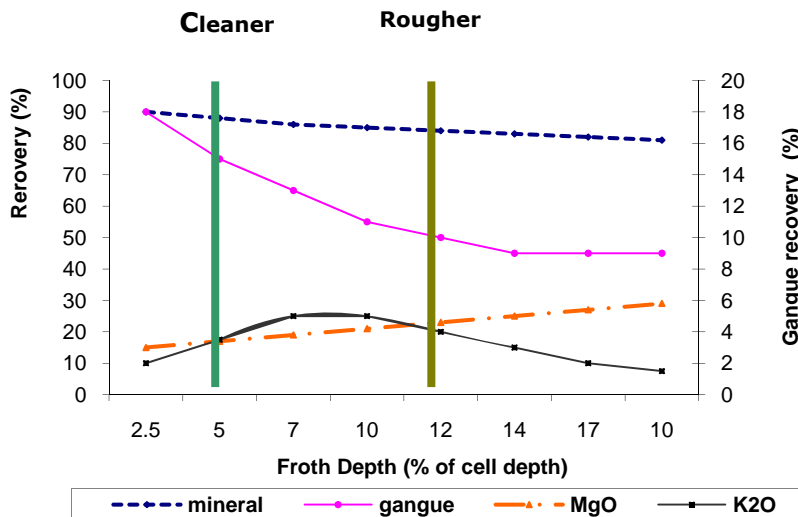


Figure 55: Froth depth model developed for pyroxenite ore in the laboratory.

It clearly shows that both roughers and cleaners can run at shallow depth because of the low gangue (potassium and magnesium) recovery.

5.3.10. Recovery vs. Liberation.

The best particle size distribution from Figure 56, is where P_2O_5 recovery is maximum. For more than 80% recovery this coincides with a particle range +38 μ m and -212 μ m.

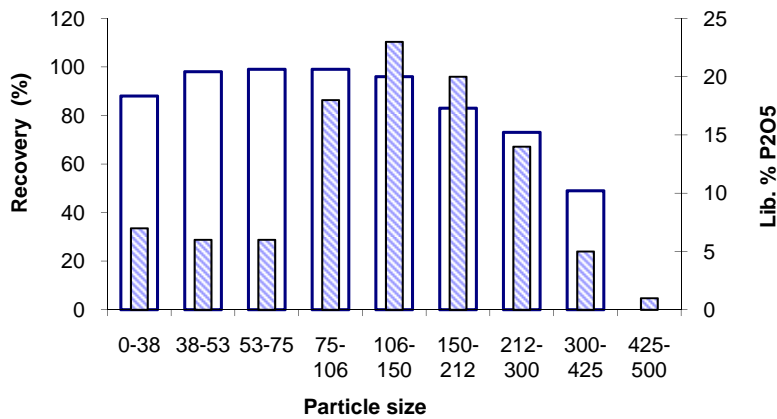


Figure 56: Recovery (blank bars) vs. liberated P_2O_5 (dashed bars).

5.3.11. Volumetric Ratio.

The volumetric ratio according to π_{17} is defined as:

$$\begin{aligned}VR_a &= D^3/d \cdot h \cdot H \\ &= (0.43)^3 / (0.22 \cdot 0.25 \cdot 0.45) \text{ [Rotor diameter} = 0.22\text{m]} \\ &= 3.2\end{aligned}$$

5.3.12. Aeration Rate and Relative aeration.

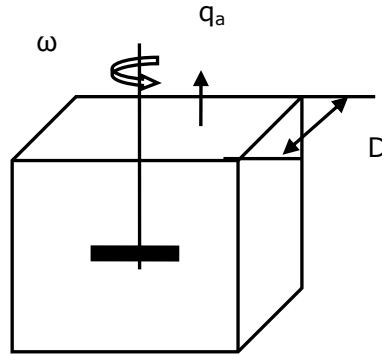


Figure 57: Model for air hold-up Q_a .

The measured air intake was measured as $q_a = 2.9 \times 10^{-3} \text{ m}^3/\text{s}$ and therefore according to π_9 and π_{18} the aeration numbers and relative aeration rate are:

$$\begin{aligned}Q_a &= 4 \times 10^{-3} / [(90 \cdot (0.43)^3)] \\ &= 5.6 \times 10^{-4} \text{ and} \\ \check{R}A_e &= 4 \times 10^{-3} / 5.6 \times 10^{-4} \\ &= 7:1\end{aligned}$$

5.3.13. Bubble Surface Area Flux.

The rotor tip Reynolds number according to π_8 is:

$$\begin{aligned}Re_t &= 1460 \cdot 9.9 \cdot 0.22 / 1.8 \times 10^{-3} \\ &= 1.766 \times 10^6\end{aligned}$$

Bubble surface area flux calculated according to Equation 56, is equal to $S_b = 69 \text{ s}^{-1}$.

5.3.14. Circulation and relative Circulation.

From pressure measurements over the mechanism the pump-ability is calculated as $q_c = 9 \times 10^{-3} \text{ m}^3/\text{s}$. According to π_{10} and π_{19} the circulation number and relative circulation is:

$$Q_c = 9 \times 10^{-3} / (90 \cdot 0.43^3)$$

$$= 1.25 \times 10^{-3}, \text{ and}$$

$$\check{R}_{\text{circ.}} = 1.25 \times 10^{-3} / 3 \times 10^{-4}$$

$$= 4:1$$

Rougher Tank Turn Around is $R_o T_a T_u = (9 \times 10^{-3} \cdot 60) / 0.08 = 6.75 \text{ m}^{-1}$.

5.3.15. Volumetric flow number.

According to π_{11} the volumetric flow number is equal to:

$$Q_p = 3 \times 10^{-4} / [90 \cdot (0.43)^3]$$

$$= 4.2 \times 10^{-5}$$

5.3.16. Power number and Tank power number.

The power consumption is = 0.56kW and according to π_{15} & π_{16} the power numbers are:

$$\check{R}PNo = 560 / [1460 \cdot (90)^3 \cdot (0.22)^5]$$

$$= 1.02 \times 10^{-3}$$

$$T_a PNo = 560 / [1460 \cdot (90)^3 \cdot (0.43)^5]$$

$$= 3.6 \times 10^{-5}$$

5.4. Full scale plant.

5.4.1. Geology and Mineralogy (pyroxenite).

It is imperative that these two factors must be the same as for pilot plant. The Phalaborwa complex accommodates basically six types of phosphate mineralogical combinations. From high phlogopite and low diopside to low phlohopite and high diopside, and any combination inside this range. Although all of them contain Apatite, they have different milling, conditioning and retention requirements. The high phlogopite ore produces a high percentage of plate like particles which absorbs reagents and therefore

require longer conditioning time than the average range. Appendix 6 shows a range of minerals from the same open pit and the different reagent suites required for each.

5.4.2. Milling and Liberation.

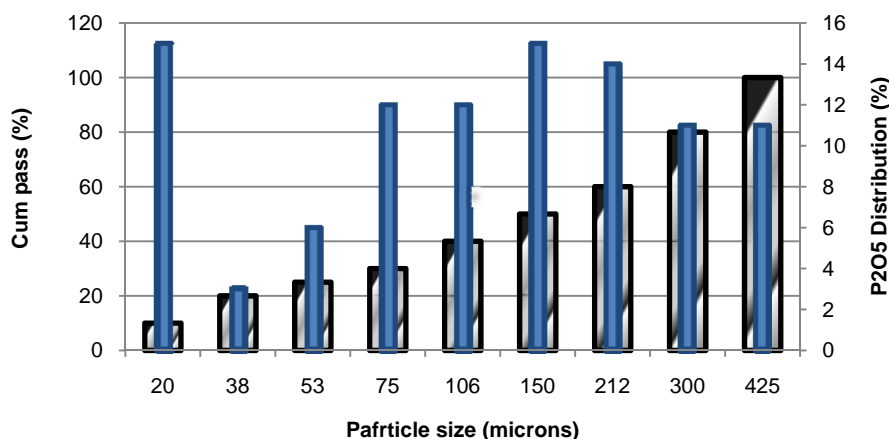


Figure 58: Mineral distribution per fraction.

Figure 58 clearly shows a much higher percentage in the -38 micron fraction and in the +212µm fraction (Solid bar). About 36% of the P₂O₅ reports in the low recovery range. The trend line shows a P₈₀ of about 370µm (Shaded bar).

5.4.3. Chemistry.

Table 23: The chemistry in the main plant.

Reagent	Dosage (g/ton)
Fatty Acid	400
Sulphonic Acid	160

The dosage quantity differs from the suite in Table 23 (Pilot plant) The main reason might be the difference in liberation and interlocked minerals. The depressant seems to be in the right range but the collector differs more than 25%. This is excessive and costly.

5.4.4. Operational Conditions.

The section consists of:

- 2 banks of 8 x roughers + 8 x scavengers of 8.5m³ each.
- 4 x cleaners + 3 x Recleaners of 4.5m³ each.
- The feed is 300 tons per hour per bank at 1350kg/m³ pulp density.

Table 24: Operating parameters for full scale plant.

Parameters	Value	Dimension
Feed rate per bank	300	Ton.h ⁻¹
Aeration rate on roughers	0.04	m ³ .s ⁻¹
Pulp density	1300	kg.m ⁻³
Pulp viscosity	1.7x10 ⁻³	kg.m ⁻¹ .s ⁻¹
Mineral specific gravity	3	-
Conditioner volume	21	m ³

5.4.5. Flow diagram.

The flow diagram is the same as for the pilot plant (Figure 51) except that the cleaners and recleaners are not the same size machines as the roughers and scavengers.

5.4.6. Conditioning.

The volume flow for the conditioning phase is:

$$q_p = 300 / (0.35 \cdot 1.3 \cdot 3600) \\ = 0.18 \text{ m}^3/\text{s}$$

Conditioning time:

$$C_o T = 21 / 0.18 \\ = 116 \text{ s (1.9 min)}$$

The conditioner mechanism $\theta = 3.5/\text{min}$.

5.4.7. Retention time.

Volume flow for retention time with 70% circulating load is:

$$q_p = 300 \cdot 1.7 / (0.35 \cdot 1.3 \cdot 3600)$$

$$= 0.3114 (\text{m}^3/\text{s})$$

$$\tau = 16.8.5 / 0.3114$$

$$= 436 \text{ s (7.2 min)}$$

The volume flow of the circulating load in a full scale plant is too large to measure with standard containers because of handling problems. In this case the use of pump system curves are the only option though very effective.

5.4.8. Volumetric Capacity.

$$VC = 7.4.5 / 16.8.5$$

$$= 0.23$$

5.4.9. Volumetric Ratio.

After inspection it was found that a 144# short rotor was installed which resulted in the following dimensional set-up:

- $D = 2.9 \text{ m}$
- $H = 1.3 \text{ m}$
- $h = 0.38 \text{ m}$
- $d = 0.67 \text{ m}$
- $b = 0.46 \text{ m}$

In the Wemco design the rotor/ draft tube/stand pipe combination represents about 15% of the total cell volume and therefore one has to consider the effect on diameter and active volume. The formulae for the volumetric ratio for the Wemco, is reduced to:

$$VR_a = (0.85 \cdot 2.9)^3 / (0.67 \cdot 0.38 \cdot 1.3)$$

$$= 45$$

5.4.10. Rotor tip Reynolds number (Agitation).

From actual measurements the $\omega = 23.5$ r/s (220rpm) and with: $v_t = 7.9$ m/s: $\rho_p = 1300$ kg.m³: $\mu_p = 1.7 \times 10^{-3}$ kg/ms: Rotor diameter = 0.67m then:

$$\begin{aligned} Re_t &= 1350 \cdot 7.9 \cdot 0.67 / 1.7 \times 10^{-3} \\ &= 4.05 \times 10^6 \end{aligned}$$

5.4.11. Volumetric Capacity.

$$\begin{aligned} VC &= 7 \cdot 4.5 / 16 \cdot 8.5 \\ &= 0.23 \end{aligned}$$

5.4.12. Aeration number.

The measured aeration rate $q_a = 0.04$ m³/s.

$$\begin{aligned} Q_a &= 0.04 / [23.5 \cdot (2.9 \cdot 0.85)^3] \\ &= 1.14 \times 10^{-4} \end{aligned}$$

5.4.13. Bubble surface area flux.

From the previous paragraphs the following from Equation 56, the bubble surface area flux is equal to $S_b = 34$ s⁻¹.

5.4.14. Circulation number.

According to the Wemco catalogue the circulation is about $q_c = 0.539$ m³/s with clean water and at $S_{gp} = 1.3$ the circulation becomes $q_c = 0.414$ m³/s.

$$\begin{aligned} \text{Therefore the circulation number } Q_c &= 0.414 / [23 \cdot (2.9 \cdot 0.85)^3] \\ &= 1.17 \times 10^{-3} \end{aligned}$$

Tank turnaround $T_a T_u = 0.414 \cdot 60 / 8.5 = 2.9$ min⁻¹.

5.4.15. Volumetric flow.

$$\begin{aligned} Q_p &= 0.3114 / 23 \cdot (2.9 \cdot 0.85)^3 \\ &= 9 \times 10^{-4} \end{aligned}$$

5.4.16. Power number.

$$\begin{aligned}\text{Based on rotor diameter} \quad \dot{R}PNo &= 28.5 \times 10^3 / [1300 \cdot (23)^3 \cdot (0.67)^5] \\ &= 13.3 \times 10^{-3}\end{aligned}$$

$$\begin{aligned}\text{Based on cell diameter} \quad T_aPNo. &= 28.5 \times 10^3 / [1300 \cdot (23)^3 \cdot (2.9 \cdot 0.85)^5] \\ &= 1.2 \times 10^{-5}\end{aligned}$$

5.5. Schedule of dimensionless numbers.

The schedule in Table 25 has been populated with the numerical information calculated in the preceding paragraphs. The mineralogy and reagent suite is not shown as it is assumed that these parameters are unchanged. Although the conditioning, retention and froth depth information has also been developed as dimensionless numbers it is shown here as dimensional information as it is just practical to display it in the same manner as the standard production information.

It is obvious from Table 25 that there is very little similarity in almost every metallurgical and hydrodynamic parameter. This is also summarised by the difference in kinetic constant. The fact that the power number based on rotor diameter complies, the same number based on tank diameter demonstrates that the energy requirement is not met. This set-up performed at a 68% recovery level producing 1850 tons of concentrate per day at a 7% P₂O₅ head grade.

5.6. Modified E-Bank.

The flotation banks at Foskor mine are divided into different alphabetical sections which represented the different minerals as indicated in the mineral spec sheets 1 to 3 in Appendix 5. The reason is that the different ores have different magnesium and potassium contents and certain fertilizer processes cannot cope with high magnesium. E bank processes pyroxenite which has a relatively simple mineralogy and reagent suite. The full scale comparison under paragraph 5.5 represents the original E-bank performance which were Wemco 120# with modified 144 rotors. Table 25 shows the schedule of dimensionless numbers for this condition.

As this bank was at the end of its maintenance life it was decided to replace the old cells with 21m³ smart cells and to increase cleaner and recleaner capacity. To improve aeration, bubble surface flux, conditioning time, retention time and grind it was decided to reduce throughput from 275tph to 240tph and increased RPM from 190 to 200RPM. Table 26 shows the improvements in operating and dimensionless parameters and Figure 57 and 58 indicate the improvement in performance. Pyroxenite ore contains diopside

which appears in conjunction with phlogopite. A high diopside content is called diopsitic pyroxenite and high phlogopite is called phlogopitic pyroxenite.

Table 25: Compliance of original main plant with specification.

FACTOR	UNITS	FORM	SPEC	INITIAL
Conditioning Time	min	cond vol/vol flow	7	1.9
Conditioner $T_a T_u$	min^{-1}		9	3.5
Ret. Time	min	NA	18	7
Froth Depth	%	FD/CD	10/5	10/5
Vol.cap.*	%	Cl.vol/R&Sc.vol	60	23
Sb	S^{-1}	Sb	19	29
P_{80}	μm	P_{80}	250	375
DR*	-	d/D	0.5	0.21
VR*	-	$D^3/d h H$	2	45
Re_s^*	-	$P_p V_s D / \mu_p$	500	60000
AR*	-	d/e	7.3	1.4
Re_t^*	-	$\rho_p V_t d / \mu_p$	1.8×10^6	4.2×10^6
A.N.*	-	$q_a / \omega D^3$	5.6×10^{-4}	1.4×10^{-4}
Circ*	-	$q_c / \omega D^3$	1.25×10^{-3}	1.27×10^{-3}
Vol.Flo.N*	-	$q_p / \omega D^3$	4.2×10^{-5}	9×10^{-4}
P.No*	-	$P / \rho \omega^3 d^5$	1×10^{-3}	13.3×10^{-3}
T.P.No.*	-	$P / \rho_p \omega^3 D^5$	3.6×10^{-5}	1.2×10^{-5}
Kinetic constant	min^{-1}	Equation 56	0.18	0.08

* =Dimensionless numbers; **Bold**=Compliance; Shaded= Non-compliance.

The phlogopitic pyroxenite floats more difficult as phlogopite is a plate like mineral which has to a certain extent a natural floatability.

This means that more depressant is required. For this reason both ores were processed a week apart and the operating teams were also changed to eliminate any training bias. According to the operators the plants were supercharged and the runs were called Shumacher runs. Comparing Figure 58 and 59 show that the same performances were

achieved with both ores. With this modification the compliance increased from 5 to 8 parameters and 9 more were improved and therefore an increase in performance. This set-up performed at a 83% recovery.

The reasons for the improved performance in the modified E-bank are the following when comparing it to the variables in the kinetic constant equation $k = F_p \cdot S_b \cdot R_f$.

- Improved conditioning time = Improved floatability (F_p).
- Improved volumetric capacity = Improved retention (T).
- Increased RPM = Improved aeration, agitation and solid suspension = Improved F_p , Re_t and S_b .
- Lower P_{80} = Improved solid suspension and viscosity = Improved F_p and S_b .
- Improved volumetric ratio = Better protection of quiet zone.
- Improved aeration = Reduction in froth retention time = Improved R_f .

Appendices 1 to 4 further demonstrate the application of the schedule of dimensionless numbers, on different phosphate banks with low performance, and demonstrate how the schedule of dimensionless numbers was applied to address these problems.

Almost every time a modification was implemented which pushed the dimensionless numbers towards similarity, an improvement was experienced. Only in severe cases such as poor liberation, did improvements in performance not materialise. With improved hydrodynamics a reduction in reagent dosage was observed for instance improved aeration resulted in a reduction of frother dosage. While measuring and calculating all variables required to compile the schedule of dimensionless numbers, certain operational deficiencies are uncovered such as level control by frother or suppressant dosage.

Table 26: Performance of modified E- bank compared with original installation.

Factor	Spec	Original	Mod. E-Bank
C _o T	7	1.9	8⁺
θ	9	3	4 ⁺
τ	19	7	12 ⁺
Fd	10/5	same	same
Vol.Cap.*	60	23	50 ⁺
Sb	19	28	33⁺
P ₈₀	250	375	300 ⁺
VR*	3	45	27 ⁺
ÅR _a *	7	1.4	1 ⁺
Re _s *	500	60000	45000
Re _t *	1.8x10 ⁶	4.2x10⁶	4.6x10⁶
A _e N.*	5.6x10 ⁻⁴	1.4x10 ⁻⁴	2x10 ⁻⁴⁺
CN.*	4.2x10 ⁻⁴	9x10⁻⁴	12x10⁻⁴
VfN*	<4.2x10 ⁻⁵	9x10 ⁻⁴	7x10 ⁻⁵⁺
ŘPNo.*	1x10 ⁻³	12x10⁻³	25x10⁻³
T ₃ PNo.*	3.6x10 ⁻⁵	1.2x10 ⁻⁵	3.3x10⁻⁵⁺
Kinetic constant	0.18	0.08	0.18
Performance	97/38	68/38	83/38

Bold= Compliance; Shaded=Non-compliance; (+)= Improvement.

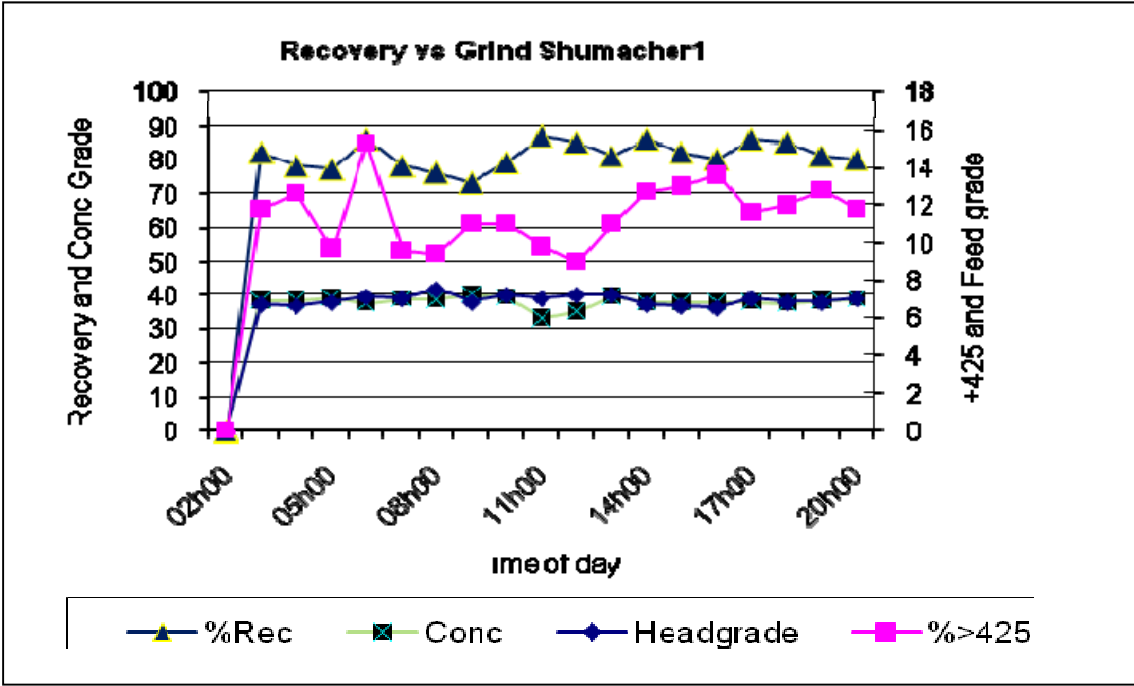


Figure 58: High Diopside ore (Test run time = 12 hours).

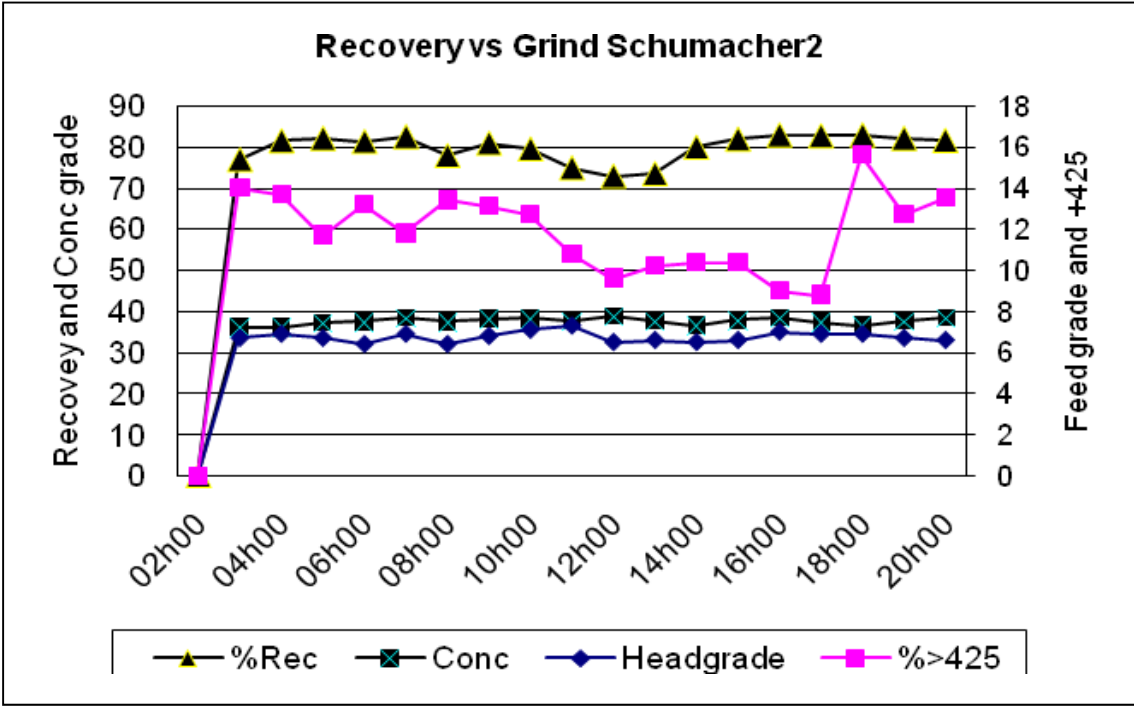


Figure 59: High Phlogopite ore.

CHAPTER 6: APPLICATION OF THE SCHEDULE OF DIMENSIONLESS NUMBERS TO A PLATINUM PLANT.

6.1. The Platinum Industry.

This case study was made difficult by the secrecy between the different South African platinum producers to protect operational and marketing advantages. Producers are also reluctant to supply pilot plant information from which to scale-up. Therefore the specification will be compiled from information gathered in the open literature, from general flotation requirements and the author's own experience. The different clients will also be referred to as Plant 1 and Plant 2. Another difficulty was to obtain an opportunity to fully apply the schedule of dimensionless to a Platinum plant, therefore this section will be dedicated to demonstrate how the schedule of dimensionless numbers was applied to identify deficiencies in these plants.

6.2. Geology.

The Bushveld complex is a massive layered intrusion approximately 2 billion years old, and is about 350 kilometres in diameter. It intruded through older sedimentary rocks, some of which contain fossils of the earliest life form. The area of interest for PGM mineral is a cyclic zone where the rocks are conspicuously layered in a repetitive fashion referred to as 'cyclic units'. The base of a cyclic unit is composed of generally dark coloured minerals, usually pyroxene, olivine or chromite. The layers above these layers often contain a mixture of these dark minerals with varying proportions of plagioclase feldspar. These multi-mineralic rocks consist of norite, gabbro, and troctolite.

6.3. Mineralogy.

Two basic mineralogy's namely Merensky and UG2 are presented in the following paragraphs.

6.3.1. Merensky.

Table 27: Approximate Merensky mineralogy.

Mineral	Pyroxenite	Plagioclase	Clino Pyr	Biotite	Talc	Others
%	70	20	4	2	small	small

The Merensky reef is situated in the basalt part of the particular cyclic unit and the approximate composition is summarised in Table 27. The PGM average composition of the Merensky minerals, as indicated in Table 28, is 6-9 gm/t.

Table 28: General PGM composition for Merensky.

Mineral	Sperrylite	Moncheite	Cooperite	Kotulskite	Braggite	Pt-Fe	Other
%	50	13	10	8	7	6	6

6.3.2. UG2 reef.

The UG2 is the second chromite layer and the approximate composition is outlined in Table 29.

Table 29: Approximate UG2 mineralogy.

Mineral	Chromite	Orthopyroxene	Plagioclase	Magnetite	Sulphides
%	75	15	10	small	small

The PGM average of the composition as indicated in Table 30 is 4-6 g/t

Table 30: PGM composition for UG2.

Mineral	Cooprite	Laurite	Braggite	Sperrylite	Pt-Fe
%	NKN	NKN	NKN	NKN	NKN

NKN = Not Known

6.4. Flotation chemistry.

The reagent suite for the flotation of minerals from the Merensky and UG2 reefs is summarised in Table 31.

Table 31: Reagent suite for Merensky and UG2 (g/t).

Reef	SIBX	FROTH	PROM	ACT	DEPR
Merensky	30	30	70	-	70
UG2	35	100	-	-	25

6.5. Operational Considerations.

The presence of talc in Merensky minerals requires special depressants and grinding control as talc mills fine easily and therefore has a natural floatability. The depressant in this case is normally a 10% starch solution. Chromite on the other hand will mill with more difficulty and having a high density will require special pumping and solid suspension requirements.

6.5.1. Conditioning.

An unconventional approach found in the platinum industry is that conditioning is replaced by stepwise dosage. This is the only industry where intimate mixing of the solids and reagents are not required as the tank turn around (Circulation) of flotation machines are far too low for this purpose. This approach also unnecessarily consumes precious retention time. About 20 minutes conditioning time is required for nickel/copper/pgm combinations and there is no reason why this won't work for Merensky and UG2. Minerals.

6.5.2. Retention.

General requirements for retention times are summarised in Table 32.

Table 32: Retention times for Merensky and UG2 (min).

Cycle	Primary Rougher	Primary Cleaner	Primary Re-cleaner	Secondary Rougher	Secondary Cleaner	Secondary Re-cleaner
Time (min)	30	60	60	30	60	60

This seems to correspond well with other plants with the same mass balance requirements.

6.5.3. Flow Diagrams.

The general flow diagram in the Platinum industry is one of grind/float/grind/float. The primary concentrates from the first rougher, cleaner and recleaner are normally final concentrates, and cleaners and recleaners are scavenging on themselves.

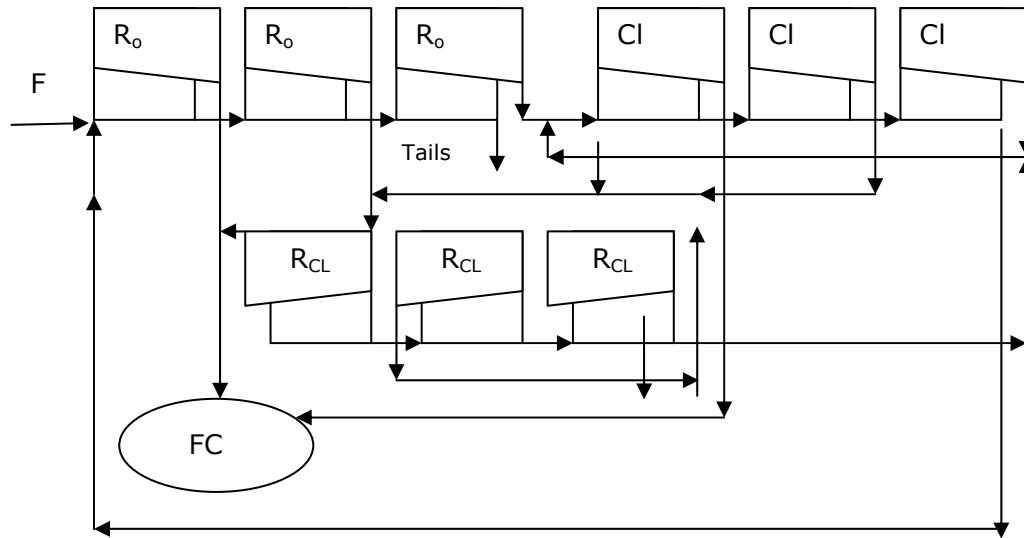


Figure 60: Typical flow diagram for PGM's.

This flow diagram is repeated as a secondary step with a grinding step in between.

6.5.4. Froth depth.

Almost no information is available on froth depth models. A confidential report on froth depth models suggested the following:

Table 33: General froth depth specification for Merensky and UG2.

Stage	Primary rougher	Primary cleaner	Primary Re-cleaner
Depth (mm)	75	90	120
Stage	Secondary Rougher	Secondary Cleaner	Secondary Re-cleaner
Depth (mm)	110	120	130

This type of specification is misleading, as it does not refer to the machine size. It is more universal to specify the froth depth as a function of cell depth. Experience showed that this did not differ much from the copper models.

6.5.5. Volumetric Capacity.

This is a function of the mass flow and required retention time. A general rule of thumb for this value of head grade is that 25% volumetric capacity is adequate.

6.5.6. Volumetric ratio, Superficial and Rotor Reynolds number.

The general scale-up specification applies. The dimensionless number for this ratio is $4 < VR_a < 16$, $Re_s < 15 \times 10^3$ and $4 \times 10^6 < Re_t > 7 \times 10^6$.

6.5.7. Circulation.

The circulation capability of the machine depends on the sinking velocity of the top 5% of particle size. This can be specified as:

Table 34: Tank turn around.

Circulation	Tank Turn-around
4.3×10^{-4}	3 – 4

6.5.8. Aeration and Bubble surface area flux and Power numbers.

The aeration and bubble surface area flux requirements are as indicated in Table 35.

Table 35: Aeration and bubble surface flux for Merensky and UG2.

Aeration Number (A_eN)	Bubble surface area flux (S_b)	Tank power number
4.1×10^{-4}	90 s^{-1}	4.2×10^{-5}

6.6. Schedule of dimensionless numbers.

The analysis shows that very little similarity was maintained during the design stage. The deficiencies could be summarised as follows:

- Some uncertainty exists, regarding exact reagent suite, as these companies are very sensitive in divulging this type of information. For some of them this information is highly secret.
- No liberation model, froth depth model and recovery vs. particle size model conditioning time and retention time models existed in some cases. The specification for comparison was decided upon after deliberation with research personnel and normally resulted in a combination of the laboratory and pilot plant information produced in the Foskor plant for a very low head grade copper

process (Head grade = 0.05-0.07% Cu) on the one hand and PGM reports in possession of the author.

Table 36: Compliance of Merensky and UG2 main plant with specification.

FACTOR	DIM	SPEC.	ME2	ME1	UG21
CT	min	20	0	0	0
τ	min	60	37	20	45
F_d^*	%	5	9	8	9
VC*	%	20		0.8	14
S_b	s^{-1}	36	65	31	43
P_{80}	μm	100	100	138	150
DR_a^*	-	0.24	0.21	0.24	0.23
VR_a^*	-	< 15	7	16	7
AR*	-	7	1.6	1.6	1.5
Re_s^*		2×10^4	14×10^4	3.2×10^4	5×10^4
Re_t^*	-	1.7×10^6	7×10^6	4×10^6	6×10^6
A_{eN}^*	-	8×10^{-5}	1.3×10^{-4}	1.1×10^{-4}	7.8×10^{-5}
Circ*	-	1.27×10^{-3}	6.3×10^{-4}	8.4×10^{-4}	1.5×10^{-3}
$T_a T_u^*$		4	0.6	2.1	2
VfN*	-	$< 3.9 \times 10^{-5}$	6.7×10^{-5}	9×10^{-5}	2.7×10^{-4}
$T_a PNo^*$	-	3.6×10^{-5}	6.4×10^{-5}	8×10^{-6}	2.8×10^{-5}
k		0.269	0.054	0.169	0.073
Performance	Re@Gr	80%@185	80%@260	90%@260	79%@260

*= Dimensionless numbers; **Bold** = Compliance; Shaded = Non-compliance.

(ME1 = Plant 1 with Merensky as ore type; ME2 = Plant 2 with Merensky as ore type; Same for UG2).

- Too high superficial Reynolds number. The superficial Reynolds number is a tool to decide on the number of parallel lines. It is possible to design plants with less units in series with the new tank cells as these cells are no longer open channels and short circuiting are limited in these designs. More parallel banks will reduce the superficial velocity and the superficial Reynolds numbers and force it towards similarity.
- Too low aeration and bubble surface flux. The supply are normally external aeration and the aeration number is below the numerical value for similarity. Bubble surface area flux is between 40-60 s⁻¹ and this is also below the process specification.
- Too low circulation. This can lead to the settlement of solid particles.
- Too high volumetric flow. This represents a dimensionless retention time and is supported by the actual retention time which is below specification. This is evident in plants where production is increased to increase output. This normally happens when the product price is high.

CHAPTER 7: CALE-UP METHODOLOGY.

7.1. New scale-up algorithm.

7.1.1. Assumptions.

Before running the algorithm the following information must be known:

- Conditioning and retention times
- Required particle size distribution
- Type of design: High or low aspect ratio

7.1.2. Algorithm.

See detail algorithm in Appendix 8.

7.2. Discussion of new algorithm.

7.2.1. The calculations in step 1 to 3 follows from the standard plant calculations in §3.10.

7.2.2. In step 4 the rotor RPM is calculated by applying the adjusted transformation number generated in Equation 36 namely $Fr_{RGA} = idem$.

7.2.3. In step 5 the power requirement is based on the Tank power number and the rotor power number is adjusted with the ratios of rotor heights for comparison with the pilot plant. The reason for the adjustment with the ratio of rotor heights is because the full scale rotor is viewed as a multi-stage version of the pilot plant rotor. If the full scale rotor was simply an adjustment of diameter then the affinity laws would have applied

7.2.4. In step 6 the circulation is again based on tank diameter and adjustment with the ratio of rotor heights for the same reason as in §7.2.3.

7.2.5. Step 7 represents the calculation of the agitation level based on rotor tip Reynolds number. To compare with pilot plant agitation the Reynolds number is adjusted with the ratio of relative particle size according to Mavros (1992).

7.2.6. Step 8 the dimensionless numbers are compared in the schedule format.

7.2.7. Finally the kinetic constant and its parameters are calculated according to Equations (46) to (62). The reasoning is that with retention time and kinetic constant = idem than the recovery should be the same

7.3. Application of the new algorithm to a standard industrial design.

7.3.1. Table 37 shows the related dimensionless numbers that must also be kept constant. The froth depth number $FD/H = idem$ is required to ensure the same concentrate grade. In this case the as there are no conditioning in this plant the dimensionless conditioning parameters $\omega\theta = idem$ and $\omega\eta = idem$ were both set equal to 1.

Table 37: The following dimensionless numbers are =idem.

Relative Particle size	Relative froth depth	Conditioning time	Tank turn around	Froth retention time	Superficial Reynolds number	
P_{80}/D	F_d/H	$\omega\eta$	$\omega\theta$	$\omega\xi$	$\rho_p J_p D / \mu_p$	

7.3.2. Table 38 shows the comparison between a pilot plant used for sulphide and non-metal floats and a 50 cubic meter cell as these designs are actively in service in the South African PGM mining industry. This machine has been installed as a rougher stage on a UG2 plant. With the improvement of rotor diameter from 0.99m to 1.16m and reducing RPM from 14r/s to 12r/s complied with the transformation requirements and resulted in an improvement of all operating and dimensionless parameters as well as a 31% improvement in floatability parameter, a 1.6% improvement in froth recovery and almost 200% improvement in the kinetic constant and end in an expected improvement of 7% points in recovery.

Table 38: Showing adjusted dimensionless numbers.

Parameters	Denver PP	BQR 500 Actual	BQR New Algorithm
Rotor Asp. Ratio	7.3	1.5	1.25
Rotor tank Ratio (%)	1.8	1.4	1.6
Tank diameter (m)	0.43	4.3	4.3
P_{80}	100	310	90
Rotor diameter (m)	0.22	0.99	1.16
Volumetric Ratio	3.5	7	6
RPM (r/s)	90	14	12
Rotor Tip Re. No	1.75×10^6	5.15×10^6	6.41×10^6
Fr	45.5	4.95	4.26
Fr_{RGA}	3.1	4.5	3.1
Aeration (m^3/s)	0.0028	0.09	0.12
Aeration number	8.4×10^{-5}	8.1×10^{-5}	1.3×10^{-4}
S_b	36	41	52
Circulation (m^3/s)	0.012	1.7	4.6
Circ. adjusted	1.7×10^{-5}	2.4×10^{-3}	4.8×10^{-3}
Power required (kW)	0.57	110	191
Rotor Power No	1×10^{-3}	31×10^{-3}	38×10^{-3}
Adjusted rotor P.No	1×10^{-3}	1.4×10^{-3}	1.22×10^{-3}
Tank Power No	3.6×10^{-5}	2×10^{-5}	5.5×10^{-5}
k	0.269	0.073	0.213
Expected improvement	-	78%	85%

7.3.3. The superficial Reynolds number based on superficial velocity is an interesting tool to verify the number of parallel banks. Presently the number of parallel banks is based on the average resident time distribution model.

Table 39: Parallel banks vs. superficial Reynolds number.

Plant	Phosphate	Copper	UG2	Nickel
TPH	600	3000	300	40
Parallel Banks	2	8	2	1
Re_s	93000	171000	23000	12723

All these plants in Table 39 comply to the requirement of $Re_s < 100000$ except the copper plant. According to the requirement $Re_s < 100000$ the copper plant should double the number of parallel banks.

7.4. Design of Tornado pilot plant.

7.4.1. Background.

Because of a lack of finances it was decided to scale down and build a pilot plant based on the Wemco design but with a specific requirement that the design must meet the same operational specification as the present pilot plant.

7.4.2. Detail design.

7.4.2.1. Cell size: Although the cells are suppose to be of the same size as the present pilot plant cells it must still meet the requirements of retention time. The total retention time required for five rougher and scavenger cells and 30% circulation load is 20 minutes. Thus 4 minutes per cell.

7.4.2.2. Volume flow $q_p = \text{Mass feed} / \phi_s \cdot S_{gp} \cdot 3600 \text{m}^3/\text{s}$

$$= 2.8 \times 10^{-4} \text{m}^3/\text{s}$$

$$\begin{aligned}
\text{Tank size} &= \tau \cdot q_p \\
&= 20 \cdot 60 \cdot 2.8 \times 10^{-4} \cdot 1.3 \text{m}^3 \\
&= 0.436 \text{m}^3 \\
&= 0.086 \text{m}^3/\text{cell}
\end{aligned}$$

A cell with a 500mm diameter and 550mm deep, represents 0.11m^3 . Assume that the froth and internal components take up about 20% of internal volume, then the free volume would be about 0.088m^3 which is sufficient.

7.4.2.3. Rotor diameter and submergence.

According to the dimensionless group π_{20}

$$d^2 \cdot b / D^2 \cdot H = 0.018$$

And the Aspect ratio of the Wemco varies from $1 < \text{AR}_a < 1.5$. For this design it was decided to start with $\text{AR}_a = 1.3$. Therefore from the above requirements the rotor diameter is:

$$D = 148 \text{mm} - \text{Say } 150 \text{mm}$$

From the dimensionless group π_{17} and Figure 62 it follows that:

$$\text{VR}_a = D^3 / d \cdot h \cdot H = 3.0. \text{ Therefore:}$$

$$h = (0.5 \cdot 0.85)^3 / 3 \cdot 0.15 \cdot 0.55$$

$$\text{Submergence} = 310 \text{mm}.$$

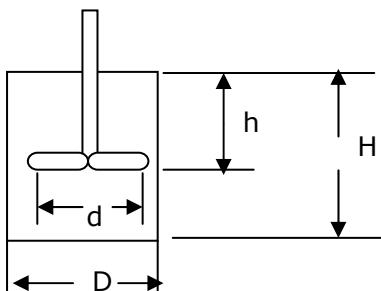


Figure 62: Proposed lay-out.

7.4.3. RPM.

RPM is calculated to meet the requirements of the Fr_{RGA} . Assume and rotational speed of $\omega = 130$ r/s then $Re_t = 1.178 \times 10^6$ and $Fr = 64.7$ and as this design will operate under the same conditions as the pilot plant then $P_{80} = 250 \mu\text{m}$ and, $\rho_p = 1450 \text{ kg/m}^3$ and $\mu_p = 1.8 \times 10^{-3}$ then $Fr_{RGA} = 3.4 \times 10^6$

7.4.3.1. Volumetric flow number (VfN).

$$\begin{aligned} \text{From the dimensionless group} \quad VfN &= q_p / \omega \cdot D^3 < 2.9 \times 10^{-5} \\ &= 2.6 \times 10^{-4} / [130 \times (0.5 \times 0.85)^3] \\ &= 2.6 \times 10^{-5} \end{aligned}$$

7.4.3.2. Rotor tip Reynolds number (Re_t).

According to the dimensionless group π_{12}

$$\begin{aligned} Re_t &= \rho_p \cdot \omega \cdot d^2 / 2 \mu_p \\ Re_t &= 1.178 \times 10^6 \end{aligned}$$

7.4.4. Power requirements.

According to the dimensionless group π_{14}

$$\begin{aligned} P / \rho \cdot \omega^3 \cdot d^5 &= 1 \times 10^{-3} \cdot (\text{Rotor height ratios}) \text{ it follows that} \\ P &= 1 \times 10^{-3} \cdot 3.8 \cdot 1450 \cdot (130)^3 \cdot (.15)^5 \\ &= 0.919 \text{ kW} \end{aligned}$$

7.4.5. Aeration, circulation and bubble surface flux.

Air flow was measured and $q_a = 0.0011 \text{ m}^3/\text{s}$.

$$\begin{aligned} \text{Therefore } Q_a &= 0.0011 / [130 \cdot (0.5 \cdot 0.85)^3] \\ &= 1.1 \times 10^{-4} \end{aligned}$$

Bubble surface flux was calculated to be $S_b = 59 \text{ s}^{-1}$.

Circulation according to Equation (54) are calculated at $q_c = 0.047 \text{ m}^3/\text{s}$. As aspect ratio is 1.3 and only 70% of the rotor will contribute to the circulation number. Therefore the circulation number is:

$$Q_c = 0.033/130 \cdot (0.5 \cdot 0.85)^3$$

$$= 3.3 \times 10^{-3}$$

7.5. Compliance to specification.

The reduced aspect ratio was specifically chosen to ensure good aeration and bubble surface flux. The next figure shows a photo of the pilot plant that was produced based on the polarised hood and the basic Wemco design but adjusted to comply with dimensionless numbers. The plant performed at a 95% recovery and 40% concentrate grade.

Because of a lack of funds and the uniqueness of this approach to some of the managers at the mine, it was decided to scale down from the full scale plant and design, build and operate a pilot plant based on the Wemco design.

The existing pilot plant design is based on the Denver design which is a self aerating machine with a very high aspect ratio rotor where the Wemco is also a self aerating machine but with a low aspect ratio rotor but with static physical barriers called dispersers and hood.

7.6. Contribution of thesis to the subject.

7.6.1. The contribution of this thesis to the subject is:

- The establishment of a new transformation equation on which to base the scale-up analysis.
- The combination of machine and process dimensionless numbers in a schedule of dimensionless numbers to analyze and identify of plant deficiencies.
- The establishment of a dimensionless kinetic constant to determine the effect of changes identified by the application of the schedule of dimensionless numbers.

7.6.2. Choosing the tank diameter as the linear independent variable focuses the attention on process requirement instead of mechanism ability.

Table 40: TORNADO design detail.

ITEM	FORM	DIM	SPEC	VANTRUT
τ	Q_t/Q_p	min/cell	5.6	6.0
Fd	% cell depth	%	9/5	9/5
VC	-	%	60	60
S_b	Form	S^{-1}	19.3	18.5
FLD	FLD	-	R_o - SC-Cl- R_{CL}	same
C_oT	$C_oVol./Q_p$	min	10	10
DR_a	d/D	-	>0.25	0.32
VR_a	D^3/dhH	-	<10	3
$\dot{A}R_a$	d/e	-	7.0	1.3
Re_s	$\rho_p vD/\mu_p$	-	500	516
Re_t	$\rho_p v_t d/\mu_p$	-	1.75×10^6	1.178×10^6
A_eN	$q_a/\omega D^3$	-	4.1×10^{-4}	1.1×10^{-4}
C.N.	$q_c/\omega D^3$	-	4.3×10^{-4}	3.3×10^{-3}
$\dot{R}.PNo.$	$P/\rho\omega^3 d^5$	-	1×10^{-3}	1×10^{-3} *
k	$F_p \cdot S_b \cdot R_f$	Min^{-1}	0.147	0.159

Bold= Compliance; Shaded= Non-compliance, * Adjusted with rotor height ratios.

7.6.3. The literature focuses on mechanism characteristics and not on the primary independent variable of recovery and kinetic constant. Rodrigues et al. showed that Froude number is not the only variable influencing recovery but also Reynolds and power number. Interesting to note that, the power number is a combination of Reynolds number and Froude number.



Figure 63: Tornado pilot plant at Foskor Pilot facility.

7.6.4. One parameter that keeps on coming up in a number of publications (Deglon et al.) is the use of partial similarity, power/m³ or power/kg. Zlokarnik concluded that this is a very ill suited parameter for dimensioning a flotation mechanism though it is probably the most common parameter surfacing in discussions with metallurgists and suppliers. Zlokarnik also showed that the ratio between full scale plant and model based on power/volume, is equal to the square root of the scale factor. In many pilot tests results, generated for clients by very reputable institutions, power/m³ is one of the process parameters specified but no application of this requirement has been found in the full scale plant. In this thesis the tank power number is used as basis for determining the power requirements and the rotor power number is calculated to establish whether the mechanism will be able to deliver.

7.6.5. Another parameter that does not appear frequently in the literature is the circulation number = $Q_c/\omega d^3$. The author combined this parameter with power number, rotor tip Reynolds number and Froude number to specify the conditions for the agitation zone to ensure sufficient solid suspension and bubble creation and at the same time protecting the quiet zone.

7.6.6. Another unique feature in the thesis is the use of the schedule of dimensionless numbers to identify plant deficiencies and to “push” the plant design towards similarity.

CHAPTER 8: CONCLUSIONS AND RECOMMENDATION.

8.1. Dimensionless analysis.

- This thesis is unique in addressing the transformation number, kinetic constant and dimensionless schedule at the same time. Comparing the transformation equation with standard industrial machines clearly showed that that these designs did not follow the scale-up criteria of $Fr = idem$. Most of these designs , especially the Wemco design, followed partial similarity of $kW/m^3 = idem$ or $Re_t \cdot Fr^{0.5} \cdot G^{0.45} \cdot \Delta R_a^{-0.2} = idem$
- The establishing of an equation for the kinetic constant based on dimensionless numbers resulted in a model built on about 16 variables. The application of this model to different designs and minerals seems to produce acceptable results.
- The validation of floatability parameter and froth recovery factor needs more attention. In this analysis the author did not try to generate dimensionless relationships for entrainment and drainage as these are implied in the overall kinetic constant. Entrainment has a detrimental effect on concentrate grade and in this case the grade is fixed by the froth depth. In this case the approach was rather to create conditions that are conducive for froth phase protection and fine particle collision conditions.

8.2. Schedule of Dimensionless numbers.

- It has also been found that the schedule of dimensional numbers is a relative simple method entailing simple measurements, calculations and comparisons. It does not require complicated measuring equipment or special conditions but simple production and maintenance tools.
- Finally it amounts to a simple comparison between simple ratios which then creates the opportunity to identify and rectify these deficiencies by entertaining improvements that will force the plant towards similitude. The deviation from the basic transformation equation of $Fr = idem$ might have something to do with economics of the time though many of these machines were designed and installed when this relationship was well known.

8.3. Main plant performance.

- It is true that full scale plants perform much worse than pilot plants to as much as 30%. These deficiencies are also independent of machine or mineral. The same deficiencies have been found in copper, phosphate, nickel, platinum and carbonate plants.
- These plants utilised the full range of equipment, with different sizes, self-aerating or external aerating machines, low and high aspect ratio rotors and high and low volumetric ratio though the deficiencies are the same.

8.4. Process Characterization.

- After discussions with metallurgists and research engineers regarding the scale-up methodology applied in their full scale designs, it percolated that they put a lot of effort in characterising the process by compiling mineralogical, metallurgical and chemical specifications and then turn it over to the suppliers of equipment to supply the appropriate equipment based on a single characteristic such as power/cubic metre. No where did the author find any hydrodynamic characteristics as part of the specification. The reason is that these metallurgists work in isolation with hardly any assistance from engineers. When one enquires about the hydrodynamic characteristics of these machines the author discovered that it exists only partially. The basis for selecting a specific machine is most of the time based on that which worked somewhere else.
- The application of dimensional similitude clearly demonstrated the simplicity of this methodology. It highlighted almost ten major deficiencies such as aeration numbers, rotor tip Reynolds number, power number, circulation number etc, in every plant. At most plants a lot of effort is put into the testing of reagents and the reason is that it is one of the highest cost items but very little time is spent on the fundamental issues of flotation such as kinetic activity and what variables influence its value.

8.5. Process specification.

In certain cases in the industry, processes have been design by “stealing” with the eyes and ears from other existing plants. Major flotation plants have been designed and built this way. When requesting process information to determine whether the plant has been constructed to specification, none was available. This clearly demonstrated the none-existence of any scale-up technique during the design of these full scale plants.

8.6. Scale-up Techniques.

Most scale-up techniques are proposals but with no prove of analysis, identification of deficiencies, suggested improvements, prediction of success and implementation. Most plants were either duplication of existing designs where the same deficiencies were repeated or some copy of another similar plant.

8.7. CFD results of Wemco machine.

The following has been established in this simulation of the mineral recovery rate of the WEMCO 120 flotation cell:

- The trajectories of the air bubbles are driven by buoyancy once they are out of the high fluid velocity area. The trajectories of the solid particles are driven by and follow the continuous liquid phase throughout the flotation cell. The solid particle sedimentation is as expected concentrated on the bottom and false floors.
- An effective procedure has been established to apply field measured data of recovery rates to the computational domain. This interpolated recovery rate values have proved effective to evaluate other important flow parameters in particular the pulp and bubble Reynolds numbers and the bubble-particle collision frequency. The most important results from the present work are the evidence that the bubble-particle collision frequency follows the same trend as the interpolated recovery rate values. Since these values are unrelated, one being interpolated from measured values and the other derived from theory one may safely continue to investigate the importance of this parameter. The same applies to the relevance of the bubble Reynolds number. This parameter has shown that the slip velocity between bubbles and liquid phase may be more important than the pulp velocity. This may be justified by the fact that initial bubble-particle collision can only take place if such a slip velocity exists, a fact inherent to the theory underlying the expression for the bubble-particle collision frequency.
- It has been shown that there exists good agreement between the interpolated measured recovery rate data and a local recovery rate found by using the bubble-particle collision frequency. The bubble Reynolds number has also shown to follow the same trend as the interpolated recovery rate values. It is suggested that more detailed evaluation of these trends are made correlating the CFD prediction of bubble-particle collision frequency and bubble Reynolds number to the interpolated recovery rate data. At this stage the bubble-collision frequency theory only predicts the probability of initial bubble-particle collisions and does not provide information on whether the solid particles will remain attached.

- Global mineral recovery rate from CFD field results. This could be achieved by developing a method to predict the overall recovery rate potential of the flotation cell by utilising the data predicted by the CFD simulation. This data should be interpreted and a method proposed.

ABBREVIATIONS.

ACT = Activator.

AP = Apatite.

$\mathring{A}R_a$ = Rotor aspect ratio.

Ar = Archimedes number.

Conc. = Concentrate.

Circ= Circulation.

CAL = Calcite.

CFD = Computational fluid dynamics.

CI = Cleaner.

CN = Circulation number.

CUM = Cumulative.

Cu 1-2 = Different copper plants.

DEPR = Depressant.

DIOP = Diopside.

DIM = Dimension.

DR_a = Diameter ratio.

FA = Fatty acid.

FC = Final concentrate.

FLD = Flow diagram.

FOR = Forsterite.

F_{RT} = Dimensionless froth retention time.

FSP = Full scale plant.

FC = Final concentrate grade (%).

G = Relative particle size ratio.

Idem = Identical value.

Lib = Liberation.

LIZ = Lizerdite.

MAG = Magnetite.

Mill = Milling (Grinding.)

Ne = Newton number.

PGM 1-2 = Different platinum plants.

PHL = Phlogopite.

PP = Pilot plant.

Pyr = Pyroxenite ore.

PROM = Promoter.

R_{CL} = Recleaner.

REC = Recovery.

ṘPNo. = Rotor power number.

ṘT_aVR_a = Rotor tank volumetric ratio.

RTD = Residence time distribution.

SA = Sulphonic acid.

Sc = Scavenger.

STD = Standard.

Tails = Tailings.

Tmf = Tails mass flow.

T_aPNo = Power number based on tank diameter.

T_aSR_a = Tank slenderness ratio.

T_aT_u = Tank-turn-round.

TPH = Tons per hour.

VC = Volumetric capacity (%).

VfN = Volumetric flow number.

VR_a = Volumetric Ratio.

VC = Volumetric capacity.

VERM = Vermiculite.

NOMENCLATURE.

Symbols.

A_c = Cell area (m^2).

$A_e N$ = Aeration number.

A_{si} = Stand pipe inlet area (m^2).

a-c = Streamline identification in potential flow.

a'-c' = Streamline identification in potential flow.

B = Reference length in the weir equation (m).

C_d = Drag coefficient.

$C_o T$ = Conditioning time (min).

d = Rotor diameter (m).

d_b = Bubble diameter (m).

d_m = Mineral particle diameter (m).

d_{32} = Sauter diameter (m).

D = Tank diameter (m) (Reference diameter).

D_h = Hydraulic diameter (m).

b = Rotor height (m).

f_t = Transformation equations.

$f_1 - f_5$ = Functions.

F = Feed rate (Tph).

F_b = Buoyancy force (N).

F_{cd} = Drag force (N).

F_d = Froth depth (%).

F_g = Gravitational force (N).

F_o = Force (N).

F_p = Floatability parameter in kinetic constant.

Fr = Froude number.

Fr_D = Froude number based on tank diameter D.

Fr^* = Froude number combined with Reynolds number.

Fr' = Special adapted Froude number.

Fr_{RGA} = Froude number combined with Reynolds number, relative particle size ratio and rotor aspect ratio.

g = Gravitational constant (9.81 m/s^2).

G = Ratio between relative particle size for full scale plant and pilot plant..

h = Rotor submergence (m).

h^* = Distance of stirrer from bottom of tank (m).

H = Tank height (m).

H^* = Filling height (m).

H_w = Water height in weir flow equation (m).

i = Constant in froth recovery factor.

j = Drainage constant in froth recovery factor.

J_g = Superficial velocity (cm/s).

J_p = Superficial pulp velocity (m/s).

k = Kinetic constant (min^{-1}).

k' = Kinetic constant modified with VR_a (min^{-1}).

k'' = Constant in propeller blade equation.

k_a = Attachment rate constant.

k_d = De-attachment rate constant.

$|k|$ = Numerical value of kinetic constant.

l = Pipe length in pipe flow equation (m).

m = Number of variables in π - theorem.

n = Number of fundamental dimensions.

n' = Constant in circulation equation for the Wemco machine.

n'' = Number of tanks in series.

N_c = Critical speed for rotating equipment.

N_m = Mineral particle number in collision model.

N_a = Air bubble number in collision model.

Ne = Newton number.

P = Power.

P_{80} = Screen size of which 80% will pass (μm) Q = Volume flow (m^3/s).

q_a = Aeration rate (m^3/s).

q_c = Circulation rate (m^3/s).

q_{acv} = Air flow in control volume in CFD model. (m^3/s).

q_p = Pulp volume feed rate (m^3/s).

q_{pcv} = Pulp flow rate in control volume in CFD model (m^3/s).

q_{rva} = Local relative aeration rate in CFD model.

Q = Volume flow (m^3/s).

Q_a = Aeration number.

Q_c = Circulation number.

Q_p = Pulp flow number.

Q_{rrp} = Recovery rate potential function.

Q_t = Tank volume (m^3).

Q_1, Q_2-Q_m = System variables.

r_c = Radius of channel where flow is equal to v_r .

r_o = Radius of channel (m).

R = Recovery (%)

$\check{R}A_e$ = Relative aeration rate.

R_{CLC} = Recleaner capacity (%).

$\check{R}F_d$ = Relative froth depth.

\check{R}_{circ} = Relative circulation.

$\check{R}p_s$ = Relative particle size.

Re_s = Superficial Reynolds number.

Re = Reynolds number.

Re_s = Superficial Reynolds number.

Re_t = Rotor tip Reynolds number.

Re_b = Bubble Reynolds number.

Re_{cv} = Reynolds number of local control volume in CFD model.

R_f = Froth recovery factor.

R_h = Rotor height (m).

R_m = Maximum expected recovery (%).

R_o = Rougher.

S = Maximum expected recovery in Klimple model (%).

S_a = Scale factor.

S_b = Bubble surface flux (sec^{-1}).

S_{bmax} = Maximum bubble surface area flux (sec^{-1}).

S_{gs} = Specific gravity of solids.

S_{gp} = Specific gravity of pulp.

S_{gcv} = Specific gravity of control volume in CFD model.

t = Real time (minutes).

T = Tailings.

T_e = Temperature ($^{\circ}$ K).

U = Forward velocity (m/s).

U_1 = Inlet velocity (m/s).

U_2 = Outlet velocity (m/s).

U_f = Liquid phase velocity (m/s).

U_a = Air phase relative velocity (m/s).

U_m = Solid phase relative velocity (m/s).

v = Linear forward velocity (m/s).

v_a = Average impeller air inlet velocity (m/s).

v_{acv} = Local air speed at control volume (m/s).

v_{pcv} = Local pulp velocity (m/s).

v_o = Free stream velocity (m/s).

v_p = Average outlet pulp velocity (m/s).

v_r = Velocity at distance r (m/s).

v_t = Rotor tip velocity (m/s).

v_s = Sinking velocity (m/s).

V_{cv} = Volume of control volume in CFD analysis (m^3).

We = Weber number.

$x_1 - x_4$ = Unknown exponents in equation for propeller blade.

x' = Exponent in equation for aeration in Wemco machine.

$y_1 - y_4$ = Unknown constants in equation for pipe flow based on Rayleigh's indicial method.

y' = Function of independent variables.

y'' = Deflection in critical speed for rotary equipment (m)

$z_1 - z_6$ = Unknown exponents in equation for pipe flow based on Buckingham's method of repeating variables.

Z = Propeller diameter (m).

Z_f = Reference pipe length in pipe flow problem (m).

Z_{pb} = Bubble particle collision rate (min^{-1}).

Greek Symbols.

α = Constant in equation for maximum bubble surface flux.

α_f = Liquid phase volume fraction.

α_a = Air phase volume fraction.

α_m = Solid phase volume fraction.

β = Exponent in equation for maximum bubble surface flux.

ω = Rotational speed (r/s).

ω_c = Critical rotational speed (radials/s).

ρ = Density (kg/m^3).

ρ_s = Density of solid material (kg/m^3).

ρ_m = Density of mineral (kg/m^3).

ρ_p = Pulp density (kg.m^3).

ρ_f = Liquid phase density (kg/m^3).

ρ_a = Air phase density (kg/m^3).

ρ_{cv} = Density of control volume in CFD analysis (kg/m^3).

ρ_{pcv} = Pulp density number for centre of control volume. (Dimensionless number)

ρ_w = Density of water (kg/m^3).

μ = Viscosity (kg/ms).

μ_p = Pulp Viscosity (kg/ms).

μ_f = Liquid phase viscosity (kg/ms).

μ_a = Air phase viscosity (kg/ms).

ξ = Froth residence time (min).

η = Conditioning time (min).

θ = Conditioner tank turn around (min^{-1}).

ϵ = Energy dissipation number.

δ = Average particle size.

ϕ_s = Mass fraction (% of solids).

Δ = Drainage component in froth recovery factor.

Δp = Pressure drop in pipe flow equation.

Φ = Linear Function.

ϕ_v = Volume fraction of solids.

π = Dimensionless group

ν = Kinematic viscosity (kgm^2/s).

σ = Surface tension (N/m).

τ = Average residence time (min)

τ_g = Gas residence time.

Υ = Dimensionless constant in pipe flow equation.

ψ = Variance of residence time distribution model.

REFERENCES

- Abrahamson, J. 1975. Collision rates of small particles in a vigorously turbulent fluid, *Chemical Engineering Science*, 30(11), 1371-1370.
- AMIRA PROJECT P9L. The Optimisation of Minerals Processes by Modelling and Simulation. Final Report (2).
- Beyers, J.H.M. 2002. CFD study of a Foskor Flotation Separator. Part 3. Evaluation of mineral recovery. Megchem Engineering and Drafting. Nico Diedericks street. Secunda, South Africa.
- Chen, F., Gomez, C.O. and Finch, J.A. 2001. Bubble size measurement in flotation machines. *Minerals Engineering*, 14(4), 427-432.
- Dai, Z., Fornasiero, D. and Ralston, J. 1999. Particle-Bubble attachment in mineral flotation. *Journal of Colloid and Interface Science*, 217(1), 70-76.
- Dai, Z., Dukhin, S., Fornasiero, D. and Ralston, J. 1998. *Journal of Colloid and Interface Science*, 97(2), 275-292.
- Dai, Z., Fornasiero, D. and Ralston, J. 2000. Particle-bubble collision models – a review. *Advances in Colloid and Interface Science*, 85(2-3), 231-256.
- Deglon, D.A., Egya-Mensah, D. and Franzidis J.P. 2000. Review of hydrodynamics and gas dispersion in flotation cells on South African platinum concentrators. *Minerals Engineering*, 13(3), 235-244.
- Deglon, D.A., Sawyerr, F. and O'Connor, C.T. 1999. A model to relate the flotation rate constant and the bubble surface area flux in mechanical flotation cells. *Minerals Engineering*, 2(6), 599-608.
- Degner, V.R. and Treweek, H.B. 1976. Large flotation cell design and development. In: M.C. Fuerstenau, Editor, *Flotation Volume 2*, AIME, New York, NY, USA, 816–837.
- Dobias, B., Klar, W. and Schwinger, K. 1992. Flotation of pigments and inks from waste paper. *Innovations in Flotation Technology*, 499-511.
- Fox, R.W., Pritchard, P.J. and McDonald, A.T. 2008. *Introduction to Fluid Mechanics*, John Wiley and Sons, Inc., NJ, USA

- Gorain, B.K., Franzidis, J.P. and Manlapig, E.V. 1997. Studies of impeller type, impeller speed and air flow rate in an industrial scale flotation cell. Part 4: Effect of bubble surface area flux on flotation performance. *Minerals Engineering*, 10(4), 367-379.
- Gorain, B.K., Franzidis, J.P. and Manlapig, E.V. 1999. The empirical prediction of bubble surface area flux in mechanical flotation cells from cell design and operating data. *Minerals Engineering*, 12(3), 309-322.
- Klimpel, R.R. 1980. Selection of chemical reagents for flotation. Ch. 45 in *Mineral Processing Plant Design*, A.J. Muller (ed), 2nd ed. 907-934.
- Koh, P.T.L., Manickam, M. and Schwarz, M.P. 2000 CFD Simulation of bubble-particle collisions in mineral flotation cells. *Minerals Engineering*, 13(14-15), 1455-1463.
- Nelson, M.G. and Lelinski, D. 2000 Hydrodynamic design of self-aerating flotation machines. *Minerals Engineering*, 13(10-11), 991-998.
- Newell, R. and Grano, S. 2007. Hydrodynamic and scale-up in Ruston turbine flotation cells: Part 1 - Cell hydrodynamics. *International Journal of Mineral Processing*, 81(4), 224-236.
- Newell, R. and Grano, S. 2006. Hydrodynamic and scale-up in Ruston turbine flotation cells: Part 2 - Flotation scale-up for laboratory and pilot cells. *International Journal of Mineral Processing*, 81(2), 65-78.
- Mavros, P. 1992. Mixing and hydrodynamics in flotation cells. In: P. Mavros and K.A. Matis, Editors, *Innovations in Flotation Technology*, Kluwer Academic.
- Rodrigues, W.J., Leal Filho, L.S. and Masini, E.A. 2001. Hydrodynamic dimensionless parameters and their influence on flotation performance of coarse particles. *Minerals Engineering*, 14(9), 1047-1054.
- Roscoe, R. 1952. The viscosity of suspensions of rigid spheres. *British Journal of Applied Physics*, 3, 267-269.
- Ruzicka, M.C. 2008. On dimensionless numbers. *Chemical Engineering Research and Design*, 86(8), 835-868.
- Schulze, H.J. 1982. Dimensionless number and approximate calculation of the upper particle size of floatability in flotation machines. *International Journal of Mineral Processing*, 9(4), 321-328.

Schubert, H. and Bischofberger, C. 1998. On the microprocesses air dispersion and particle-bubble attachment in flotation machines as well as consequences for the scale-up of macroprocesses. *International Journal of Mineral Processing*, 52(4), 245-259.

Sleigh, P. A. and Noakes, C. 2009. Lecture Notes: An Introduction to Fluid Dynamics. CIVE 1400. School of Civil Engineering. University of Leeds, Leeds, United Kingdom (<http://www.efm.leeds.ac.uk/CIVE/FluidsLevel1/Unit00/index.html>)

Van der Linde, G.J. 1980. *’n Studie van die Wisselwerking tussen Reagense en Minerale by die Flottasie van Apatiet*. Proefskrif vir die graad "Doktor in die Natuurwetenskappe". Randse Afrikaanse Universiteit, Johannesburg, South Africa.

Vera, M., Franzidis, J.P. and Manlapig, E. 1999. The JKMRRC high bubble surface area flux flotation cell. *Minerals Engineering*, 12(5), 477-484.

Wills, B.A. and Napier-Munn, T.J. 2006. *Mineral Processing Technology*, 7th ed. Elsevier Publishers, Netherlands.

Wittrup, K.D. 2007. Chemical and Biological Reaction Engineering. Spring 2007. Lecture 10. Massachusetts Institute of Technology.

Yoon, R.H. 2000. The role of hydrodynamic and surface forces in bubble-particle interaction. *International Journal of Mineral Processing*, 58(1-4), 129-143.

Zlokarnic, M. and Judat, H. 1967. Rohr- und Scheibenrührer - zwei leistungsfähige Rührer zur Flüssigkeitsbegasung, *Chemische Ingenieurstechnik*, 39(20), 1163-1168.

Zlokarnic, M. 1972. Criteria based on the Theory of Similarity for Dimensioning Flotation Cells. Presentation to the 13th session of the Working Committee on Flotation of the Expert Committee on Ore Processing of the GDMB, Bad Grund. (Herz).

Zlokarnic, M. 1991. *Dimensional Analysis and scale-up in Chemical Equipment*. Springer-Verlag, Berlin, Germany.

Zlokarnic, M. 1998. Problems in the application of dimensional analysis and scale-up of mixing operations. *Chemical Engineering Science*, 53(17), 3023-3030.

Zlokarnic, M. and Judat, H. 1969 Tube and propeller stirrers – An effective stirrer combination for simultaneously Gassing and Churning Chem-Ing Tech 41, 1270-1273.

APPENDIX 1: I-BANK PILOT PLANT

1.1. I-Bank operational conditions.

Table 41: Showing the operational conditions for I-Bank pilot plant.

Parameter	Dimension	Value
Tank size	L	300
RPM	r/s	58
Rotor diameter	m	0.27
Rotor height	m	0.05
Rotor submergence	m	0.6
Tank diameter	m	0.63
Tank Height	m	0.75
Tank width	m	0.63
Conditioner volume	m	0.57
Pulp density	kg/m ³	1400
Power Installed (Consumed)	kW	2 (1.6)
Rotor aspect ratio	-	5

I-bank pilot plant has been built a few years after the Foskor research pilot plant as a tool to investigate production problems with the same feed from the main plant. (Same mineralogy and grind: $P_{80} = 310$ micron). For this reason the pilot plant was built underneath the mill building. This plant is the next size Denver machine use in the Foskor pilot plant and it was decided to use it as an interim scale-up phase before modifying the main plant. The question was what parameters should be modified to comply to the Foskor pilot plant specification The machines are all Denver # 12 machines. The configuration is 3x roughers + 2x scavengers + 2x cleaners + 1x recleaner. The characteristics of the individual cells are as per Table 41.

1.2. Geometrical similarity.

Dimensionless groups which are within 10% of numerical similarity are labeled as: OK, otherwise NOK

1.2.1. Diameter ratio from π_7 .

$$\begin{aligned}DR_a &= 0.27/0.63 \\ &= 0.43 \text{ (OK)}\end{aligned}$$

1.2.2. Volumetric ratio from π_{16} .

$$\begin{aligned}VR_a &= (0.63)^3/(0.27 \cdot 0.6 \cdot 0.75) \\ &= 2.1 \text{ (OK)}\end{aligned}$$

1.2.3. Ratio of Rotor volume to Tank volume π_{17} .

$$\begin{aligned}\acute{R}T_a VR_a &= 0.27^2 \cdot 0.05 / (0.63^2 \cdot 0.75) \\ &= 2.9\%\end{aligned}$$

1.3. Metallurgical similarity.

1.3.1. Conditioning time.

Before we can calculate the CT we need to decide on the feed rate. Let us assume 2 tph

$$\begin{aligned}q_p &= 2 / (0.42 \cdot 1.4 \cdot 3600) \\ &= 9.5 \times 10^{-4} \text{ m}^3/\text{s}\end{aligned}$$

Therefore $CT = 0.572 / 9 \times 10^{-4}$

$$= 635 \text{ s [10.5 min] (OK)}$$

Conditioner mechanism $\theta = 7$ (OK)

1.3.2. Retention time.

The flow diagram is the same as pilot plant then there would be 3 x roughers and 2x scavengers and therefore:

$$\begin{aligned}\tau &= 5 \times 0.297 / (9 \times 10^{-4} \cdot 1.3) \\ &= 1269 \text{ s [21 min] (OK)}\end{aligned}$$

(The factor = 1.3 allows for circulating load)

1.4. Hydrodynamic similarity.

1.4.1. Rotor tip Reynolds number.

Rotor tip velocity = $58 \cdot 0.27/2$

$$= 7.8 \text{ m/s}$$

Therefore $Re_t = 1400 \cdot 7.8 \cdot 0.27 / 1.8 \times 10^{-3}$

$$= 1.7 \times 10^6 \text{ (OK)}$$

1.4.2. Aeration number.

$$Q_a = 6 \times 10^{-3} / [58 \cdot (0.63)^3]$$

$$= 4.8 \times 10^{-4} \text{ (NOK)}$$

1.4.3. Circulation and relative circulation.

No info available

1.4.4. Froude number.

$$Fr_D = \omega^2 \cdot d^2 / 4 \cdot g \cdot D$$

$$= 9.9 \text{ (NOK)}$$

1.4.5. Bubble surface area flux (Gorain model).

From Equation 56 the bubble surface area flux is equal to 31 s^{-1} (OK)

1.4.6. Volumetric flow.

$$VfN = 9 \times 10^{-4} \cdot 1.3 / [58 \cdot (0.63)^3]$$

$$= 8 \times 10^{-5} \text{ (OK)}$$

1.4.7. Power number.

$$\dot{R}PNo = 1600 / 1400 \cdot 58^3 \cdot 0.27^5$$

$$= 4.3 \times 10^{-3} \text{ (OK)}$$

$$T_aPNo. = 1700 / (1400 \cdot 58^3 \cdot 0.63^5)$$

$$= 6.3 \times 10^{-5} \text{ (OK)}$$

1.5. Remarks.

- 1.5.1 It is obvious that there is a slight deficiency in aeration rate and bubble surface flux. The rest of the dimensionless groups are within acceptable limits (OK).
- 1.5.2 From the new scale-up methodology the ratio of P_{80} /tank diameter ratio is far from specification. This is a result of coarse grinding.
- 1.5.3 The combination of $Re_t \times Fr^{0.5} = 8$ is also below specification.
- 1.5.4 According to the Denver catalogue the rotor diameter was suppose to be 0.31m and upon inspection it was found that the rotor diameter has been reduced to 0.27m. This has probably been done to match the installed power. With a reduced rotor diameter the RPM should be 70r/s. This would have resulted in a $Re_t \cdot Fr^{0.5} = 11.5 \times 10^6$ which is very close to the requirement of 12×10^6 .
- 1.5.5 The Denver design utilises a spigot for recirculation which allows pulp to be drawn into the eye of the rotor and as a result increase circulation and aeration. Inspection of this spigot reveals that the spigot was too small. After replacing the spigot with the correct size the plant performed at 93% recovery and high concentrate grade.
- 1.5.6 The reason for the lower performance was a result of a lack of liberation and incorrect size of the sand relieve valve which hampered proper froth depth control.

APPENDIX 2: H-BANK RECONFIGURED

2.1. Operating Conditions.

2.1.1. Historical background.

H-bank has originally been designed to upgrade the <45 micron fraction of the final concentrate from about 35% P₂O₅ to 40% P₂O₅ and at the same time reduce the Magnesium to an acceptable level (<2%). The laboratory experiments (Table 42) proved that this could be done:

Table 42: Results of laboratory experiment to reduce magnesium.

No	Particle	Reagent	S _{gp}	Feed	Feed	Conc.	Rec	Conc.
1	<45	None	1.1	34.2	1.46	37.4	92.7	0.8
2	<45	FA 0.25	1.1	31.8	2.1	35.6	81.4	0.7
3	<45	None	1.1	25.9	3.23	37.1	65.5	0.8
4	<45	None	1.1	31.5	3.4	35.5	82.6	1.7

2.1.2. The original installation.

The original installation consisted of:

- 14x164 # Wemco cells (eff. volume = 24.5m³) – As roughers
- 8x144 # Wemco cells (eff. volume = 13.7m) – As Scavengers
- 11x120 # Wemco cells (eff. volume = 8.2m³) – As cleaners
- 8x84# Wemco cells (eff. volume = 3.7m³) – As Recleaners

No provision was made for conditioning in the original lay-out.

2.2. New design.

As the original installation could not perform the upgrade, the request was to reconfigure the equipment to float a very special type of Phosphate mineral called PP&V.

The specification for the mineral is given on spec sheet no.11. in Appendix 6. The feed rate would be 300tph with P₈₀ < 300µm to comply to the retention time requirements.

2.2.1. Conditioner volume.

$$\begin{aligned}\text{Conditioner volume} &= C_o T \cdot q_p \\ &= 10 \cdot 60 \cdot 0.142 \\ &= 85\text{m}^3\end{aligned}$$

2.2.2. Rougher & Scavenger volume.

$$\begin{aligned}(\text{R}_o \text{ \& Sc}) \text{ volume} &= T \cdot q_p \cdot 1.5 \text{ (50\% circulating load)} \\ &= 22 \cdot 60 \cdot 0.142 \cdot 1.5 \\ &= 281\text{m}^3\end{aligned}$$

2.2.3. Scavenger volume.

$$\begin{aligned}\text{Sc volume} &= 0.4 \cdot 281 \\ &= 112\text{m}^3\end{aligned}$$

Then rougher volume = 169m³.

2.2.4. Cleaner & Recleaner volume required.

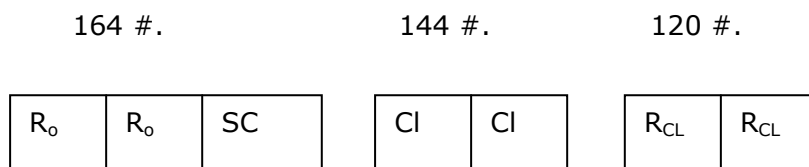
$$\begin{aligned}(\text{Cl \& R}_{\text{CL}}) \text{ volume} &= 0.6 \cdot (\text{R}_o \text{ \& Sc}) \text{ volume} \\ &= 0.6 \cdot 281 \\ &= 168\text{m}^3\end{aligned}$$

2.2.5. Recleaner volume.

$$\begin{aligned}\text{Recleaner volume} &= 0.4 \cdot (\text{Cl \& R}_{\text{CL}}) \text{ volume} \\ &= 0.4 \cdot 168 \\ &= 67\text{m}^3\end{aligned}$$

Then available cleaner volume = 101m³

2.2.6. Flow diagram.



Four parallel streams will bring down the superficial Reynolds number to 20734.

Table 43: Superficial Reynolds number for present lay-out.

Mechanism	q _p .	Area	v	D	Re _s
164	0.05	8.4	0.0063	4.2	20734

2.2.7. Volumetric ratio.

$$VR_a = (4.2 \cdot 0.8)^3 / (0.76 \cdot 0.97 \cdot 2.35)$$

$$= 21.8$$

2.2.8. Rotor tip Reynolds number with $\omega = 20r/s$.

$$Re_t = 1400 \cdot 7.6 \cdot 0.76 / 1.8 \times 10^{-3}$$

$$= 4.5 \times 10^6$$

2.2.9. Aeration number and relative aeration.

$$A_e N = 0.196 / [20 \cdot (4.2 \times 0.8)^3]$$

$$= 2.5 \times 10^{-4} \text{ (To low)}$$

$$\check{R}A_e = 4:1 \text{ (To low)}$$

2.2.10. Bubble surface flux.

Table 44: Analysis of different mechanisms for bubble surface flux.

Mechanism	Q _a	A _{cell}	J _g	v _t	Constant	S _b
164	0.15	11.8	1.27	7.6	0.1	38
144	0.12	9.6	1.25	7.3	0.1	37
120	0.08	6.7	1.2	7.6	0.1	36

The constant in this case = $(\dot{A}R_a)^{-0.019} \times (P_{80})^{-0.4} = 0.102$

2.2.11. Circulation and relative circulation and volumetric flow.

$$q_c = 0.79/[20(4.2 \cdot 0.85)^3]$$

$$= 8.7 \times 10^{-4}$$

$$R_{\text{circ}} = 15:1$$

$$VfN = 0.053/20(4.2)^3$$

$$= 5.8 \times 10^{-5}$$

2.2.12. Power number.

$$\dot{R}PNo = 48 \times 10^3/[1400 \cdot (20)^3 \cdot (0.76)^5]$$

$$= 17 \times 10^{-3}$$

$$T_a PNo = 7 \times 10^{-6}$$

2.3. Remarks.

The aim of the exercise was to utilise the existing equipment to the best possible extent and therefore it is expected that there will be some shortcomings:

2.3.1. The Scavenger volume is only 50% of the rougher volume but maybe this deficiency will be offset by the slight increase in retention time.

2.3.2. Volumetric ratio is typical of the Wemco design.

2.3.3. Superficial Reynolds number is higher than the specification but it is significantly lower than the main plant.

2.3.4. Aeration rate, relative aeration and bubble surface area flux are below specification. The key here is to improve P80 as all the other parameters are fixed.

2.3.5. Volumetric flow is acceptable.

2.3.6. Power is insufficient.

2.4. Result.

2.4.1. This modification was never implemented but the plant was recommissioned as is and never performed up to standard because of the reasons mentioned in paragraph 2.

APPENDIX 3: 42 m³ SMART CELL.

3.1. Background.

As part of a new extension planned at Foskor a comparison test was made between two 42 m³ Smart cells from two suppliers and utilising the same feed. The schedule of dimensionless numbers was utilised to identify and explain the differences in geometry, hydrodynamics and performance. The mineralogy, conditioning, grinding and chemistry were the same for both machines.

3.2. Experimental set-up and hydrodynamic performance.

Table 45: Comparison between 42 m³ Smart cells with pyroxenite ore.

Factor	dim	Spec	Cell A	Cell B
F _d	%	10	10	10
S _b	s ⁻¹	66	53 ⁺	28
DR	-	0.5	0.25	0.21
VR	-	4	28	4
Re _t	-	2x 10 ⁶	7x10⁶	8x10⁶
A.N.	-	4.1x10 ⁻⁴	3.5x10 ⁻⁴⁺	1.5x10 ⁻⁴
Circ	-	4.3x10 ⁻⁴	1.4x10⁻³	3x10⁻³
ŘP.No	-	1.78x10 ⁻³	16x10⁻³	15x10⁻³
T _a PNo	-	3.4x10 ⁻⁵	3.3x10⁻⁵	2.4x10⁻⁵
Performance	Rec/Grade	-	55%/30%P	21%/30P

Bold = Compliance; Shaded = Non-compliance; (+) = Better.

3.3. Results and conclusions.

Cell A performed at 55% recovery while cell B performed at 21% recovery. Both with the same feed and concentrate grade. It was obvious that the better performance of cell A could be attributed to a higher bubble surface flux, aeration rate, power number and power intensity. After doubling the aeration rate and increasing the RPM by 10% on Cell B, the performance was equal to that of Cell A.

APPENDIX 4: BANK 15.

4.1. Background.

According to Macros (1972), the separation zone must be protected from the turbulence and agitation from the agitation zone, and for this reason a low volumetric ratio is required. To accomplish this, "bank 15 experiment" has been designed to test the sensitivity of the process to the change in agitation and quiet zone. To achieve this a modified (shortened) Wemco #164 rotor has been installed in a #120 cell (Bank 15) and compared with a #144 short rotor in a #120 cell (Bank 13). (See Figure 64 & 65) This modification reduced the volumetric ratio of bank 15 to 27 and this has been compared with the bank 13 which has been refurbished with new 144 short components and volumetric ratio of 45. (See Table 46.)

Table 46: Performance comparison between bank 13 and bank 15.

ITEM	BANK 13	BANK 15
Volumetric ratio	45	27
Average rougher conc	27.9	28.1
Feed (% P ₂ O ₅)	14.2	12.1
Tails (%P ₂ O ₅)	10.8	9.75
Recovery (%)	39.5	30.5
Froth depth (mm)	200	200

4.2. Machine Changes.

The disappointing performance of bank 15 as indicated in Table 45 were investigated and the following were discovered:

- Bank 15 retention time was 20% less than bank 13 because of the bigger mechanisms.
- The hood was the so called high energy hood with less open area.
- No gap between disperser and draft tube.

The following changes were made:

- To reduce the retention time an orifice was installed in the feed lines.
- The standard hood was installed.
- The disperser has been shortened to create a 25mm gap between disperser and draft tube.

The metallurgical and hydrodynamic result of these changes are summarised in Table 41 and the operational performance taken over three weeks are shown in Table 47.

Table 47: Metallurgical and Hydrodynamic comparison between bank 13 and bank 15.

ITEM	BANK 13	BANK 15
Retention (min)	4	4
$S_b(s^{-1})$	34	28
Circulation	8×10^{-4}	5×10^{-4}
Aeration Number	2.2×10^{-4}	2.3×10^{-4}
Volumetric ratio	45	27
Rotor tip Reynolds No	4.4×10^6	4.5×10^6
Ave Recovery (%)	26.6	34.4

4.3. Conclusions.

- 4.3.1. It seems that the modification to protect the separation zone contributed to the improvement in performance.
- 4.3.2. Even with an inferior circulation and bubble surface area flux, bank 15 still performed better than bank 13.

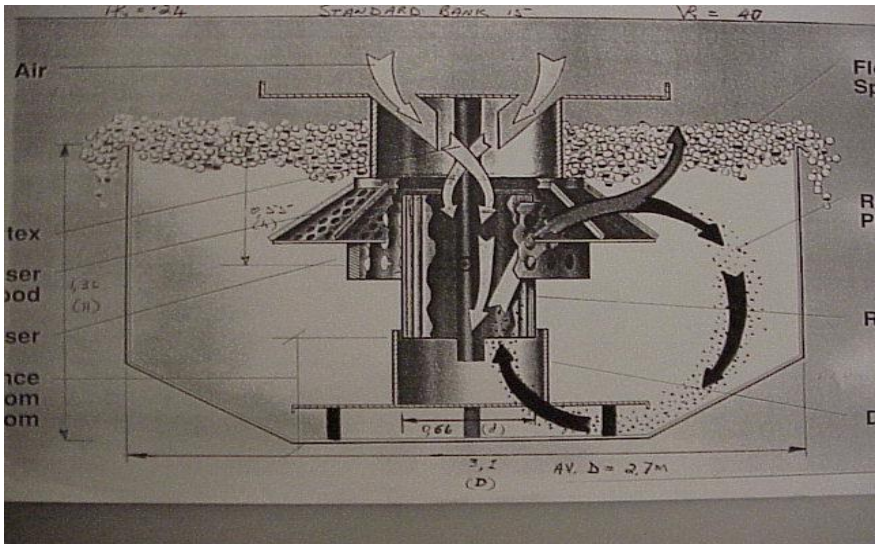


Figure 65: Standard Wemco-Bank 13.

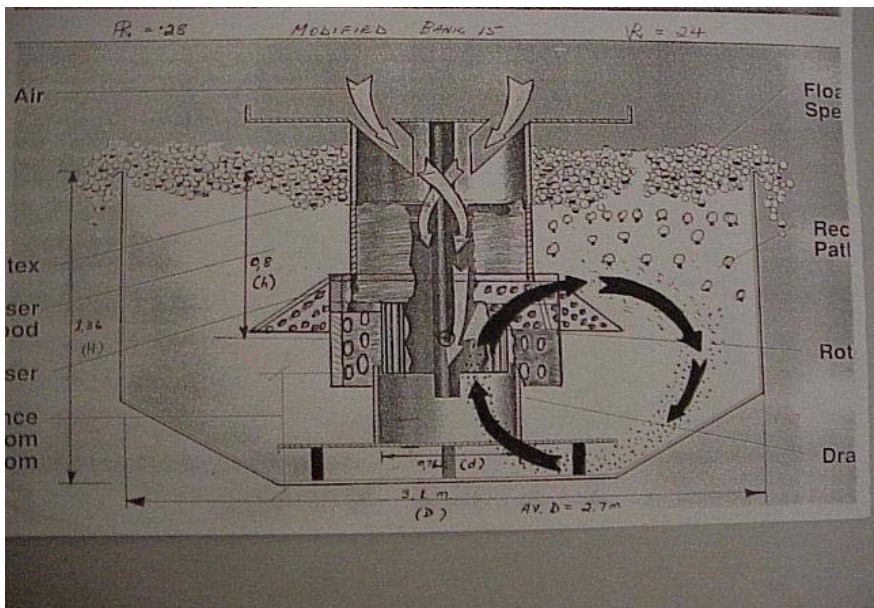


Figure 66: Modified Wemco-Bank 15.

APPENDIX 5: MINERAL SPECIFICATION

MINERAL SPECIFICATION SHEET NO.1.

MINERAL: PYROXENITE ORE.

Mineral	AP	PHL	LIz	MAG	DIOP	CAL	FOR	VERM	-
%	18	24	2	0	54	0.3	0.2	2	-
Grind	F10	F50	F 60	F80	F100	-	-	-	-
µm	50	150	250	300	425	-	-	-	-
Chem.									
type	FA	WG	PGE	SA	GUM	-	-	-	-
gm/t	400	0	0	160	0	-	-	-	-
Metal									
Factor	τ	F_d	VC	S_b	FLD	C_oT	pH	-	-
dim	min	%	%	sec^{-1}	PP	min	-	-	-
factor	30*	9/5+	60*	>60	PP	10	9	-	-
Hyd.									
Factor	VR_a	$\dot{A}R_a$	Re_s	Re_t	A_eN	Circ.	Vf.N	$\dot{R}PNo$	$T_aPNo.$
factor	4	1	500	2×10^6	4.1×10^{-4}	4.3×10^{-4}	2.9×10^{-5}	1×10^{-3}	4.3×10^{-5}

*Based on rougher and scavenger capacity.

+ Based on cell depth.

MINERAL SPECIFICATION SHEET NO.2.

Mineral: FOSKORITE-CARBONATITE ORE.

Mineral	AP	FL	LIS	DIOP	KAL	DOL	FOR	FOR	-
%	16	10	7	5	42	14	4	4	-
Grind	F10	F50	F60	F80	F100	-	-	-	--
µm	50	150	250	300	425	-	-	-	-
Chem.									
type	FA	WG	PGE	SA	GUM	-	-	-	-
gm/t	204	347	164		>60	-	-	-	-
Met									
type	τ	F _d	VC	S _b	FLD	C _o T	pH	-	-
dim	min	%	%	sec ⁻¹	PP	min	-	-	-
factor	25*	9/5 ⁺	12*	>60	PP	10	9	-	-
Hyd									
type	VR _a	ÅR _a	Re _s	Re _t	A _e N	Circ	VfN	ÍPNo	T _a PNo
factor	4	1	500	2x10 ⁶	4.1x10 ⁻⁴	>4.3x10 ⁻⁴	2.9x10 ⁻⁴	1x10 ⁻³	4.3x10 ⁻⁵

*Based on rougher and scavenger capacity.

+ Based on cell depth.

MINERAL SPECIFICATION SHEET NO.3.

MINERAL: FOSKORITE ORE.

Mineral	AP	FL	LIS	DIOP	KAL	FOR	Mag	-	-
%	20	26	15	25	5	7	15	-	-
Grind	F10	F50	F60	F80	F100		-	-	-
µm	50	50	250	300	425		-	-	-
Chem.									
type	FA	WG	PGE	SA	GUM		-	-	-
gm/t	388	0	129	0	0		-	-	-
Met									
type	τ	F _d	VC	S _b	FLD	CT	pH	-	-
dim	min	%	%	sec ⁻¹	PP	min	-	-	-
factor	28*	5/2 ⁺	60*	>60	p	10	9	-	-
Hyd									
Type	VR _a	ÅR _a	Re _s	Re _t	A _e N	Circ	Vf.N	ŘPNo	T _a PNo
Factor	4	1	500	2x10 ⁶	4.1x10 ⁻⁴	4.3x10 ⁻⁴	2.9x10 ⁻⁵	1x10 ⁻³	4.3x10 ⁻⁵

*Based on rougher and scavenger capacity.

+ Based on cell depth.

MINERAL SPECIFICATION SHEET NO.4.

MINERAL: ARE 9 LA ORE.

Mineral	AP	FL	LIS	MAG	DIOP	KAL	FOR	VERM	
%	18	38	11	1	26	5	1	1	
Grind	F10	F50	F60	F80	F100	-	-	-	-
Dim	μm	μm	μm	μm	μm	-	-	-	-
μm	50	150	250	300	425	-	-	-	-
Chem.									
type	FA	WG	PGE	SA	GUM	-	-	-	-
gm/t	754	43754	86	-	-	-	-	-	-
Met									
type	τ	F _d	VC	S _b	FLD	C _o T	pH	-	-
dim	min	%	%	sec ⁻¹	PP	min	-	-	-
factor	28*	5/2 ⁺	60*	>60	PP	10	9	-	-
Hyd									
type	VR _a	ÅR _a	Re _s	Re _t	A _e N	Circ	VfN	ŘPNo	T _a PNo
factor	4	1	500	2x10 ⁶	4.1x10 ⁻⁴	4.3x10 ⁻⁴	2.9x10 ⁻⁵	1x10 ⁻³	4.3x10 ⁻⁵

*Based on rougher and scavenger capacity.

+ Based on cell depth.

MINERAL SPECIFICATGION SHEET NO.5.

MINERAL: ARE 9 LG ORE.

Mineral	AP	FL	LIS	MAG	DIOP	KAL	DOL	FOR	-
%	20	30	21	1	14	7	1	6	-
Grind	F10	F50	F60	F80	F100	-	-	-	-
µm	50	150	250	300	425	-	-	-	-
Chem.									
type	FA	WG	PGE	SA	GUM	-	-	-	-
gm/t	785	55	86	-	-	-	-	-	-
Met									
type	τ	F _d	VC	S _b	FLD	C ₀ T	-	-	-
dim	min	%	%	sec ⁻¹	PP	min	-	-	-
factor	28*	5/2 ⁺	60*	>60	PP	10	-	-	-
Hyd.									
type	VR _a	ÅR _a	Re _s	Re _t	A _e N	Circ	VfN	ŘPNo	T _a PNo
factor	4	1	500	2x10 ⁶	4.1x10 ⁻⁴	4.3x10 ⁻⁴	2.9x10 ⁻⁵	1x10 ⁻³	4.3x10 ⁻⁵

*Based on rougher and scavenger capacity.

+ Based on cell depth.

MINERAL SPECIFICATION SHEET NO.6.

MINERAL: ARE 9 SW ORE.

Mineral	AP	FL	LIS	MAG	DIOP	KAL	DOL	FOR	-
%	21	21	9	1	36	4	2	5	-
Mill	F10	F50	F60	F80	F100	-	-	-	-
µm	50	150	250	300	425	-	-	-	-
Chem.						-			
type	FA	WG	PGE	SA	GUM	-	-	-	-
gm/t	387	21	54	-	-	-	-	-	-
Met									
type	τ	F_d	VC	S_b	FLD	C_oT	-	-	-
dim	min	%	%	sec^{-1}	PP	min	-	-	-
factor	28*	5/2 ⁺	60*	>60	PP	10	-	-	-
Hyd									
type	VR_a	$\dot{A}R_a$	Re_s	Re_t	A_eN	Circ	VfN	$\dot{R}PNo$	$T_aPNo.$
factor	4	1	500	2×10^6	4.1×10^{-4}	4.3×10^{-4}	2.9×10^{-5}	1×10^{-3}	4.3×10^{-5}

*Based on rougher and scavenger capacity.

+ Based on cell depth.

MINERAL SPECIFICATION SHEET NO.7.

MINERAL: ARE 9 F11A ORE.

Mineral	AP	FL	LIS	MAG	DIOP	KAL	DOL	FOR	-
%	18	40	11	1	17	4	2	6	-
Grind	F10	F50	F60	F80	F100	-	-	-	-
µm	50	150	250	300	425	-	-	-	-
Chem.									
Type	FA	WG	PGE	SA	GUM	-	-	-	-
gm/t	672	43	129	-	-	-	-	-	-
Met									
Type	τ	F _d	VC	S _b	FLD	C _o T	pH	-	-
Dim	min	%	%	sec ⁻¹	PP	min	-	-	-
factor	28*	5/2 ⁺	60*	>60	PP	10	9	-	-
Hyd									
type	VR _a	ÅR _a	Re _s	Re _t	A _e N	Circ	VfN	ŘPNo	T _a PNo
factor	4	1	500	2x10 ⁶	4.1x10 ⁻⁴	4.3x10 ⁻⁴	2.9x10 ⁻⁵	1x10 ⁻³	4.3x10 ⁻⁵

*Based on rougher and scavenger capacity.

+ Based on cell depth.

MINERAL SPECIFICATION SHEET NO.8.

MINERAL: ARE 9 F12W ORE.

Mineral	AP	FL	LIS	MAG	DIOP	KAL	DOL	FOR	-
%	18	37	8	1	23	11	0.5	1	-
Grind	F10	F50	F60	F80	F100	-	-	-	-
µm	50	150	250	300	425	-	-	-	-
Chem.									
Type	FA	WG	PGE	SA	GUM	-	-	-	-
gm/t	462	20	113	-	-	-	-	-	-
Met									
Type	τ	F _d	VC	S _b	FLD	C _o T	-	-	-
Dim	min	%	%	sec ⁻¹	PP	min	-	-	-
factor	28*	5/2 ⁺	60*	>60	PP	10	-	-	-
Hyd.									
type	VR _a	ÅR _a	Re _s	Re _t	A _e N	Circ	VfN	ŘPNo	T _a PNo
factor	4	1	500	2x10 ⁶	4.1x10 ⁻⁴	4.3x10 ⁻⁴	2.9x10 ⁻⁵	1x10 ⁻³	4.3x10 ⁻⁵

*Based on rougher and scavenger capacity.

+ Based on cell depth.

MINERAL SPECIFICATION SHEET NO.9.

MINERAL: ARE 9 F12 ORE.

Mineral	AP	FL	LIS	MAG	DIOP	KAL	DOL	FOR	-
%	15	55	7	1	20	-	2	-	-
Grind	F10	F50	F60	F80	F100	-	-	-	-
µm	50	150	250	300	425	-	-	-	-
Chem.									
Type	FA	WG	PGE	SA	GUM	-	-	-	-
gm/t	431	26	52	-	-	-	-	-	-
Met									
Type	τ	F _d	VC	S _b	FLD	C _o T	-	-	-
Dim	min	%	%	sec ⁻¹	PP	min	-	-	-
factor	28*	5/2 ⁺	60*	>60	PP	10	-	-	-
Hyd.									
type	VR _a	ÅR _a	Re _s	Re _t	A _e N	Circ	VfN	ŘPNo	T _a PNo
factor	4	1	500	2x10 ⁶	4.1x10 ⁻⁴	4.3x10 ⁻⁴	2.9x10 ⁻⁵	1x10 ⁻³	4.3x10 ⁻⁵

*Based on rougher and scavenger capacity.

+ Based on cell depth.

MINERAL SPECIFICATION SHEET NO.10.

MINERAL: PMM TAIL DAM ORE.

Mineral	AP	FL	LIS	MAG	DIOP	KAL	DOL	FOR	-
%	20	8	15	3	5	20	-	-	-
Grind	F10	F50	F60	F80	F100	-	-	-	-
µm	10	105	150	300	500	-	-	-	-
Chem.									
Type	FA	WG	PGE	SA	GUM	-	-	-	-
gm/t	388	350	150	0	60	-	-	-	-
Met									
Type	τ	F_d	VC	S_b	FLD	C_oT	pH	-	-
Dim	min	%	%	sec^{-1}	PP	Min	-	-	-
factor	25*	9/5 ⁺	60*	>60	PP	10	9	-	-
Hyd									
type	VR_a	$\dot{A}R_a$	Re_s	Re_t	A_eN	Circ	VfN	$\dot{R}PNo$	T_aPNo
factor	4	1	500	2×10^6	4.1×10^{-4}	4.3×10^{-4}	2.9×10^{-5}	1×10^{-3}	4.3×10^5

*Based on rougher and scavenger capacity.

+ Based on cell depth.

MINERAL SPECIFICATION SHEET NO.11.

MINERAL: PP&V ORE.

Mineral	AP	FL	LIS	MAG	DIOP	KAL	DOL	VERM	-
%	20	6	-	-	55	-	-	20	-
Grind	F10	F50	F60	F80	F100	-	-	-	-
µm	50	150	250	300	425	-	-	-	-
Chem.									
Type	FA	WG	PGE	SA	GUM	-	-	-	-
gm/t	400	-	-	50	-	-	-	-	-
Met									
Type	τ	F _d	VC	S _b	FLD	C _o T	-	-	-
Dim	min	%	%	sec ⁻¹	PP	min	-	-	-
factor	30*	9/5 ⁺	60*	>60	pp	10	-	-	-
Hyd									
Type	VR _a	ÅR _a	Re _s	Re _t	A _e N	Circ	VfN	ŘPNo	T _a PNo
factor	4	1	500	2x10 ⁶	4.1x10 ⁻⁴	4.3x10 ⁻⁴	2.9x10 ⁻⁵	1x10 ⁻³	4.3x10 ⁻⁵

*Based on rougher and scavenger capacity.

⁺ Based on cell depth.

APPENDIX 6: VISCOSITY IN PULP.

6.1. Method by Roscoe (1952).

One of the most difficult parameters to measure is pulp viscosity. Roscoe developed an empirical model which gives relatively good results with conservative solids loading

$$\mu_p = \mu_w(1-\phi_v)^{-2.5} \quad (88)$$

Where ϕ_v = volume fraction of solids and μ_w = viscosity of water. For a pulp specific gravity of $S_{gp} = 1.4$ the viscosity works out to $1.67 \times 10^{-3} \text{kg/ms}$.

6.2. Helephi's model (1997).



Figure 67: Showing the modification to the hand drill and design of the shear plate for the Helephi's viscometer.

This model is dedicated to my laboratory assistant who developed the model, built and calibrated the viscometer. The viscometer was constructed by modifying a hand held drill to increase the sensitivity of its amp meter and also providing the grip with a trigger mechanism to start at the same amp reading for calibration purposes. The drill was also fitted with an extended shaft and a shear disc. The reasoning here was that:

$$\text{amps} = \text{torque} = \text{shear} = \text{viscosity}. \quad (89)$$

Helepi then calibrated the meter with known fluids and obtained a relationship between viscosity and amps.

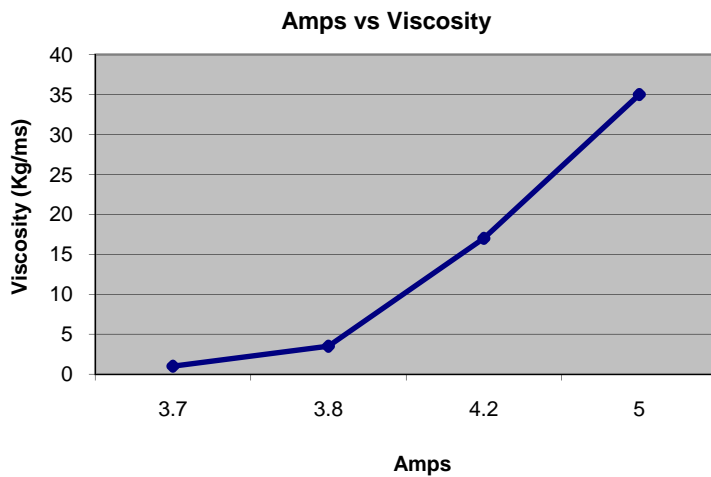


Figure 68: Relationship between viscosity and Amps.

Helepi then measured pulp density and viscosity in an active cell and produced the following result:

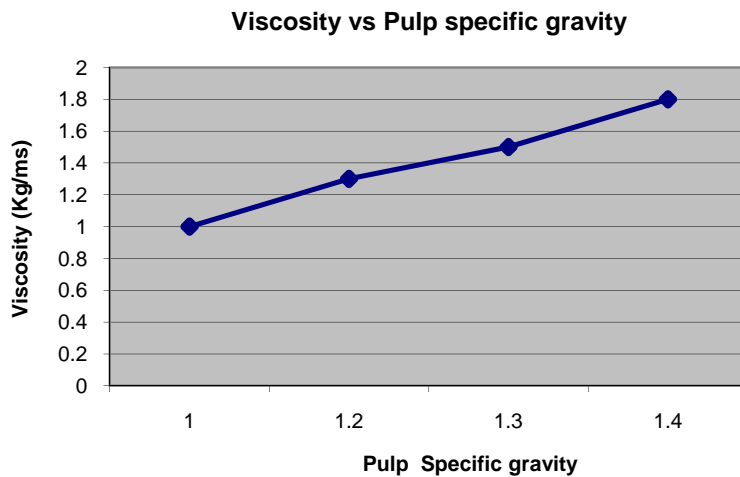


Figure 69: Viscosity vs. Pulp specific gravity for Helepi's method.

This result compares favourably with that of Roscoe and renders a $\mu_p = 1.8$ kg/ms at $S_{gp} = 1.4$

6.3. Germans' Method.

This method entails the measurement of a pressure drop over a fix length. The pressure drop is a function of the velocity distribution and viscosity. The experiment produced significantly higher viscosities because

- The pulp was a copper pulp
- No air was present
- No reagents were present
- Particle size was not known.

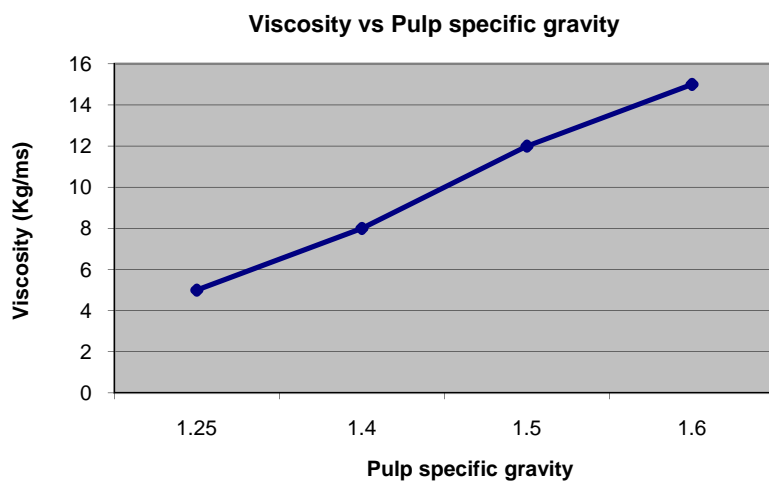


Figure 70: Viscosity vs. Pulp specific gravity for German's method.

APPENDIX 7: DETAIL DIMENSIONLESS ANALYSIS.

7.1. Variables.

Table 6 contains the relevant list for a mechanically agitated flotation process. The technique chosen for dimensional analysis is the method of repeating variables. In this case three repeating variables are chosen (Because three dimensions exist) and a fourth one is added to form a dimensionless group by equating the function to one. (π -group). The choice of repeating variables are:

Pulp density = ρ_p (ML^{-3})

Some linear velocity = v (LT^{-2})

Tank diameter = D (L)

7.2. Developing of π -groups.

7.2.1. Geometrical groups.

7.2.1.1. Rotor diameter: d (m) - π_1

$$\rho_p^x \cdot v^y \cdot D^z \cdot d = 1 \quad (89)$$

Replace variables with dimensions and equate to zero:

$$[ML^{-3}]^x \cdot [LT^{-1}]^y \cdot [L]^z \cdot [L] = 0$$

Compare exponents for each dimension:

$$M: x = 0$$

$$L: y + z + 1 = 0 \Rightarrow y + z = -1$$

$$T: -y = 0$$

$$X = 0 : y = 0 : z = -1$$

Substitute in (89):

$$\pi_1 = d/D \text{ (Diameter ratio).}$$

When rotor diameter is replaced with any other linear variable then it will result in a similar group as π_1 .

7.2.1.2. Geometrical dimensionless groups

$$\pi_1 = \text{Diameter ratio (DR}_a) = d/D$$

$$\pi_2 = \text{Relative particle size (}\check{R}p_s) = P_{80}/D$$

$$\pi_3 = \text{Tank slenderness ratio (T}_a\text{SR}_a) = H/D$$

$$\pi_4 = \text{Relative froth depth (}\check{R}F_d) = F_d/D$$

$$\pi_5 = \text{Submergence ratio (Su) = h / D}$$

$$\pi_6 = \text{Rotor height (R}_h) = e/D$$

7.2.2. Kinematic groups.

7.2.2.1. Aeration: q_a (m^3/s) - π_7 and circulation: q_c (m^3/s) - π_8

$$\rho_p^x \cdot v^y \cdot D^z \cdot q_a = 1 \tag{90}$$

Replace variables with dimensions and equate to zero:

$$[ML^{-3}]^x \cdot [LT^{-1}]^y \cdot [L]^z \cdot [L^3T^{-1}] = 0$$

Compare exponents for each dimension:

$$M: x = 0$$

$$L: y + z + 3 = 0 \Rightarrow y + z = -3$$

$$T: -y - 1 = 0 \Rightarrow y = -1$$

$$X = 0 : y = -1 : z = -2$$

Substitute in (90)

$$\pi_7 = q_a / vD^2$$

When v is replaced by ωD then equation becomes:

$$\pi_7 = q_a / \omega D^3 \quad (\text{Aeration number})$$

The same applies to the circulation requirement:

$$\pi_8 = q_c / \omega D^3 \quad (\text{Circulation number})$$

7.2.2.2. Conditioning time η (s) $-\pi_9$, froth retention time ξ (s) $-\pi_{10}$ and Conditioner Tank turn Around θ (s⁻¹)

$$\rho_p^x \cdot v^y \cdot D^z \cdot \eta = 1 \tag{91}$$

Replace variables with dimensions and equate to zero:

$$[ML^{-3}]^x \cdot [LT^{-1}]^y \cdot [L]^z \cdot [T] = 0$$

Compare exponents for each dimension:

$$M: x = 0$$

$$L: y + z = 0 \Rightarrow y = -z$$

$$T: -y + 1 = 0 \Rightarrow y = 1$$

$$X = 0 : y = 1 : z = -1$$

$$\pi_9 = v\eta/D$$

Replace v with ωD

$$\pi_9 = \omega\eta \text{ (Dimensionless conditioning time)}$$

The same manipulation for ξ and θ :

$$\pi_{10} = \theta/\omega \text{ (Dimensionless Tank turn around)}$$

$$\pi_{11} = \omega\xi \text{ (Dimensionless froth retention time)}$$

7.2.2.3. Viscosity μ (kg/ms) - π_{12} and gravity g (m/s²) - π_{13}

$$\rho_p^x \cdot v^y \cdot D^z \cdot \mu = 1 \tag{92}$$

Replace variables with dimensions and equate to zero:

$$[ML^{-3}]^x \cdot [LT^{-1}]^y \cdot [L]^z \cdot [ML^{-1}T^{-1}] = 0$$

Compare exponents for each dimension:

$$M: x + 1 = 0 \Rightarrow x = -1$$

$$L: -3x + y + z - 1 = 0 \Rightarrow y + z = -2$$

$$T: -y - 1 = 0 \Rightarrow y = -1$$

$$X = -1 : y = -1 : z = -1$$

Replace in equation (92)

$$\pi_{12} = \mu/\rho_p \cdot v \cdot D$$

or

$$\pi_{12} = \rho_p \cdot v \cdot D / \mu \text{ (Superficial Reynolds number)}$$

When μ is replaced by gravity then:

$$\rho_p^x \cdot v^y \cdot D^z \cdot g = 1 \quad (93)$$

Replace variables with dimensions and equate to zero:

$$[ML^{-3}]^x \cdot [LT^{-1}]^y \cdot [L]^z \cdot [LT^{-2}] = 0$$

Compare exponents for each dimension:

$$M: x = 0$$

$$L: y + z + 1 = 0 \Rightarrow y + z = -1$$

$$T: -y - 2 = 0 \Rightarrow y = -2$$

$$X = 0 : y = -2 : z = 1$$

Replace in equation (93)

$$\pi_{13} = gD/v^2$$

Replace v with ωd and invert, then π_{13} becomes

$$\pi_{13} = \omega^2 d^2 / gD \text{ (Froude number based on tank diameter)}$$

7.2.2.4. Kinematic dimensionless groups

$$\pi_7 = \text{Aeration number (A}_e\text{N)} = q/\omega \cdot D^3$$

$$\pi_8 = \text{Circulation number (CN)} = Q_c/\omega \cdot D^3$$

$$\pi_9 = \text{Dimensionless Conditioning time (C}_o\text{T)} = \omega \eta$$

$$\pi_9 = \text{Conditioner tank turn around } (\theta) = \theta/\omega$$

$$\pi_{11} = \text{Dimensionless Froth retention time (F}_{RT}\text{)} = \omega \cdot \xi$$

$$\pi_{12} = \text{Superficial Reynolds number } (Re_s) = \rho_p \cdot \omega \cdot D^2 / \mu_p$$

$$\pi_{13} = \text{Froude No } (Fr) = \omega^2 D / g$$

7.2.3. Dynamic groups.

7.2.3.1. Absorbed power P (kW) - π_{14}

$$\rho_p^x \cdot v^y \cdot D^z \cdot P = 1 \quad (94)$$

Replace variables with dimensions and equate to zero:

$$[ML^{-3}]^x \cdot [LT^{-1}]^y \cdot [L]^z \cdot [ML^2T^{-3}] = 0$$

Compare exponents for each dimension:

$$M: x + 1 = 0 \Rightarrow x = -1$$

$$L: -3x + y + z + 2 = 0 \Rightarrow y + z = -5$$

$$T: -y - 3 = 0 \Rightarrow y = -3$$

$$x = -1 : y = -3 : z = -2$$

Replace in equation (94)

$$\pi_{14} = \rho^{-1} \cdot v^{-3} \cdot D^{-2} \cdot P$$

Replace v with ωD and invert, then π_{14} becomes:

$$\pi_{14} = P / \rho \cdot \omega^3 \cdot D^5 \text{ (Tank power number)}$$

7.2.3.2. Surface tension σ (N/m) - π_{15}

$$\rho_p^x \cdot v^y \cdot D^z \cdot \sigma = 1 \quad (95)$$

Replace variables with dimensions and equate to zero:

$$[ML^{-3}]^x \cdot [LT^{-1}]^y \cdot [L]^z \cdot [MT^{-2}] = 0$$

Compare exponents for each dimension:

$$M: x + 1 = 0 \Rightarrow x = -1$$

$$L: -3x + y + z = 0 \Rightarrow y + z = -3$$

$$T: -y - 2 = 0 \Rightarrow y = -2$$

$$X = -1 : y = -2 : z = -1$$

Replace in equation (95)

$$\pi_{15} = \rho^{-1} \cdot v^{-2} \cdot D^{-1} \cdot \sigma$$

Replace v with ωD and invert, then π_{15} becomes:

$$\pi_{15} = \rho \cdot \omega^2 \cdot D^3 / \sigma \text{ (Weber number)}$$

APPENDIX 8: NEW SCALE -UP ALGORITHM

